Titre: Title:	Decoding Distributed Neuronal Activity in Extrastriate Cortical Areas for the Visual Prosthetic Applications
Auteur: Author:	Armin Najarpour Foroushani
Date:	2020
Type:	Mémoire ou thèse / Dissertation or Thesis
Référence: Citation:	Najarpour Foroushani, A. (2020). Decoding Distributed Neuronal Activity in Extrastriate Cortical Areas for the Visual Prosthetic Applications [Thèse de doctorat, Polytechnique Montréal]. PolyPublie. https://publications.polymtl.ca/5494/

POLYTECHNIQUE MONTRÉAL

Affiliée à l'Université de Montréal

Decoding Distributed Neuronal Activity in Extrastriate Cortical Areas for the Visual Prosthetic Applications

ARMIN NAJARPOUR FOROUSHANI

Institut de génie biomédical

Thèse présentée en vue de l'obtention du diplôme de Philosophiae Doctor

Génie biomédical

Novembre 2020

POLYTECHNIQUE MONTRÉAL

Affiliée à l'Université de Montréal

Cette thèse intitulée :

Decoding Distributed Neuronal Activity in Extrastriate Cortical Areas for the Visual Prosthetic Applications

présentée par **Armin NAJARPOUR FOROUSHANI**

en vue de l'obtention du diplôme de Philosophiae Doctor

a été dûment acceptée par le jury d'examen constitué de :

Nikola STIKOV, président
Frédéric LESAGE, membre et directeur de recherche
Mohamad SAWAN, membre et codirecteur de recherche
Christopher PACK, membre et codirecteur de recherche
Benjamin DE LEENER, membre
André ACHIM, membre externe

DEDICATION

To my wife

ACKNOWLEDGEMENTS

I am grateful to thank people who encouraged and helped me during several years of working on PhD project. I would like to express my gratitude to my supervisor and co-supervisors, Prof. Mohamad Sawan, Prof. Christopher Pack, and Prof. Frédéric Lesage, for guiding me on both scientific and personal levels and helping me to target PhD goals. I would also like to acknowledge Bennett Csorba, Sujaya Neupane, Yann Aublet-Longpré, and Matthew Krause, at Pack Lab McGill, who provided me with clean datasets and commented on my work.

Finishing a PhD needs a lot of time and dedication and requires a balance between work and personal life. And I really like to thank my wife Fatemeh, who helped me emotionally, logically, and scientifically during my PhD. I also would like to thank my parents, grand parents, and my brother, who were always supportive in everything. I am also grateful for having good friends at Polytechnique and McGill, who involved in both academic and fun aspects of my PhD life.

RÉSUMÉ

Les prothèses visuelles corticales sont planifiées pour restaurer la vision chez les individus non-voyants en appliquant du courant électrique à des sites discrets sur le cortex visuel. À ce jour, la qualité de la vision rapportée dans la littérature est celle d'un petit nombre de phosphènes (percept de spots lumineux spatialement localisés) sans organisation pour générer un percept significatif. Le principal défi consiste à développer des méthodes pour transférer les informations d'une scène visuelle dans un schéma de stimulation compréhensible pour le cerveau. Une connaissance clé pour résoudre ce défi est de comprendre comment les caractéristiques du phosphène (ou en général, les caractéristiques visuelles) sont représentées dans le modèle distribué d'activité neuronale. Une approche pour obtenir ces connaissances consiste à déterminer dans quelle mesure les réponses neuronales bien réparties peuvent détecter les changements dans une caractéristique visuelle spécifique des stimuli. Pour atteindre cet objectif, nous avons étudié la capacité de discrimination des zones corticales extrastriées V4 chez les singes macaques. Ces zones extrastriées ont de petites régions rétinotopiques qui offrent la possibilité d'échantillonner une grande région de l'espace visuel à l'aide de réseaux de microelectrodes standard telles que celles de l'Université d'Utah. Cela aide à construire des prothèses mini-invasives.

Notre contribution concerne la résolution spatiale des potentiels de champs locaux (LFP) dans la zone V4 pour déterminer les limites de la capacité des prothèses visuelles à induire des phosphènes à plusieurs positions. Les LFP ont été utilisés car ils représentent une activité neuronale sur une échelle de 400 microns, ce qui est comparable à la propagation de l'effet de microstimulation dans le cortex. La zone visuelle extrastriée V4 contient également une carte rétinotopique de l'espace visuel et offre la possibilité de récupérer l'emplacement des stimuli statiques. Nous avons appliqué la méthode «Support vector machine» (SVM) pour déterminer la capacité des LFP (par rapport aux réponses à plusieurs unités - MUA) à discriminer les réponses (phosphènes) aux stimuli à différentes séparations spatiales. Nous avons constaté que malgré les grandes tailles de champs récepteurs dans V4, les réponses combinées de plusieurs sites étaient capables de discrimination fine et grossière des positions. Nous avons proposé une stratégie de sélection des électrodes basée sur les poids linéaires des décodeurs (en utilisant les valeurs de poids les plus élevées) qui a considérablement réduit le nombre d'électrodes requis pour la discrimination avec une

augmentation des performances. L'application de cette stratégie présente l'avantage potentiel de réduire les dommages tissulaires dans les applications réelles.

Nous avons conclu que pour un fonctionnement correct des prothèses, la microstimulation électrique devrait générer un schéma d'activité neuronale similaire à l'activité évoquée correspondant à un percept attendu. De plus, lors de la conception d'une prothèse visuelle, les limites de la capacité de discrimination des zones cérébrales implantées doivent être prises en compte. Ces limites peuvent différer pour MUA et LFP.

ABSTRACT

Cortical visual prostheses are intended to restore vision to blind individuals by applying a pattern of electrical currents at discrete sites on the visual cortex. To date, the quality of vision reported in the literature is that of a small number of phosphenes (percept of spatially localized spots of light) with no organization to generate a meaningful percept. The main challenge consists of developing methods to transfer information of a visual scene into a pattern of stimulation that is understandable to the brain. The key to solving this challenge is understanding how phosphene characteristics (or in general, visual characteristics) are represented in a distributed pattern of neural activity. One approach is to determine how well neural responses can detect changes in a specific characteristic of stimuli. To this end, we have studied the discrimination capability of V4 extrastriate cortical area in macaque monkeys. Extrastriate cortical areas have small retinotopic maps that can provide an opportunity to sample a large region of visual space using standard devices such as Utah arrays. Thus, this helps to build minimally invasive prosthetic devices.

Our contribution relates to the spatial resolution of local field potentials (LFPs) in area V4 to determine the limits in the capability of visual prosthetic devices in generation of phosphenes in multiple positions. LFPs were used because they represent neural activity over a scale of 400 microns, which is comparable to the spread of microstimulation effects in the cortex. Extrastriate visual area V4 also contains a retinotopic map of visual space and offers an opportunity to recover the location of static stimuli. We applied support vector machines (SVM) to determine the capability of LFPs (compared to multi-unit responses) in discriminating responses to phosphene-like stimuli (probes) located with different spatial separations. We found that despite large receptive field sizes in V4, combined responses from multiple sites were capable of fine and coarse discrimination of positions. We proposed an electrode selection strategy based on the linear weights of the decoder (using the highest weight values) that significantly reduced the number of electrodes required for discrimination, while at the same time, increased performance. Applying this strategy has the potential to reduce tissue damages in real applications.

We concluded that for the correct operation of prosthetic devices, electrical microstimulation should generate a pattern of neural activity similar to the evoked activity corresponding to an expected percept. Moreover, in the design of visual prosthesis, limits in the discrimination

capability of the implanted brain areas should be taken into account. These limits may differ for MUA and LFP.

TABLE OF CONTENTS

LIST OF TABLES

LIST OF FIGURES

LIST OF SYMBOLS AND ABBREVIATIONS

AMD	Age-related Macular Degeneration
AUC	Area under the curve
fMRI	Functional Magnetic Resonance Imaging
FPR	False positive rate
LDA	Linear Discriminant Analysis
LFP	Local field potential
LGN	Lateral geniculate nucleus
MT	Middle temporal visual cortex
MUA	Multiunit Activity
NHP	Non-Human Primates
RBF	Radial Basis Function
RF	Receptive field
ROC	Receiver Operating Characteristic
RP	Retinitis Pigmentosa
SD	Standard deviation
SE	Standard error
SVM	Support vector machines
tDCS	Transcranial Direct Current Stimulation
TMS	Transcranial Magnetic Stimulation
TPR	True positive rate
V1	Primary visual cortex
V4	Visual area V4
V2	Visual area V2

LIST OF APPENDICES

CHAPTER 1 INTRODUCTION

Based on global data on visual impairment in 2010, the number of visually impaired people was estimated to be 285 million (4.25% of world population in 2010), of whom 39 million were legally blind [1]. Visual prostheses are intended to restore vision in individuals with visual impairment by restoring their ability to recognize objects [2]. They apply direct electrical stimulation at some functioning points in the visual pathway located beyond the damaged site [3]. In normal vision, retina performs spatial, temporal, and chromatic processing on the visual input and transfers information via optic nerves to lateral geniculate nucleus (LGN). LGN then relays visual information to the primary visual cortex (V1) [4] and from there information transfers to the extrastriate areas where they apply more complex processing.

Electrical stimulation can target several places on the visual pathway, such as the retina, optic nerve, LGN, or visual cortex. Some types of visual impairment can result in non-functional retina such as Age-related Macular Degeneration (AMD), Retinitis Pigmentosa (RP), and diabetic retinopathy [5]. In these cases, a retinal prosthesis will not be helpful. Moreover, the optic nerve and LGN are not easily accessible due to their anatomical locations in the head [6, 7]. Thus, cortical visual prostheses can be the solution.

Applying electrical current stimulation at discrete sites in the visual pathway produces perception of punctate, isolated, and spatially localized spots of light called phosphenes [2, 8-11]. Multielectrode arrays provide the possibility of injecting a pattern of activity and thereby produce a pattern of phosphenes. Generating a meaningful percept requires having control over the characteristics of multiple phosphenes such as their spatial position, duration, size, brightness, and color. These characteristics depend on various factors including physical parameters of the implanted arrays, their location on the cortex, and the properties of applied stimulation currents, as well as behavioural and environmental factors. For example, with intracortical stimulating electrodes, increasing the current amplitude leads to an increase in the brightness [9].

To date, even in experiments that make use of many electrodes, the quality of vision reported in the literature is that of a small number of phosphenes with no organization to generate a meaningful percept [2, 9-12]. The main challenge is in developing a method to transfer information of a visual scene into a pattern of electrical stimulation that is understandable to the brain. The brain hardly detects unfamiliar patterns of neural activity. Thus, extensive training sessions will be required.

Because of the effect of neuroplasticity, training changes neural circuitry to support the detection of new activity patterns. Although this procedure makes the microstimulation detectable, it still introduces unfamiliar patterns of neural activity to the downstream neurons. This problem can be solved if the induced neural activity patterns are similar to the naturally-evoked responses to the visual stimuli. However, reaching this goal requires two research directions to progress in parallel, which explore: 1) how are phosphene characteristics (or in general, visual characteristics) represented in the distributed neural activity? 2) How can a pre-designed pattern of distributed neural activity be generated by applying a pattern of electrical microstimulation? For example, it is still unclear whether the position of an induced phosphene depends on the current amplitude. Moreover, electrical current stimulation may activate neurons that encode different positions in visual space. Therefore, it is important to control the extent of the induced neural activity.

We published a review paper entitled "Cortical visual prostheses: from microstimulation to functional percept" [13] which comprehensively discussed the above challenges. The focus of this PhD project is toward the first direction (above): how are visual characteristics represented in the distributed neural activity? Specifically, we study the discrimination capability of distributed neural activity in the extrastriate cortical areas of macaque monkeys. In this thesis, we use the term “neural activity” to mean both spikes and local field potentials (LFPs). We used sighted macaque models to circumvent the complexities resulting from changes that occur in the organization of the visual cortex after the onset of blindness and challenges associated with human experiments. It is worth mentioning that macaques have a similar visual cortex anatomy and function as humans.

Although most existing cortical visual prosthetic devices have targeted V1 because of the simplicity of encoding pixels as phosphenes in a retinotopic map and slightly lower current threshold [14], this area is quite large relative to standard recording arrays. Therefore, a multielectrode array in V1 can sample only a tiny region of visual space. In contrast, retinotopic maps in extrastriate visual areas (Figure 1.1) are physically smaller, while the receptive fields are much larger than those in V1 [15-17]. This provides the opportunity to sample a larger region of visual space, using standard devices such as Utah arrays [18, 19], and therefore, an extrastriate prosthetic could be minimally invasive. Thus, in this project, we focus on the extrastriate visual cortices.

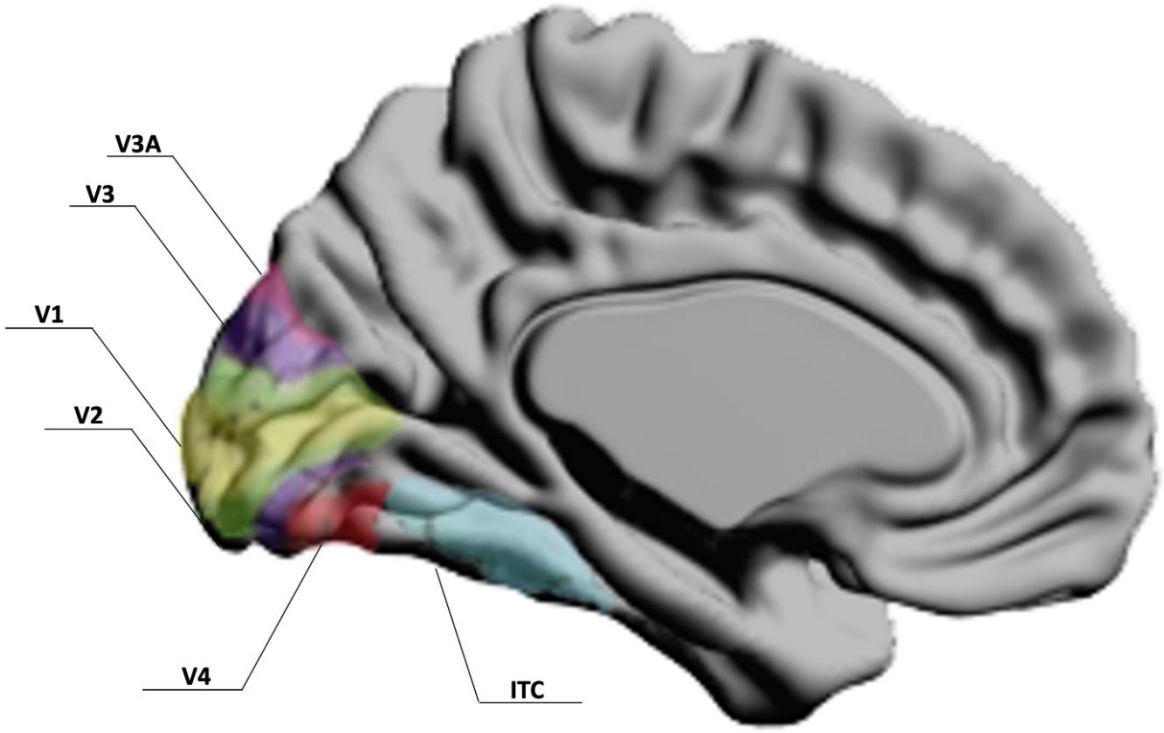

Figure 1.1 Medial view of the visual cortical areas. Primary visual cortex (V1) is shown in yellow and extrastriate cortical areas are presented in different colors.

Our contribution concerns the spatial resolution of extrastriate cortical area V4. The paper on this study, entitled "Spatial resolution of local field potential signals in macaque V4," was published in 2020 [20]. To generate a phosphenated percept, a pattern of spatially localized phosphenes must be induced. A preliminary step toward this goal is to determine how well responses to different spatial positions can be discriminated. This puts a limit on the capability of prosthetic devices to induce phosphenes at multiple positions. Area V4 contains a retinotopic map of visual space and offers an opportunity to recover the location of static stimuli. We analyzed the ability of local field potentials and Multiunit activity (MUA) from V4 in discriminating two-dimensional positions. Support vector machines (SVM) were used to discriminate responses associated with phosphene-like stimuli presented (probes) at different separations. We proposed an electrode selection strategy using linear weights of classifier to find the minimum number of electrodes for fine

discriminations, which will be applicable in the design of compact prosthetic devices. We also determined the effect of removing trial-to-trial fluctuations in response (noise correlations) on the decoding performance from two different perspectives.

1.1 Summary of hypotheses and contributions

This section summarizes our hypotheses and contributions in this PhD project. The main hypothesis is that the local field potentials in V4 are capable of fine and coarse spatial discriminations. Our sub-hypotheses and related contributions for this project are as follows:

Hypothesis 1: Local field potentials can precisely discriminate positions close enough to the fovea with 4° separations.

Contribution 1: We presented discrimination performance as a function of cortical distance and eccentricity to examine this hypothesis (Chapter 4).

Hypothesis 2: A smaller subset of electrodes, if selected correctly, can provide the same level of discrimination performance as the whole set of electrodes. In other words, they contain the same amount of information as the whole set of electrodes.

Contribution 2: We compared two methods for selecting a smaller set of electrodes and presented the results of the decoding for each group (Chapter 4).

Hypothesis 3: Information about the spatial positions are encoded in wideband LFPs rather than band-limited LFPs.

Contribution 3: We determined and compared the spatial resolution of wideband LFPs and band-limited LFPs (Chapter 4).

Hypothesis 4: Correlated variability (noise correlations) in the neural responses plays role in the decoding.

Contribution 4: We followed two perspectives introduced by Averbeck et al., 2006 (encoding and decoding perspectives). We trained our decoder on the correlation-removed responses but tested it once on the correlation-removed responses (encoding perspective in Chapter 5) and the other time on the original correlated responses (decoding perspective in Chapter 4). We compared the performance of each one to the original correlation-aware decoder.

Hypothesis 5: More important electrodes have a lower level of correlated variability.

Contribution 5: We presented correlated variability as a function of importance values (Chapter 4).

The entire structure of this thesis is designed toward the main objective as mentioned above: understanding the discrimination capability of distributed neural activity in the extrastriate cortical areas and the potential applications for developing better prosthetic devices. Therefore, the remaining chapters are organized as follows. In chapter 2, we review the experimental progress toward generating phosphenes and modulating their associated perceptual characteristics. We will then discuss the key challenges facing the generation of meaningful functional percepts (the review paper). In chapter 3, we present the methodology that was used in this thesis. In chapter 4, we analyze the spatial resolution of LFPs (as well as MUA) in the extrastriate cortical area V4 and propose an electrode selection strategy intended to build more compact prosthetic devices. In chapter 5 we present the theory and results for the encoding perspective and will compare them to the results of the decoding perspective. In chapter 6, we discuss the findings presented in the previous chapters. Finally, in chapter 7, we will present the conclusions from all the work in this PhD project.

CHAPTER 2 LITERATURE REVIEW

2.1 Article 1: Cortical visual prostheses: from microstimulation to functional percept

This manuscript has been published in Journal of Neural Engineering – IOPscience on February 2018, Volume 15, Issue 2, Pages 021005.

Title: Cortical visual prostheses: from microstimulation to functional percept

DOI: https://doi.org/10.1088/1741-2552/aaa904

Authors: Armin Najarpour Foroushani[1], Christopher C. Pack[2] and Mohamad Sawan[1]

Affiliations:

[1]Polystim Neurotech Lab, Institute of Biomedical Engineering, Polytechnique Montreal, Montreal, QC, Canada

[2]Montreal Neurological Institute, McGill University, Montreal, QC, Canada H3A 2B4

2.1.1 Abstract

Cortical visual prostheses are intended to restore vision by targeted electrical stimulation of the visual cortex. The perception of spots of light, called phosphenes, resulting from microstimulation of the visual pathway, suggests the possibility of creating meaningful percept made of phosphenes. However, to date electrical stimulation of V1 has still not resulted in perception of phosphenated images that goes beyond punctate spots of light. In this review, we summarize the clinical and experimental progress that has been made in generating phosphenes and modulating their associated perceptual characteristics in human and macaque primary visual cortex (V1). We focus specifically on the effects of different microstimulation parameters on perception and we analyse key challenges facing the generation of meaningful artificial percepts. Finally, we propose solutions to these challenges based on the application of supervised learning of population codes for spatial stimulation of visual cortex.

2.1.2 Introduction

As of 2010, the number of people estimated to be living with a visual impairment was around 285 million, and the number of legally blind people was around 39 million [1]. Visual prostheses are used to restore the function of vision in blind individuals by restoring their ability to recognize objects and to navigate in an unfamiliar environment [2]. Since blindness results from a dysfunction in the normal signal flow in the visual pathway, visual prostheses are frequently used to apply direct electrical stimulation to the visual pathways at some still functioning points located beyond the damaged site [3]. Employing electrical current stimulation to the functioning visual pathway at discrete sites evokes a perception of phosphenes; these are punctate, isolated, and spatially localized coloured or non-coloured spots of light appearing close to the center of the visual field [2, 8-11]. Electrical stimulation of the visual pathway through multielectrode arrays provides the possibility of injecting a spatiotemporal pattern of activity, thereby inducing a pattern of phosphenated perception (perception of images made of phosphenes). The aim is for the evoked visual percept to be a phosphenated version of the visual scene in the form of a score-board (bit-mapped) image [6, 21].

Electrical stimulation can target different areas of the visual pathway, such as the retina, optic nerve, lateral geniculate nucleus (LGN), optic radiations, and the visual cortex, depending on the impaired region of the visual pathway. In normal vision, the retina performs spatial, temporal, and chromatic processing on the visual input and produces sequences of spikes to transfer to the LGN. From the LGN signals project to V1, the primary visual cortex [4]. Region V1 is thought to be an ideal site for implanting electrode arrays for a number of reasons: it has uniform thickness and density of cells for central vision and peripheral vision and also has a well-organized mapping of visual space onto neurons (visuotopic map) [22]. In addition, it has enough area for implantation of electrodes [23] and is easy to access, compared to the retina, optic nerve or LGN [6, 7]. The primary visual cortex also has a large magnification factor [24, 25] which means that more cortical tissue is devoted to a given visual field angle and thus, the receptive field mapping on the cortex can be covered with more electrodes (if required) and higher resolution images can be evoked [26]. Furthermore, for patients with non-functional retinae or optic nerves, such as when complete blindness results from Age-related Macular Degeneration (AMD), Retinitis Pigmentosa (RP),

glaucoma, or diabetic retinopathy, a retinal prosthesis would not be helpful [5]. Figure 2.1 shows a simplified graphical illustration for a cortical visual prosthesis implanted in human V1.

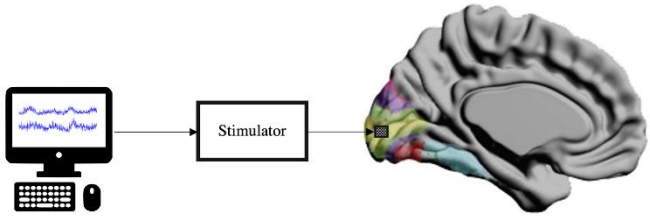

Figure 2.1 Graphical schematic of implanted electrode arrays in the primary visual cortex to electrically stimulate the brain, induce perception of phosphenes, and restore vision.

2.1.2.1 Surface stimulation

Prior to 1990, experiments with cortical visual prostheses were performed on humans and with surface electrode arrays. The first cortical visual prosthesis was made in 1968. It was capable of producing percepts of discrete, clustered, and diffuse points of light [11]. The prosthesis was based on a surface array of 80 electrodes implanted in the right occipital pole and could generate 32 individual phosphenes from 39/80 of electrodes. While, this approach was not sufficient to produce a functional percept in blind subjects, it motivated further work on cortical visual prostheses [8, 10, 12]. Using surface electrode arrays, Dobelle showed that phosphenes can be generated so as to help patients in reading Braille characters [12]. Using a camera and image processing algorithms, in 2000, Dobelle was able to provide a patient with very limited object recognition and independent mobility, using surface electrodes to generate up to 21 phosphenes [2].

2.1.2.2 Intracortical stimulation

The first stimulation of visual cortex using intracortical microelectrode arrays in a human in 1990 showed that discriminable phosphenes can be evoked by electrodes 700 µm apart and with 100 times less current than was necessary with surface microstimulation [27]. In 1996, it was demonstrated that intracortical microstimulation can evoke phosphenes in a patient who could not perceive phosphenes from surface stimulation [9].

After 2000, research started to be performed more often on non-human primates, mainly on rhesus macaque monkeys using intracortical microelectrode arrays [6, 7, 28-30], because they had a similar visual cortex anatomy and function to humans but with central visual field representation on the V1 surface that made it easier to access with most electrode arrays. In 2005, monkeys trained in a memory saccade task were able to saccade to the phosphene location generated by intracortical electrical stimulation [7]. In 2011, the effects of different microstimulation factors on behavioural responses in macaque monkeys were documented [28]. Although working on monkeys is not as ethically complicated as working on humans, the identification of phosphene quality is necessarily more complicated because of the lack of effective communication. Monkey studies therefore rely on psychophysical measures to identify the percept [6, 7, 28-30].

In parallel to the progress made in phosphene induction, different implantable electronic systems also were developed for the controllable microstimulation of the visual cortex in order to modulate phosphenes efficiently and with very low power consumption devices [31-34]. These systems are now are part of two products by Second Sight Medical Products that were published as US patents in 2016 [35, 36].

The work of Dobelle (2000) showing very limited object recognition and mobility with only 21 phosphenes [2] was a major advance, but to date even experiments with many electrodes have failed to approximate functional vision with inputs constructed from phosphenes [2, 9-12], and no cortical visual prosthesis has obtained regulatory approval to date [37]. The quality of vision reported in the literature is that of a small number of phosphenes with no organization sufficient to generate a meaningful percept. The most significant barrier is in developing a method to transfer information of a visual scene into a spatiotemporal stimulation pattern that is understandable to the brain. Here, in section 2 we first review how phosphene induction and perceptual characteristics can be influenced by the properties of electrical microstimulation. Section 3 concerns detailed analysis about the challenges facing the construction of functional visual percept from phosphenes and proposed solutions to overcome the difficulties of inducing meaningful percepts. Finally, the conclusions about the issues discussed in this paper will be presented.

2.1.3 Phosphene induction and the effect of microstimulation

The quality of phosphenes is influenced by different factors, including the implanted electrodes and the applied stimuli, as well as behavioural and environmental factors, and the characteristics of the neural tissue interfacing the implanted electrodes. In the following section we review how different factors affect the generation, detection, duration, and characteristics of the phosphenes. A summary of the effects of different factors on phosphene induction is provided in Table 2.1.

2.1.3.1 Phosphene generation

To induce perception of a phosphene in a subject, a minimum amount of current, termed phosphene threshold or current threshold, is required. In human patients, phosphene threshold can be determined by various methods. For example, in the successive approximation convergence technique [9], the current is initialized to one-half of the maximum current and the perception of phosphenes is reported by the subject after each stimulation train. If the phosphene is perceived, the next current tested is half the difference between the present value and 0 μA or between the present value and the highest current for which a phosphene has not been perceived. If a phosphene was not perceived, the next stimulation current is half the difference between the present value and the lowest current value for which a phosphene was perceived (or the maximum current value for which phosphene was induced). This process continues until the change in current is less than 0.1 μA, with the phosphene threshold as the lowest current for which a phosphene was perceived.

The phosphene threshold depends on stimulation parameters such as frequency, pulse duration, and amplitude [9-11] and also depends on location and depth of the electrode tips in the cortical layers and the impedance of the electrodes [28]. In macaque monkeys after two years of implantation, electrical stimulation could still generate a visual percept [29], indicating that the functionality of electrodes for phosphene generation can persist for a long period of time. Here, we present the effect of different factors on phosphene generation.

2.1.3.1.1 Electrode array parameters and tissue interface

Table 2.1 The effect of different factors on the phosphene threshold based on the summary of the literature. ↑: Increasing that factor increases the phosphene threshold; ↓: Increasing that factor decreases the phosphene threshold; N.E.: No Effect; N.R.: Not Relevant; N.K.: Not Known

	Electrode Depth	**Distance Between Electrodes**	**Repeated Stimulation**	**Pulse Amplitude**	**Frequency**	**Pulse Duration**	**Train Length**	**Number of stimulating electrodes**
Phosphene Threshold	↓	↓	↑	N.R.	↓ Effective in 100-200Hz	↓ Effective in 0.01-1ms	↓	↓
Phosphene Duration	N.K.	N.K.	N.K.	High amplitudes increase the duration	N.K.	N.R.	↑ With limits on train length	N.K.
Phosphene Location	Not known exactly	Influences number of phosphenes	N.E.	N.E.	N.E.	N.E.	N.E.	Depends on the location of electrodes
Phosphene Brightness	↑	N.K.	↓	↑	↑	↑	↑	N.K.
Phosphene Size	↓	Depends on electrodes position & eccentricity	N.K.	↑ But for intracortical electrodes depends on location	N.K.	N.K.	↑	N.K.
Phosphene Colour	Colourful phosphenes reported with intracortical stimulation	N.K.	N.K.	Higher or lower than current threshold influence the colour	N.K.	N.K.	N.K.	N.K.

Although Dobelle's finding showed little effect of different *electrode sizes* on subjective perception [10], it is reported that lower currents coming from smaller electrodes are possibly able to generate smaller phosphenes [38]. The *depth of electrode tips* shows significant effects on phosphene generation. Increasing the depth of the electrode tips in the cortex from the surface decreases the threshold for phosphene elicitation [27, 39, 40], with the threshold becoming minimal in layers V and VI in the visual cortex [41]. This is the reason that intracortical electrodes need less current to

induce phosphenes compared to surface electrodes [9, 27]. Surface electrodes require current in the range of 1 mA-15 mA to elicit phosphenes [10, 11, 42] which is unsafe for simultaneous stimulation, increases the risk of seizure, and elicits pain [10]. In addition, they cannot evoke a high-resolution pattern of separated phosphenes, as they cause interactions between phosphenes. Intracortical microelectrodes positioned in the depth of 2 mm in human V1 region can elicit phosphenes with only 1.9-25 µA [9]. Thus, intracortical visual prostheses are already used as an alternative solution which need much lower power and higher microelectrode density to induce phosphenes [7, 9]. The first intracortical visual prosthesis used in humans showed that phosphenes were perceived with 100 times lower electrical current (20 µA) at depth of approximately 2.25 mm compared to what was necessary with surface electrodes [27]. In addition, blind patients who were unable to perceive phosphenes with surface electrode stimulation could perceive phosphenes with intracortical electrode arrays [9].

Phosphene threshold is not a constant value; it can change over time after repeated stimulation. The *distance between electrodes* plays a role in the current thresholds of other electrodes after repeated stimulation. Repeated anodic-first (then cathodic) stimulation of an intracortical electrode results in a substantial increase in the phosphene threshold of the stimulating electrodes and a decrease in the phosphene threshold of an unstimulated electrode within 250 µm distance [9]. The results of this work for electrodes with 500 µm distance showed that repeated sub-threshold stimulation of one electrode also decreased the phosphene threshold. However, for electrodes with distance 750 µm, sub-threshold stimulation of one electrode did not affect the phosphene threshold of other electrodes.

2.1.3.1.2 Stimulation parameters and phosphene threshold

Stimulation parameters concern the current stimulation waveform given to the cortical tissue from each electrode. These parameters are *amplitude*, which is the intensity of the stimuli, *pulse polarity*, which can be cathodic-first or anodic-first, *frequency*, which is the inverse of time between pulses, *pulse duration*, which is the duration of a phase of the pulse, *train length*, which is the duration of the pulse burst, and *inter-train interval*, which is the time between two successive trains [9]. Phosphene threshold is a function of all these parameters. Changing stimulation parameters affects the phosphene threshold but does not produce different phosphenes [10]. For a patient with 22

years of blindness implanted with intracortical electrodes, satisfactory phosphenes were generated with a frequency of 200 Hz, pulse duration 200 µs, inter-phase interval 0, train length 125 ms; the measured phosphene thresholds for most of the electrodes were less than 25 µA [9].

The *pulse amplitude* required to generate a phosphene is distinct for every electrode and for different subjects. The probability of phosphene perception increases with increasing the stimulus current amplitude (Figure 2.2), as tested on two monkeys implanted with intracortical microelectrodes [28]. In this regard, it was found that repeated electrical stimulation (higher or lower than phosphene threshold) reduced the ability to detect the phosphene and increased the level of stimulation required to produce a behavioural response [28, 41]. However, increasing the time between the stimulations could avoid this issue.

The leading phase of biphasic stimulation pulse or *pulse polarity* can affect the phosphene threshold. It has been reported that for surface macroelectrodes there is no difference in phosphene threshold between cathodic-first and anodic-first pulses [10]. However, for intracortical microelectrodes, cathodic-first pulses are more effective than anodic-first pulses in generating phosphenes [9]. As illustrated in Figure 2.3, with intracortical electrodes, a lower threshold is required for cathodic-first compared to anodic-first stimulation.

Frequencies above 30 Hz can produce steady phosphene [9-11, 27], but the most effective frequencies to generate phosphenes in humans are in the range of 100-200 Hz [9, 10]. Decreasing pulse frequency was shown to increase the phosphene threshold [9, 10]. It was reported that using intracortical stimulation with frequencies in the range 150-200 Hz, the threshold current was constant but increased by 50% for a frequency of 75 Hz [9].

The effective *pulse duration* to evoke phosphenes has been reported to be 0.01-1 ms [9-11], with pulse durations longer than 1ms failing to generate phosphenes. Results on human subjects showed that the threshold decreased with increased pulse duration [9-11]. An interesting result was that the subject preferred the wider pulse duration (≥400 µs) [9], which was in contrast to the results obtained with surface electrodes [10]. This work ([9]) also reported a current threshold increase of 52% as the experiment progressed, but this increase reached 20% when pulse duration became two times more. Thus, to decrease the current threshold, pulse duration can be increased over the course of experiment which is also less unpleasant for the subject. This increase can continue to the point

that variations in the phosphene threshold are reduced, so that at higher pulse durations the threshold becomes nearly stable [9]. The relationship between pulse duration and current threshold when four contiguous electrodes were stimulated could be fitted to a hyperbolic function specifying Chronaxie and rheobase [29] by the mathematical expression: $I * t = I_{rh} * (t + \tau_{SD})$. In this expression I was the threshold current, I_{rh} was the rheobase current, t was the pulse duration, and τ_{SD} was the chronaxie.

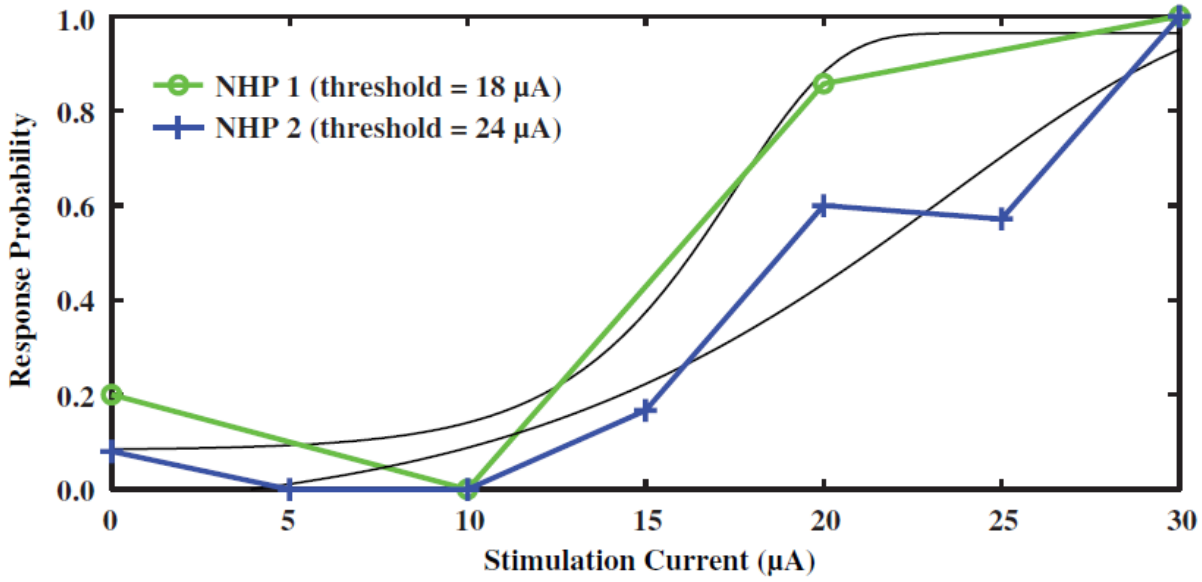

Figure 2.2 Behavioural responses to various microstimulation current values from a single electrode for two Non-Human Primates (monkeys) NHP 1 and NHP 2. The stimulation parameters were: 40 cathodic-first pulses, 200 µs pulse width, and 200 Hz frequency. The results show increase in probability of behavioural response by increasing current amplitude. Used with permission from [28].

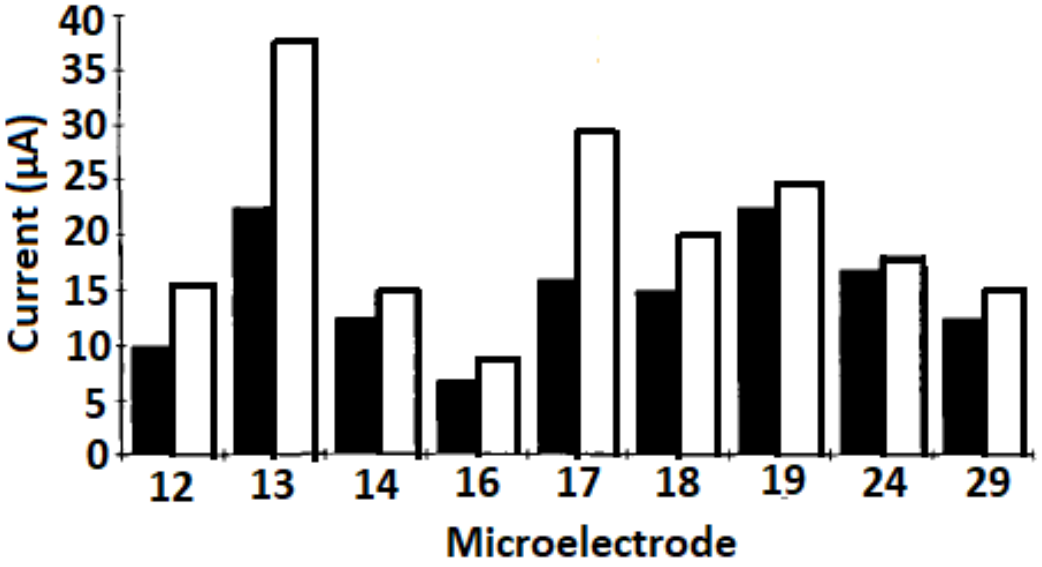

Figure 2.3 How anodal and cathodal stimulations affect the threshold. Cathodal-first stimulation that is shown in black needs less current to attain the phosphene comparing to the anodal first stimulation that is shown in white. Adapted from [9].

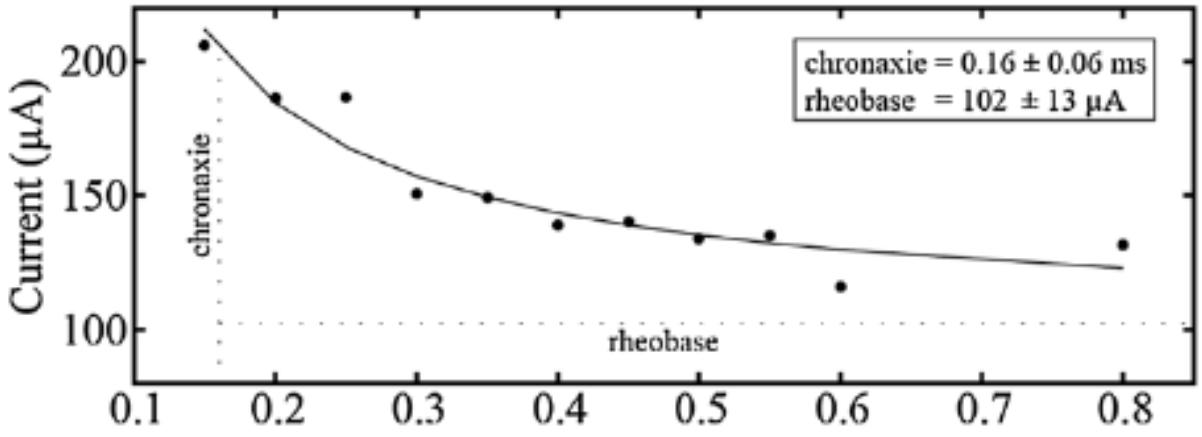

Figure 2.4 Relationship between threshold current and pulse duration for stimulating four contiguous stimulating electrodes. The stimulation current was 40 symmetric biphasic cathodic-first pulses with 200 Hz frequency. Chronaxie and rheobase were calculated to be 0.16±0.06 ms and 102±13 μA. Used with permission from [29].

The relationship between current threshold and pulse duration for four contiguous electrodes with 40 biphasic cathodic-first pulses at frequency 200 Hz is illustrated in Figure 2.4 [29]. *Train length* also exerts an influence on the phosphene threshold: At fixed frequencies, decreasing the train length from 250 ms to 125 ms increased the phosphene threshold 20%, but at a train length of 250 ms, the phosphene was more recognizable and with longer duration [9].

2.1.3.1.3 Spatial characteristics of stimulation

The *number of stimulating electrodes* is an important parameter in evoking phosphene perception and induction of a desirable percept. By stimulating through single intracortical electrodes implanted in a monkey, only 8/82 resulted in behavioural responses [28]. However, increasing the number of stimulating electrodes increased the probability of evoking a visual percept and reduced the required phosphene threshold for generating behavioural responses [29]. With systematic stimulation through individual electrodes with currents up to 200 μA, only 19 out of 96 electrodes could evoke behavioural responses. When two contiguous electrodes were used for stimulation, only two of eight groups of electrodes with 300 μA per electrode could produce behavioural responses. By increasing the number of electrodes in a group to four, 26 out of 32 groups generated consistent responses, and psychometric curves generated with 204±49 μA current per electrode. When the number of contiguous electrodes reached nine, all eight groups could induce behavioural responses with 91±25 μA per electrodes (Figure 2.5) [29]. These results showed that increasing the number of simultaneously stimulated electrodes decreases the current threshold per electrode required to produce a behavioural response and increases the probability of generating a visual percept. It was also shown that increase in the current threshold over time is less for nine contiguous electrodes than for four contiguous electrodes. Although these results show lower threshold and higher probability of phosphene generation, there is no evidence that more electrodes produce better performance on a visual task. In addition to electrodes that are able to generate phosphenes, performance depends on the area of the visual cortex that is stimulated by the electrode array and the spatial distance between electrodes [37].

2.1.3.2 Training to detect electrically-induced phosphenes

Training is an important factor in performance of prosthesis. Without training sessions, subjects could not detect even intense stimulation, presumably because they were unable to register an artificial spatial and temporal distribution of activity. However, following training, behavioural thresholds improve [43]. In one experiment [9], a blind patient was unable to detect the phosphene in the first experimental trial, but after eight stimulation sessions she could detect phosphenes reliably. The patient was also able to detect the onset of stimulation with lower current levels and shorter latencies than the offset of stimulation [9].

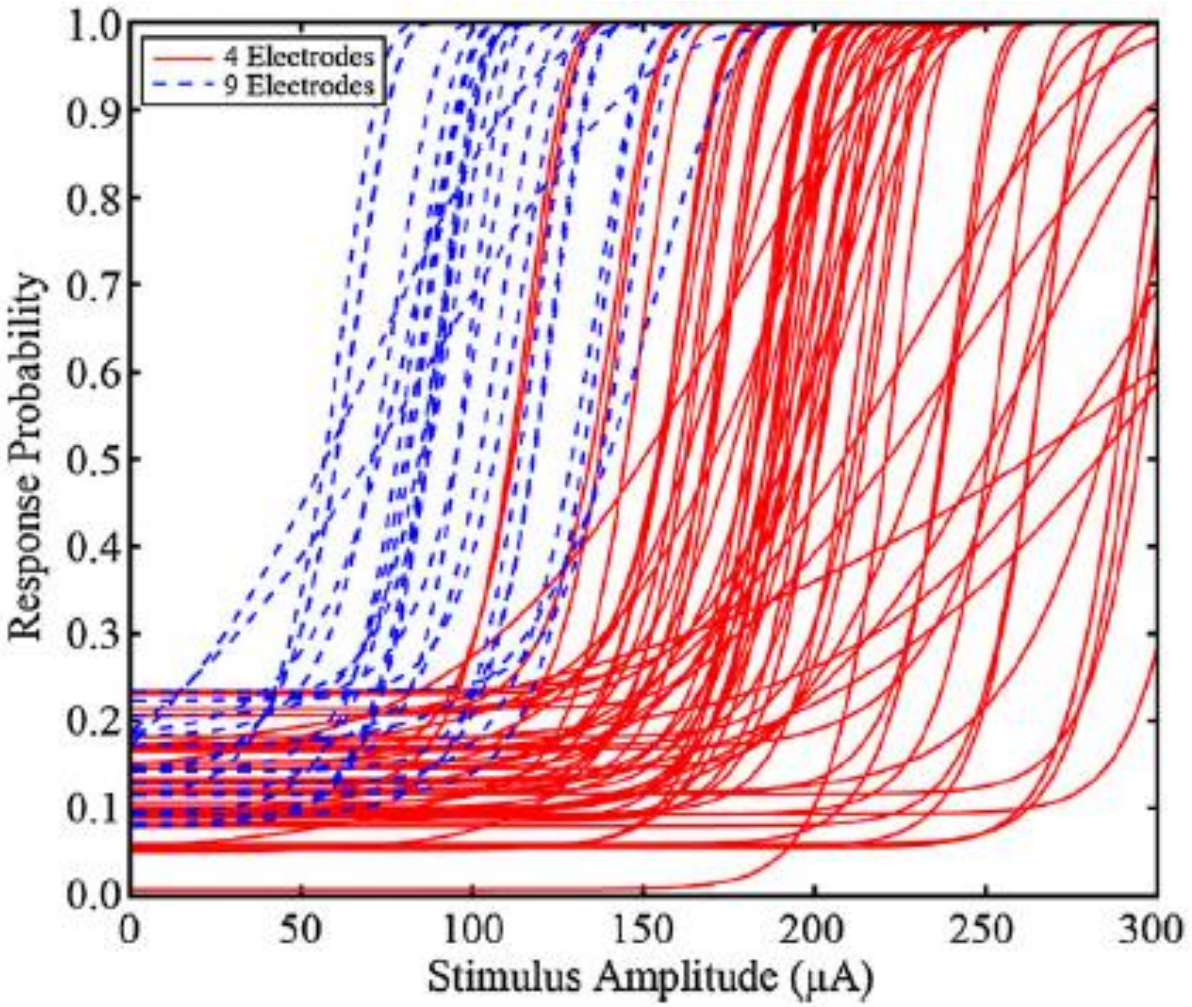

Figure 2.5 The relationship between number of contiguous stimulating electrodes and the current threshold per electrode required to induce behavioural response. These curves are Weibull functions fitted to psychometric data for stimulating with four and nine contiguous electrodes.

Current threshold for four contiguous electrodes is 204±49 μA while for nine electrodes it is 91±25 μA. Used with permission from [29].

To measure the effect of training on the ability of animals to detect intracortical microstimulation at different sites in V1, rhesus monkeys were trained on a two interval forced-choice detection task [44] with visual stimuli. When the threshold for detecting visual stimuli became stable (after around 4 months) the visual stimulation was replaced with a 250 ms anodal-first, biphasic pulse train microstimulation with frequency 200 Hz and amplitude of no more than 50 μA (weak stimulation). Each site was defined as a 3 mm ×3 mm region with 5mm distance from the other sites. For each site, training reduced the current threshold. Initially monkeys were unable to detect the phosphenes, but after 2-4 weeks of training, thresholds converged to a stable asymptote (around 6.2-6.6 μA).

Training to detect microstimulation in one site is very specific to the trained location, as further training is required to achieve asymptotic thresholds at an untrained site [44]. However, the effects of training are long-lasting: Retesting a previously trained site after one year showed that the threshold remained stable without practice. Interestingly, at a specific cortical site, training to detect electrical stimulation elevated detection threshold of the visual stimuli by factor of 1.5-7 and retraining to detect visual stimuli elevated the detection threshold of electrical stimulation 3-fold at each site. However, both changes in threshold were reversible [45].

On the other hand, the effect of training in a memory saccade task to detect phosphene location in monkeys showed that after a period of training with some stimulating electrodes they were able to detect the phosphenes induced by other electrodes that had not been used before [7]. Following training, they were able to detect a 5% change in frequency [41] and 5-10% change in current. They were also able to detect 20 ms or more of delay between stimulations delivered through separate electrodes [41]. In general, monkeys can detect stimulation of every site throughout the visual cortex, possibly as a consequence of extensive training [14].

Microstimulation changes neuronal response properties, and thus during the training sessions the neuronal connections likely change to support them [46]. It appears that after training, the microstimulation signals are processed as if they were generated naturally, and in some situations subject cannot distinguish between natural and artificial neuronal stimulation [47]. This suggests

that adult cortex has enough plasticity to learn to process new neural activity patterns [48]. For future prostheses with a large number of stimulating electrodes (e.g. more than 100), detection of multiple phosphenes will likely require extensive training and more advanced psychophysical techniques.

2.1.3.3 Phosphene duration

The duration that a phosphene is perceptible depends on the stimulation onset and cessation. Phosphenes typically appear immediately after the onset of stimulation and disappear immediately after stimulus cessation (Figure 2.6 a) [9-11]. There is also a reaction time for the onset of phosphene detection and cessation that differs for different electrodes and is influenced by stimulation frequency [9]. Strong stimulation, however, can result in persistence of phosphenes beyond the stimulation offset (Figure 2.6 b) [10, 11]. Increasing the stimulation train length initially yields phosphenes of slightly longer duration than the train length. However, larger increases cause phosphenes to disappear before the termination of stimulation. This occurs when the stimulation train length is greater than 10-15 s for surface microelectrodes [10] or 1 s for intracortical microstimulation (Figure 2.6 c) [9]. To increase the duration of phosphene perception when a long stimulation train is used, brief interruption should be applied during the stimulation train [9]. In particular, it was shown that stimulation with 12 trains of length 125 ms with inter-train intervals of 50 ms can produce perception of multiple phosphenes appearing close together in time. However, decreasing the inter-train interval to 25 ms produces a percept of a single phosphene perceived throughout the period of stimulation, which disappears shortly after the cessation of stimulation. It has been shown that the neural elements of V1 that mediate phosphene induction are mainly pyramidal fibres [10, 11, 39, 41, 42], while GABAergic fibres mediate phosphene termination [49].

2.1.3.4 Phosphene characteristics

According to studies of phosphene induction in blind patients [2, 10-12], the perceptual characteristics associated with phosphenes are shape, size, brightness, colour, flicker, spatial location, multiplicity, and edge. It has been observed that the shapes of cortical phosphenes are spot-like, round, and diffuse [11]. The sizes of most phosphenes are in the range of 0.5-2º of visual

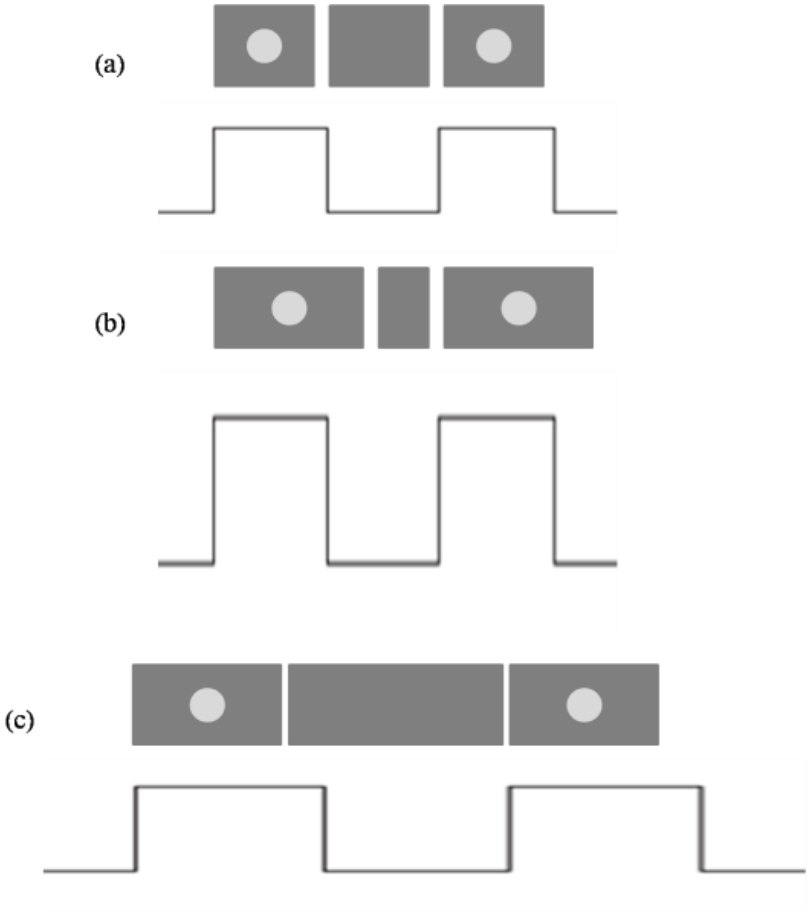

Figure 2.6 Phosphene onset, duration, and extinction depend on the microstimulation pulse amplitude, and pulse duration. (a) phosphene appears with the stimulus onset and disappears with stimulation offset. (b) With an increase in current stimulation amplitude, the phosphene stays longer and does not disappear immediately with the offset of stimulus. (c) When a stimulus pulse duration is longer than 1 s for intracortical electrodes or 10-15 s for surface electrodes, the phosphene disappears before the offset of stimulus.

angle [8-11, 50]. In colour, they are most likely to be colourless (white) [2, 10], yellow [42], and gray. However, blue [42], red, green [9], brown, and orange [10] phosphenes are also observed. The flicker of phosphenes is variable, and depending on the microstimulation factors, they can flicker or not [9]. The spatial location of phosphenes is pseudo-corticotopic and only roughly follows the visuotopic map [10, 11, 28]; phosphenes usually appear around the horizontal and vertical meridians. A single stimulation site sometimes may produce multiple phosphenes [9-11].

The edges of phosphenes are sharper in the foveal and parafoveal visual field and are more fuzzy at higher eccentricities [11]. Here, we present the effects of different microstimulation factors on the main phosphene characteristics, according to the experimental results obtained on human and monkey.

2.1.3.4.1 Phosphene location

The location of phosphenes and the effectiveness of electrical stimulation in producing a percept depend on the location and extent of the electrodes across the visual cortex. With implantation of intracortical electrodes near the right occipital pole [51, 52], all the phosphenes were generated in a small area of the visual field in the left hemi-field with the majority above the horizontal meridian and at an eccentricity of 22° [9]. A phosphene map is the ensemble of locations of the induced phosphenes associated with all the stimulating electrodes. Figure 2.7 a is an example of a two-dimensional phosphene map from a human subject implanted with an electrode array on the top side of the right occipital lobe (Figure 2.7 b) [2]. For human subjects, two mapping methods were presented in [9]. The first method used a dart board with five radial and five concentric annular segments (to represent the fovea and visual periphery); for each phosphene the subject placed a dart in the corresponding board location via tactile localization (Figure 2.8 a). The second method used computer mapping of each phosphene by having subjects indicate the direction between two phosphenes induced by activating two electrodes when one phosphene was a reference phosphene (previously mapped) and the second phosphene was the one to be mapped. The subject indicated the direction vector between two phosphenes using a joystick with 16 different directions (Figure 2.8 b). The results showed fairly good correspondence between the location of electrodes in the visual cortex and the computer-based phosphene map. Phosphene mapping in animals is more difficult and entails the initial step of training them to provide information about what they have perceived. The memory saccade task can be used for this purpose [6, 7, 29]. In the memory saccade task, the animal fixates on a spot for around 1-1.5 s, and during this fixation time a small spot flashes for around 100 ms in a random location within the receptive field (as previously mapped) of the neurons. After a delay, the animal is required to saccade to the remembered location of the flashed spot (stimulus) to receive a reward. In the next step, the fixation point is presented visually, and then the electrical stimulation is applied. It is expected that the animal will treat the phosphene

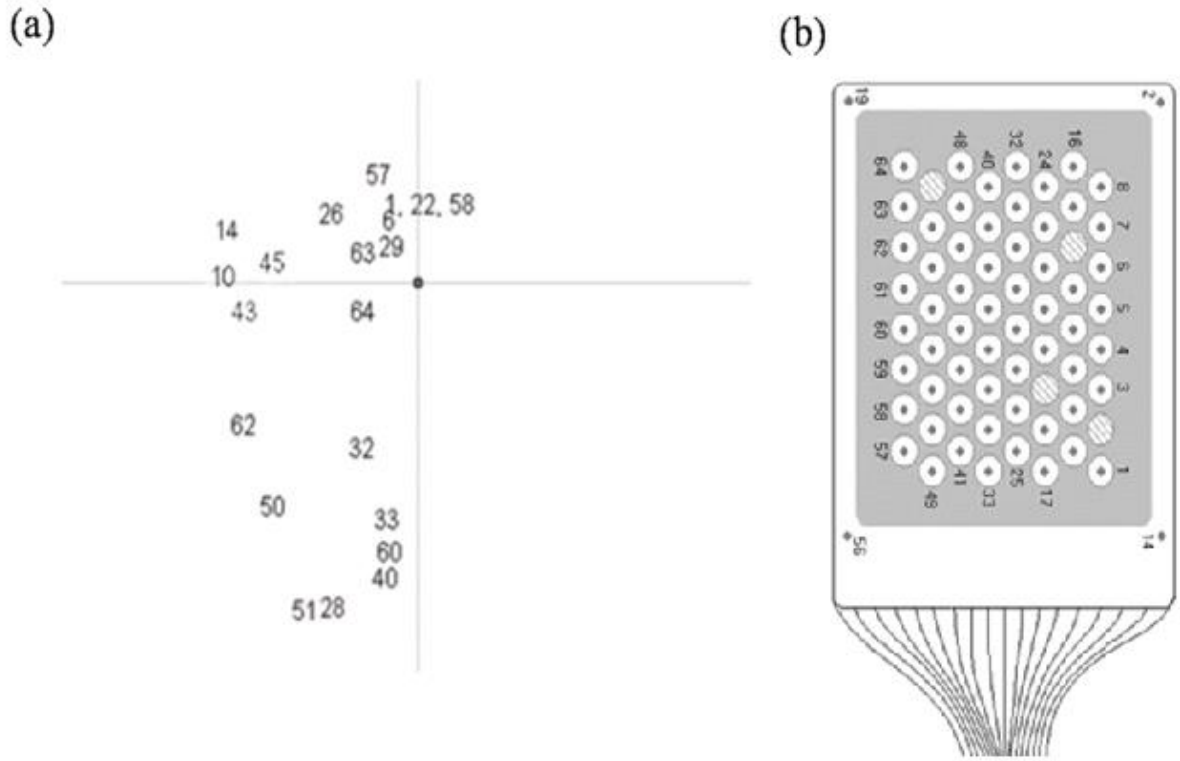

Figure 2.7 Phosphene map in the visual space of a blind subject reported by Dobelle (2000). (a) Location of phosphenes mapped in the visual field of the blind subject. Each number corresponds to an electrode number as shown on the right. The phosphenes are induced on the left visual field in the 8 inch×3 inch area (b) the electrode array numbering used for stimulation. The array is implanted on the top side of the right occipital lobe. Used with permission from [2].

similarly to the visual stimulus and perform a saccade to the location of the phosphene in the receptive field. Saccade endpoints can then be considered a readout of the location of the induced phosphene. The reason that saccade should be made to the remembered location is that when the eyes move, the phosphenes move with the eye, as reported in human experiments [9]. An important point that is usually considered in the experiments is interleaving visual and electrical stimulation, so that the animals are motivated to perform the saccade for both types of stimuli. Although this memory saccade task works for sighted monkeys, it may not be applicable for blind human subjects where the eye muscles do not function in a normal way. The results of studying phosphene location in monkeys showed a significant correlation between saccade endpoint and receptive field location

for each electrode [6, 7, 53, 54], and significant increases in this correlation were observed after several months of training.

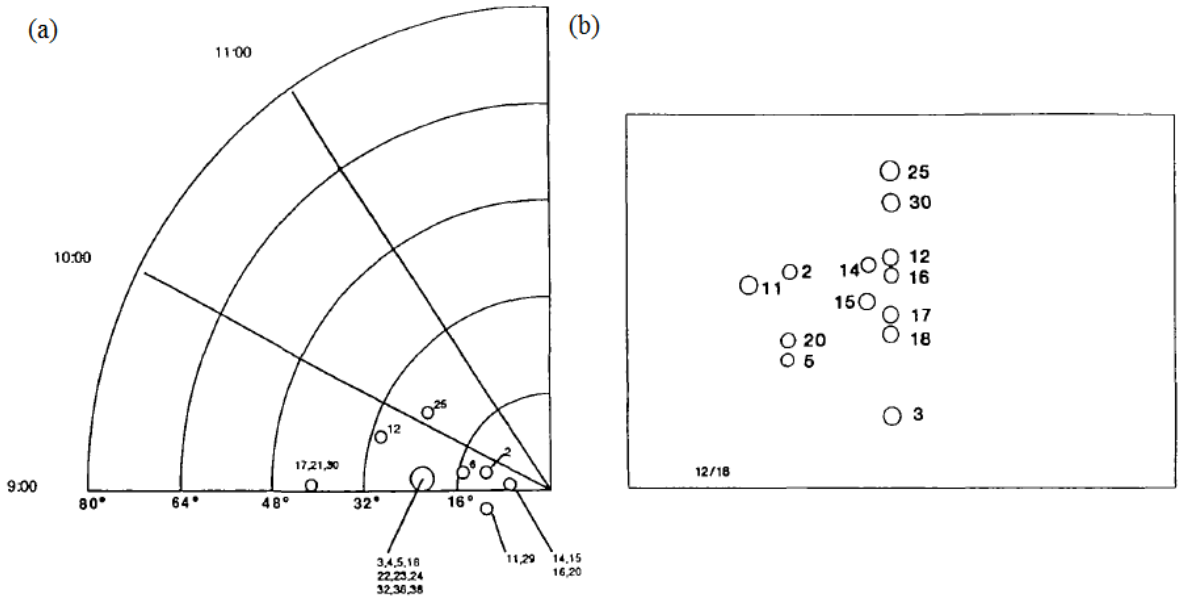

Figure 2.8 Different methods of phosphene mapping as used in [9]: (a) dart board map, which refers to the subjective center of gaze and (b) computer-coupled joystick mapping. The circles show the perceived location of phosphenes in the visual space (showed by the number of phosphenes). Used with permission from [9].

Stimulating with new electrodes that were not used for training the monkey on the saccade-to-phosphene task also showed a high correlation between receptive field centers and the saccade end points [7]. This suggests that the monkeys had not simply learned to perform the saccade based on the stimulation per se, but rather had learned to respond to the evoked phosphene. On the other hand, the results of stimulating V1 with higher than 5 mm distance showed that stimulation with new electrodes that were not used for training cannot be detected without further training session [45]. Comparing saccade endpoints and visual targets that were presented in eccentricity equal to zero, showed 2.5 times higher standard deviation (SD) for saccade endpoints and an increase in their SD with increases in eccentricity [7]. Thus, a saccade to a visual target is more precise. Performance of the memory saccade task in concert with electrical stimulation of three groups of nine contiguous electrodes implanted anterior to the Calcarine sulcus and lateral to the sagittal

fissure showed that the animal could discriminate percepts induced by different groups (Figure 2.9) [29]. However, these results did not indicate whether the monkey had perceived more than one phosphene.

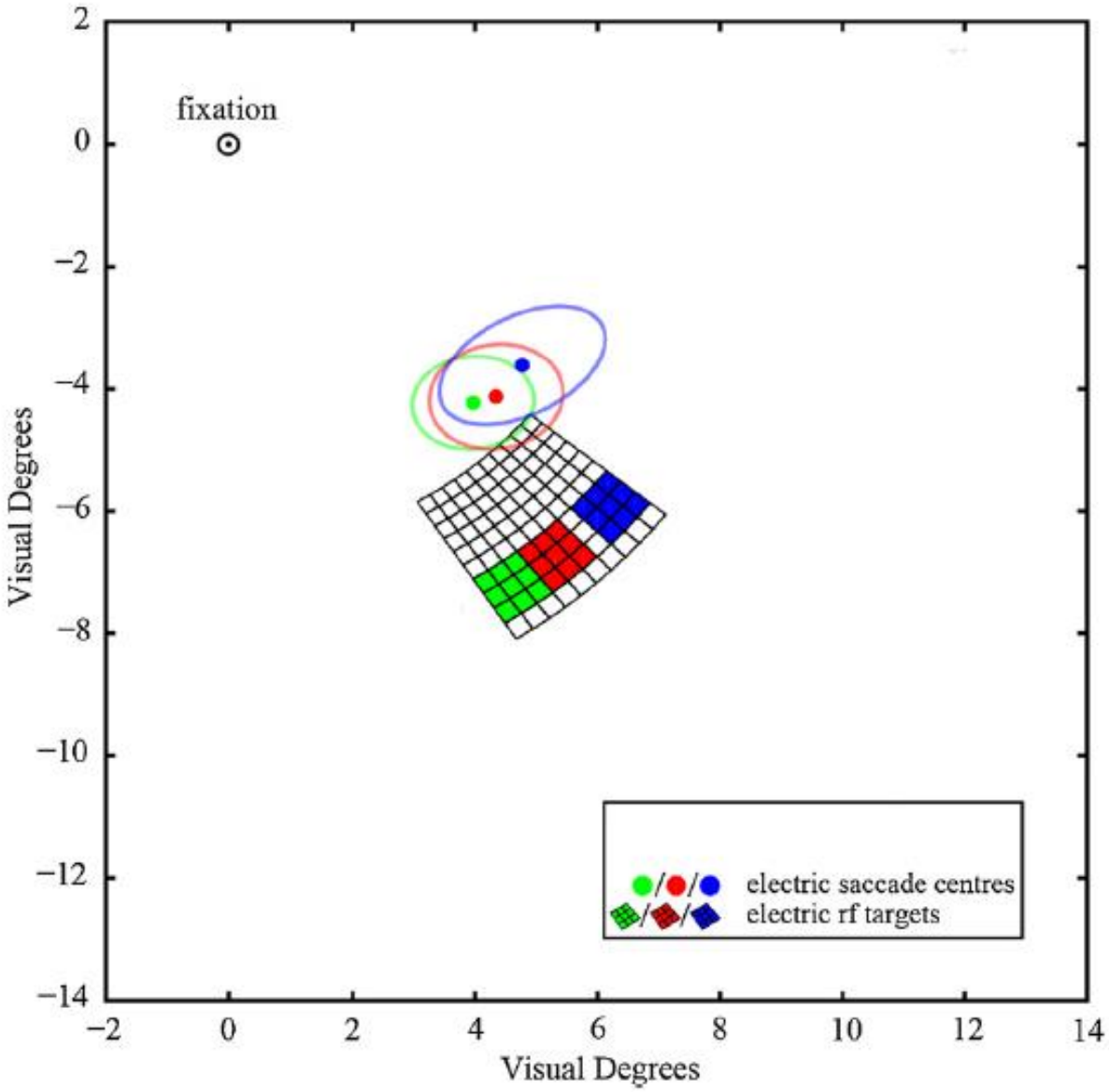

Figure 2.9 Saccade end points of three different percepts induced by electrical stimulation of three groups of nine contiguous electrodes as represented by three different colours. This shows that the monkey can discriminate between different stimulation groups. The distance between these groups of electrodes was 16±0.3 mm on the array and 1°±0.2° on the electrodes. Used with permission from [29].

The visuotopic (or retinotopic) map is a well-organized map of the visual (retinal) coordinate system onto points (neurons) in the visual cortex (Figure 2.10) [55]. To compare the visuotopic map with the phosphene map in macaque monkeys, the receptive fields of both Local Field Potential (LFP) and Multiunit Activity (MUA) signals for several electrodes were measured [28]. Then, applying electrical stimulation through the same electrodes, it was observed that the spatial locations of evoked phosphenes were similar to the spatial location of the receptive fields for the corresponding neurons but do not follow a conformal map [28]. Based on this observation and other experimental studies, it was concluded that the phosphene map is not very regular and only roughly follows the receptive field properties of the V1 visuotopic map [2, 10-12]. The relationship between the phosphene map and the V1 visuotopic map is thus somewhat unclear [28].

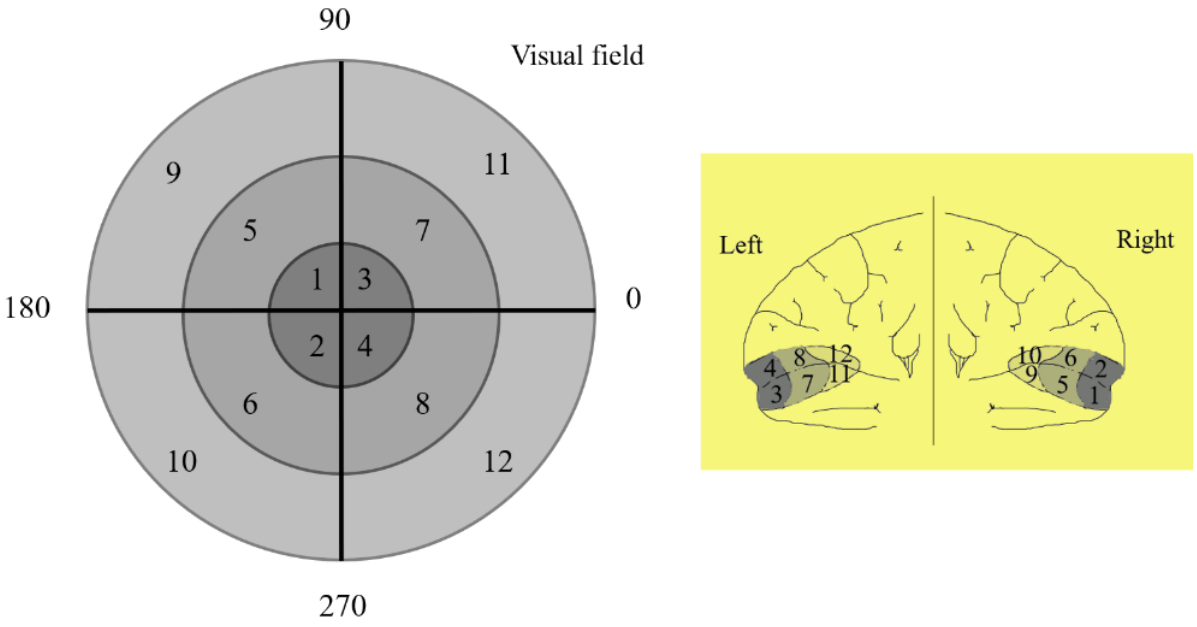

Figure 2.10 Visuotopic map of the primary visual cortex. Different locations in the visual field are mapped onto the activity of neurons in different regions of V1 as shown by numbers and gray colors.

2.1.3.4.2 Phosphene brightness

Electrical stimulation can modulate the perceived brightness of phosphenes. It generates phosphenes brighter than the background [2, 9-11]. It was reported by one subject that at least 12 brightness levels could be distinguished [42]. With surface macroelectrodes, increasing the current

initially yielded an increase in the brightness of the phosphene. With further increase in current, the size of the phosphenes expands [10, 42]. It is not known if brightness can change independently of the phosphene size [56]. The depth of the implanted electrodes also has a direct relationship with the brightness of the phosphenes. For intracortical stimulating electrodes, increasing current amplitude was reported to increase the brightness [9]. Increasing pulse duration or train length using either intracortical electrodes [9] or surface electrodes [10, 11] increases the brightness of evoked phosphene [9-11]. Increasing pulse frequency from 100 to 200 Hz increased the brightness of phosphenes [9, 10]. Unlike human, in monkeys, the phosphene brightness was reported to be 2.6%-10% (contrast), and most of the times darker than the background (Figure 2.11 a) [30]. Small changes were observed with variation in the current levels.

Brightness accommodates to repeated bouts of electrical stimulation for both surface and intracortical electrodes and for both blind and sighted subjects [9, 10, 42]. In other words, by repeating stimulation for periods of minutes, the phosphene brightness dropped gradually. Fifty repetitions of a pulse train of 125 ms with 0.1 ms pulse duration and frequency of 200 Hz led to a decrease in phosphene brightness of 80% (Figure 2.12) [9]. In this work, increasing pulse duration to 0.2 ms decreased the rate of change in the brightness accommodation, and increasing it to 0.4 or 0.8 ms resulted in a brightness decrease for the first 25 trials and relatively no change for the next trials. The effect of brightness accommodation should therefore be considered in the design of visual prostheses.

2.1.3.4.3 Phosphene size

The size of phosphenes ranges from that of a pin point to that of a 20 mm diameter coin (around 0.5-2° and less than 3° visual angle) at arm's length [9, 10]. It differs from subject to subject and from trial to trial. For rhesus macaque monkeys, the sizes of phosphenes were reported to be in the range of 9-26 min of arc in diameter (Figure 2.11 b) [30], which overlaps with values reported for phosphenes induced by stimulation of the human foveal representation [9, 11]. It was observed that the phosphenes produced by intracortical microelectrodes are smaller in size than phosphenes induced by surface electrodes [9]. When surface electrodes were used, increasing the current increased the size of the resulting phosphene [10, 11, 42]. However, when intracortical

microelectrode arrays were used, the effect of an increase in current amplitude on size depended on the location of electrode in the cortex [42].

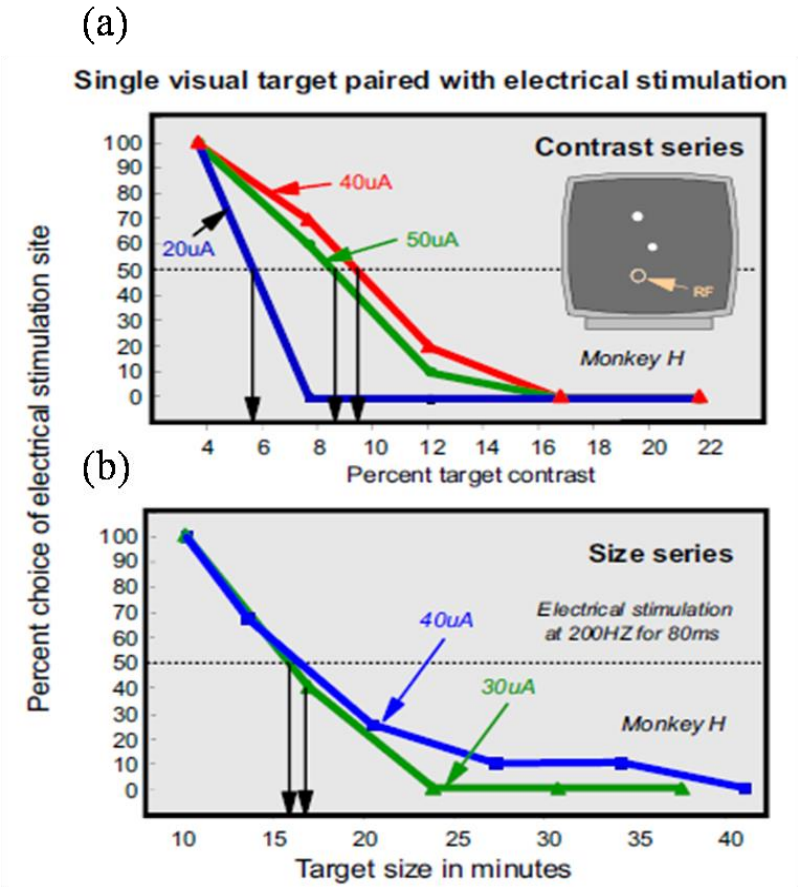

Figure 2.11 The (a) contrast and (b) size of phosphenes induced by electrical stimulation using a paired target task on a rhesus macaque monkey. The above figures show the percentage of the performing saccade to the location of the receptive field of the electrically stimulated neuron as a function of the contrast and size of visual stimulus for different current levels. The 50% crossover shows the equivalence in visual target and percept made by electrical stimulation. Used with permission from [30].

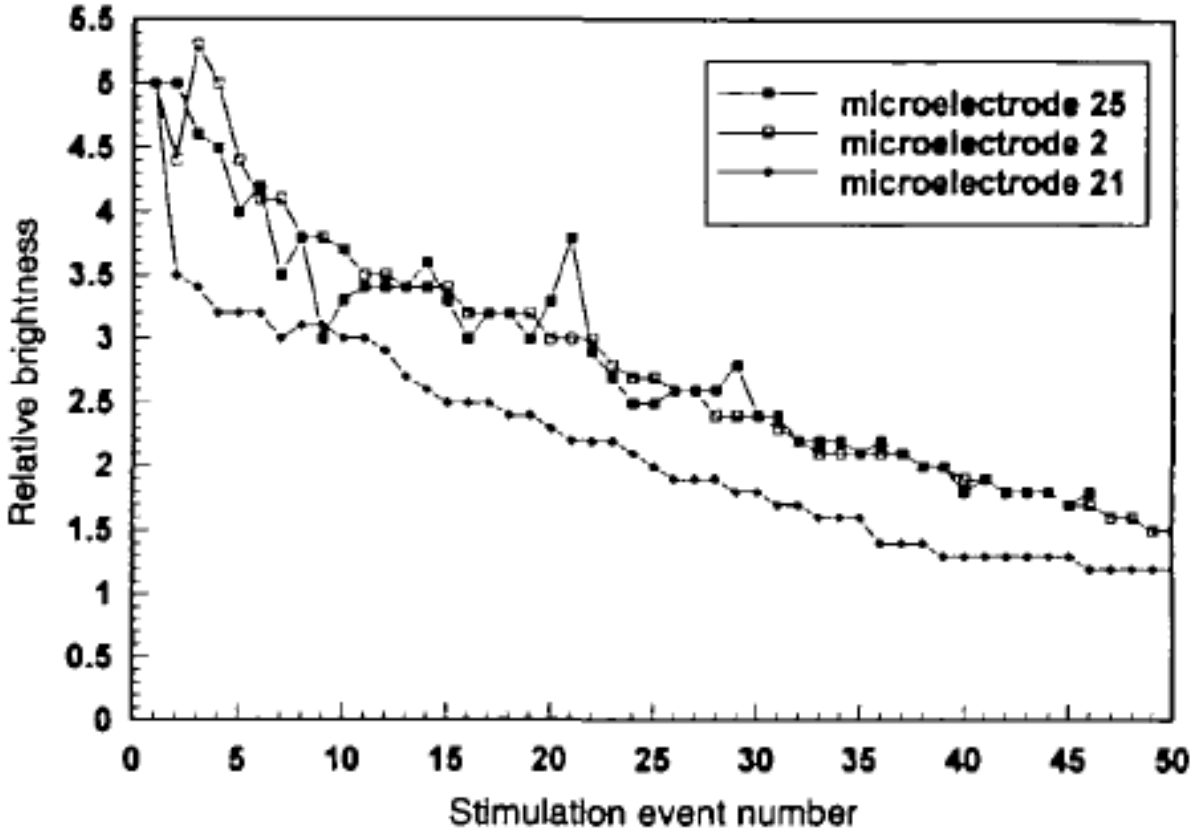

Figure 2.12 Reduction in relative phosphene brightness resulted from accommodation to stimulus repeated for 50 times as tested for three different intracortical electrodes implanted on a blind subject. Stimulation parameters are: pulse train 125 ms, pulse duration 0.1 ms, and frequency 200 Hz. Used with permission from [9].

Depending on the site of stimulation, increased current could lead to increased or decreased phosphene size, or in some cases a size increase followed by a decrease [9, 42]. Stimulation with intracortical electrodes showed that increasing the train length (200 ms-500 ms) increased the phosphene size [9].

For rhesus monkeys, determining phosphene characteristics, such as size, contrast, and colour, can be challenging. To address this problem, the two-target task has been proposed as a method to determine the contrast or size of the visual percept induced by electrical stimulation of V1 [30]. In this task, the animal is presented with two visual targets on the monitor, one with constant size and contrast, and the other with variable size or contrast. The monkey is trained to saccade to the one

with higher contrast or larger size. Electrical stimulation with fixed parameters is then delivered, and it is paired with a single visual target whose contrast or size changes systematically. In this way, the contrast or size of the phosphene can be determined by comparison to the visual target. Phosphene size estimated in this way can be seen in Figure 2.11 b.

The sizes of evoked phosphenes also depend on the eccentricity. By increasing the distance of the microstimulating site from the foveal representation of V1, the sizes of evoked phosphenes increase from fraction of a degree to around three degrees [9, 11]. Thus, given a fixed stimulation current, increasing the eccentricity increases the size of the phosphenes (Figure 2.13) [57]. The eccentricities of phosphenes also differ from subject to subject and trial to trial. For example, for Dobelle (2000) it was 20° [2], and for Brindley (1968) it was about 35° [11]. In the same eccentricities however, current stimulation parameters influence the size of phosphene. For example, at eccentricity 4° from the fovea, currents of 25 μA, 50 μA, and 100 μA affect 0.31°, 0.39°, and 0.58° of the visual field [57].

2.1.3.4.4 Phosphene colour

Previous attempts to control phosphene colour using electrical stimulation in humans have not been successful [10]. Specifically, manipulating the current pulse leads to changes in the colour of the phosphenes that cannot be disentangled from changes in luminance. In a subject who had been blind for 22 years and subsequently implanted with intracortical microelectrodes, for stimulation levels near the threshold (current less than 10 μA), phosphenes with distinct colours (yellow, red, blue) were induced, but increasing the current beyond 12.5 μA evoked white, greyish, or yellowish phosphenes [9]. The reason for this result can be activation of neurons in more cortical columns with different color preferences by high current stimulation well above the threshold (e.g. 80 μA). Surface electrodes in blind patients failed to produce coloured phosphenes [10, 11]. In the work of Dobelle in 2000 with cortical surface electrodes, the patient reported colourless phosphenes [2]. This was in contrast to sighted patients implanted with intracortical electrodes near the occipital pole, who reported blue and yellow phosphenes [27].

To determine the colour of phosphenes perceived by rhesus monkeys, a shifted background task was used [30]. In this task, the luminance or colour of the background was shifted before the presentation of the visual or electrical stimulation. The background colour and contrast then

changed up to the point that the monkey was unable to perceive a visual stimulus or phosphene percept. From this work it was concluded that the background colour and luminance are the same as those of the perceived phosphene. The results showed that electrical stimulation produces coloured phosphenes with relatively unsaturated colours in a macaque monkey with full block on CIE (International Commission on Illumination [58]) 0.304/0.206 [30].

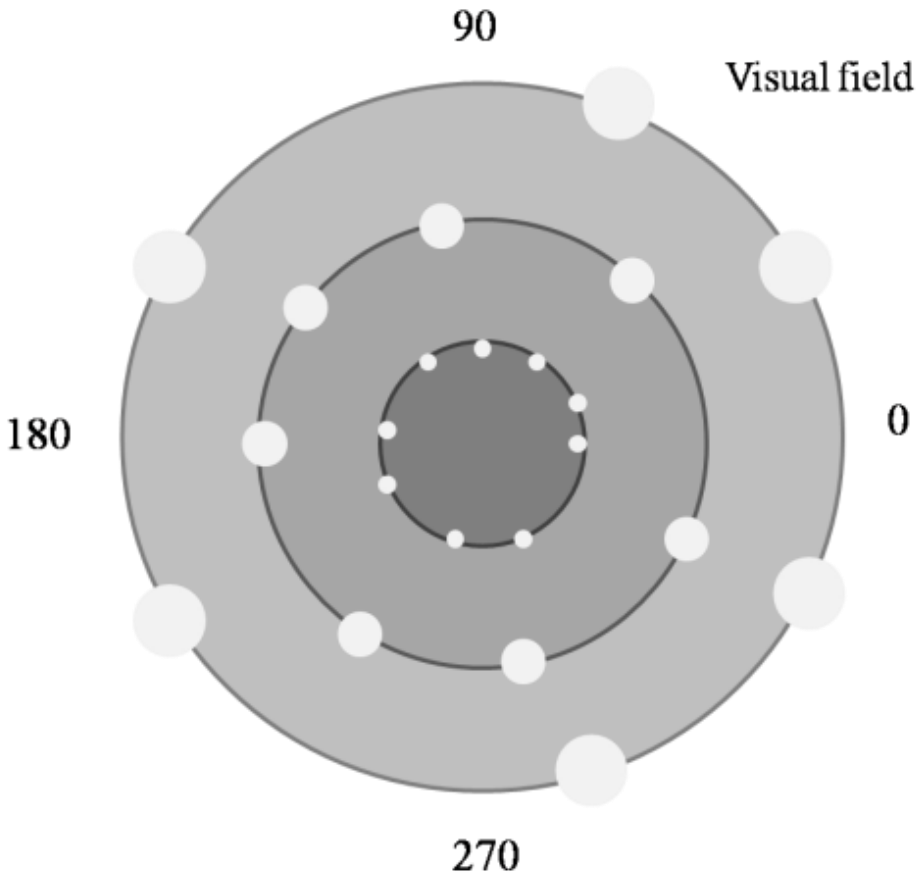

Figure 2.13 By increasing the eccentricity in the visual field and for stimulations with the same current levels, the sizes of phosphenes (white circles) increase. In other words, by increasing the distance of microstimulation site from foveal representation the size of phosphenes induced by the same current level will increase. Theoretically, if phosphenes follow the visuotopic map at the same distance from the centre of visual field, they should be approximately the same size [57].

2.1.3.4.5 Flicker

Depending on the experimental setting, phosphenes may appear to flicker [8, 11, 50] or not [9, 27]. The flicker fusion frequency at low stimulation frequencies is around 50 Hz [2], which is higher than what is found in normal vision (typically around 20Hz). The reported rate of flicker for both of Brindley's subjects was 10 s^{-1} [11, 50] regardless of stimulation parameters. It was reported by Dobelle (2000) that the flicker frequency was independent of pulse, repetition frequency, or any other physiological function such as cardiac pulse [2]. Using intracortical electrodes, static phosphenes (not flickering) were induced [9, 27].

2.1.3.5 Multiple Phosphenes

Depending on the depth of cortical stimulation, using implanted electrodes that are on the cortical surface [11] or intracortical [27], and depending on the distance between the electrodes, electrical stimulation from multiple electrodes can produce multiple phosphenes. Intracortical electrodes with ≥500 µm inter-electrodes distances can generate separate phosphenes, with a minimal interaction when a maximum of 30 µA current is applied [9, 27]. This 500 µm inter-electrodes distance is five times smaller than the distance (~3 mm) between surface electrodes used to evoke separate phosphenes [10, 11]. These reports show that intracortical electrodes have a much greater resolution in producing phosphene perception. Stimulating multiple electrodes can produce patterned percept but the interaction between stimulated currents can produce overlapped phosphenes and interfere with perception [9, 12].

Patterns of four phosphenes were generated with four electrodes but sometimes with complex interactions [10]. Two electrodes situated 4.4 mm apart were reported to produce two phosphenes in close proximity, with characteristics depending on stimulation parameters [9]. While each of those electrodes stimulated separately evoked phosphenes with different sizes and colours, stimulating them alternately with different inter-train-interval values ≥1 s resulted in a loss of the individual characteristics of the phosphenes. A reduction of the inter-train-interval when alternately stimulating those two electrodes rendered the two phosphenes more distinct, while maintaining the perceived distance between them [9].

Stimulation from some electrodes can produce a second phosphene that has a higher threshold [10]. These phosphenes can appear to have different colours and different sizes. Thus, two different

maps, one for low-threshold and one for high-threshold phosphenes, can be generated [11]. Using cortical surface electrodes, Dobelle (2000) reported that each electrode can create 1-4 closely spaced cluster of phosphenes, each up to the diameter of a pencil at arm's length [2]. By increasing the current of an intracortical electrode, the second closely spaced phosphene was described as 'fuzzy' [9]. In this work, stimulation with a single stimulation train, regardless of train length or multiple stimulation trains, with inter-train interval shorter than 25 ms, generated a static phosphene, while multiple stimulation trains with inter-train intervals longer than 25 ms produced two temporally separate phosphenes. In addition, when two or more phosphenes appeared simultaneously at different distances from the subject, their distances changed to make them appear at the same distance or in the same plane.

2.1.3.6 Computer Vision

In addition to training programs, using computer vision and image processing algorithms such as edge detection can help patients to improve shape and letter recognition gradually by extracting and converting specific image features into patterned stimulation [2]. Increasing the number of phosphenes would call for an additional preprocessing step to extract some image features prior to reconstruction of the image through the stimulation. The work of Dobelle (2000) was the only clinical study that used image processing algorithms on a cortically implanted subject [2]. Development of future cortical visual prostheses necessitates advanced algorithms for compression and transfer of particular features of an image into a specific area of the visual cortex.

2.1.3.7 Phosphenes move with eye movement

Phosphenes move proportionally with voluntary eye movements [2, 8-11]. When up to six phosphenes were simultaneously generated, they moved along with the eye movement [9]. This complicates generation of a consistent phosphene map. Therefore, eye tracking technology is required to ensure the stability of images during the eye movement. More detailed reviews on this topic can be found in Tehovnik et al. (2005) and Tehovnik et al. (2009) [57, 59].

2.1.3.8 Clinical Outcomes

The functional performance of a cortical implant must be verified quantitatively. This assessment should encompass the capacity of the cortical implant to create useful perception across different

tasks, such as motion perception, light perception, and obstacle avoidance [60, 61]. For example, in [12] the performance of the implant was tested by the ability of the subject to read Braille characters and conventional letters, while in [2] it was tested by the ability of the patient to recognize shapes using Landolt rings and Snellen charts. Additionally, the visual acuity of the implant recipient - achieved via head scanning - was estimated to be 20/1200. Since publication of [2], no further report of visual acuity in cortical visual prosthesis recipients has been published [37]. One of the main concerns in this area is the absence of standard methods and scoring systems to assess functional performance [62].

2.1.4 Major challenges and suggested solutions

There are challenges associated with different aspects of cortical visual prosthesis, such as surgical aspects, postoperative care, stability of the electrode–brain interface, seizure risks, chronic inflammation, and neurodegeneration as explained and discussed in [37]. However, in this review we focus on those challenges that exist in controlling phosphene characteristics by applying electrical stimulation and discuss the main difficulties facing image-to-electrical stimulation pattern transformation.

A phosphenated image is the downsampled grayscale version of the original image with different pixel count, density, size, brightness, and overlap [21, 63]. As discussed above, the goal of many cortical visual prostheses is to induce a meaningful percept made of phosphenes by applying electrical stimulation to the visual cortex. Most of the studies presented in the previous sections have focused on the experimental and/or clinical generation and characteristics of phosphenes as a function of changing stimulation parameters or the physical properties of the electrodes (such as their depth). Among these studies, there has been no report of systematic control over the location, brightness [6], colour, or size of the phosphenes. No study has been able to induce phosphenated perception by converting images into spatiotemporal electrical stimulation patterns in V1 region. A hypothetical (theoretical) topography for electrode positioning in V1 was presented in [64], and argued to be likely the generated percept made of phosphenes.

Using feature extraction algorithms and a blinking phosphene in a simulated prosthetic vision environment resulted in attention of the subject to the relevant parts of an image and thus, improvement in object avoidance [65]. One study using a psychophysical experiment with a

portable phosphene simulation device on a normally sighted human subject showed that 625 pixels were sufficient to support text reading and navigation [21]. However, one criticism of this work is that the 625 pixels provided to the subjects were still processed by the retina, LGN, and visual cortex, so that direct electrical stimulation of the cortex still might not be sufficient to produce useful visual percepts, even if 625 electrodes could be implanted and operated effectively [66]. In addition, these simulations were performed using a monitor masked by an opaque perforated film of varying density and pixel count to provide the likely percept experienced by a prosthesis recipient. However, these simulated studies were not experimentally validated using implanted microelectrodes. To date there have been no experimental demonstrations of meaningful visual perception using phosphenes generated with spatiotemporal microstimulation patterns [6].

Using spatiotemporal electrical stimulation to control phosphene characteristics and creating meaningful perception poses diverse challenges which can be classified into two major categories: 1) challenges related to generation and detection of phosphenes; and 2) challenges related to the quality of the induced percept. Solving these challenges requires an understanding of all aspects of visual prosthesis such as encoding different visual features into distinct neuronal population activity, transducing a desired population activity into microstimulation parameters, monitoring dynamic variation of visuotopic organization from the onset of blindness, selecting specific cortical areas for implantation of the visual prosthesis, and adaptively updating stimulation parameters based on recorded neural responses.

2.1.4.1 Challenges related to generation and detection of phosphenes

Neuroplasticity plays a key role in the detection and generation of phosphenes. Weak electrical microstimulation is not easily detectable without training, because the neural activity produced by microstimulation is unfamiliar to the brain. On the other hand, after the onset of blindness, neuroplasticity causes the visual cortex to begin to process other sensory inputs. The positive and negative effects of neuroplasticity are very important consideration for the development and operation of a cortical visual prosthesis.

2.1.4.1.1 Training to detect phosphenes

Microstimulation changes neural circuitry during training to support detection of new neuronal activity patterns. However, we don't know if after training those neuronal activity patterns change and associate with different percept. Thus, further clinical assessment is required to track the dynamic changes in perception as subjects are trained to detect microstimulation. In addition to this plasticity during training, each electrode site may require a separate training session that may take up to 4 weeks. Therefore, for future visual prosthesis applications with many electrodes, extensive training will likely be needed. Fortunately, such plasticity is long lasting, so that trained sites typically do not retraining, even many months after the initial training [44].

2.1.4.1.2 Neuroplasticity and changes in visuotopic map of V1 after onset of blindness

Understanding the cortical plasticity that follows the onset of blindness is also important for the success of cortical visual prostheses [3]. Some studies show little change in V1 organization after retinal damage, so that a phosphene can be perceived by electrical stimulation for a decade after the onset of blindness [12, 67]. Indeed, it is likely that V1 shows relatively little plasticity beyond the critical period during early development [68, 69]. Thus, when blindness starts after the period of normal development, such as in the case of AMD and RP, visuotopically organized visual cues should be able to be evoked using electrical stimulation, even decades after the onset of blindness [26]. Thus, for cases in which blindness occurs after the critical period of normal development, there remains the possibility of reconstructing normal visual activity based on knowledge of the distribution of current achieved by artificial brain stimulation and the encoding strategies used by the normal visual system. Absent this knowledge, training is unlikely to be sufficient for subjects to interpret artificially-induced neuronal activity patterns.

On the other hand, some studies show a significant change in the architecture and connectivity of V1 after retinal damage (sensory deprivation) resulting from preserved neuroplasticity in adults [70-76]. Following the onset of blindness, visual cortex areas that are normally involved in vision begin to process inputs from other sensory modalities (Figure 2.14) [77-80], such as somatosensation [78, 81, 82]. An interesting example of this cross-modality adaptation has been shown with the inactivation of the occipital cortex, either experimentally with Transcranial Magnetic Stimulation (TMS) in early and late blind subjects [83-85] or following a stroke [86]. In

either case, blind subjects are impaired in Braille reading following occipital inactivation, suggesting that this region has been co-opted for tactile processing.

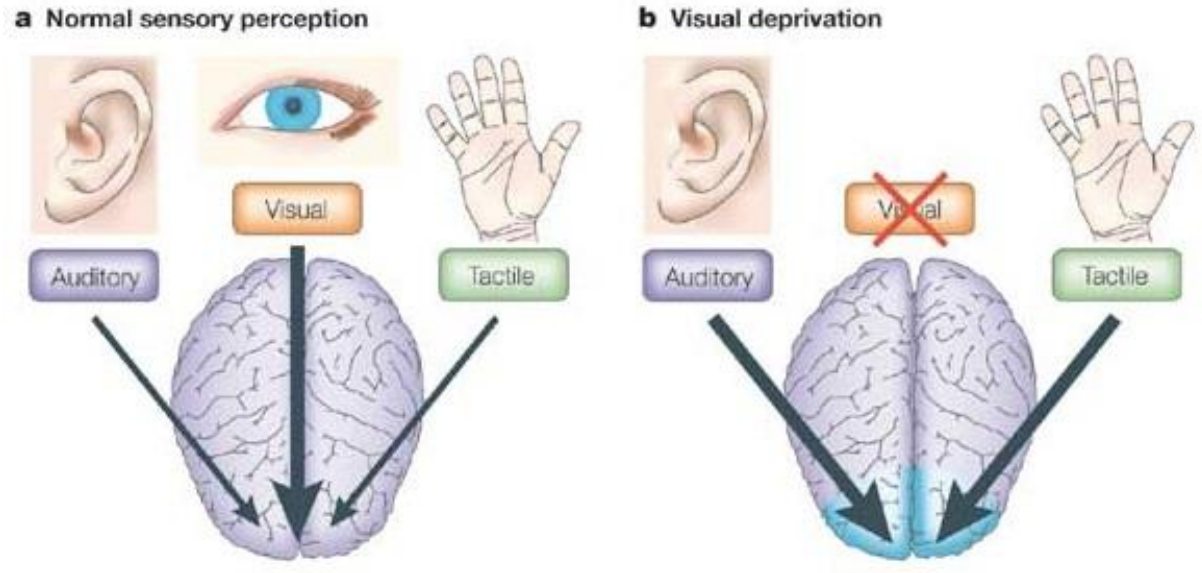

Figure 2.14 The effect of neuroplasticity in the visual cortex after onset of blindness (a) In normal sensory perception visual cortex processes mainly the visual information (b) after onset of blindness and visual deprivation since visual cortex is not employed for processing the visual information it will be adapted to process other modalities including auditory and tactile processing. Used with permission from [3].

The occipital cortex can also be employed for processing auditory information [87] and speech comprehension [88] in blind subjects. Further evidence for the neural reorganization of V1 after the onset of blindness is that sighted subjects can perceive both light and dark phosphenes and can discriminate 2000 levels of illumination, while dark phosphenes can very rarely be perceived by blind subjects, and they can only discriminate around 10 levels of phosphene brightness [9-11, 42]. This suggests that changes have occurred in the V1 after onset of blindness. It has been reported that coloured phosphenes are also less likely to be perceived by blind subjects than sighted subjects [2, 8, 10], and a patient who had been blind for 57 years from the age of 5 was unable to experience

phosphenes by stimulation of V1 [2]. Thus, the amount of information that can be transferred to V1 through microstimulation can be significantly reduced because of reorganization in V1. This is the negative effect of the neuroplasticity on visual prosthesis development. Although neuroplasticity can have a positive effect on the operation of the cortical visual prosthesis by helping the neuronal networks adapt to the new situation during the training period after implantation, it can also limit the degree of adaptation, in favour of processing other modalities [89, 90]. For example, when cross-modal plasticity changes the auditory cortex to restore auditory function, the auditory cortex can fail to respond to cochlear stimulation appropriately [91] or as mentioned above stimulation with TMS could impair accuracy of the Braille reading [84] that may occur for the case of intracortical stimulation too. Thus, there remains the possibility that a cortical visual prosthesis may not generate meaningful and interpretable vision, as a consequence of cross-modality adaptation. The extent and magnitude of neuroplastic changes are influenced by the cause, onset, and duration of blindness. As microstimulation changes the neural circuitry, coupling it with extensive training sessions may reverse these cross-modal effects. In addition, the dynamic changes in the neural responses of visual cortex after onset of blindness should be studied, so that microstimulation can be applied optimally.

2.1.4.2 Challenges related to controlling the phosphene characteristics

After generation and detection of phosphene, methods to control the characteristics of the induced percept are needed. For this purpose, it is required to have control over the location, brightness, size, colour, and duration of multiple phosphenes. Based on different studies on the phosphene location and map in V1, it is still unclear if the location of the induced phosphene depends only on the location of current stimulation site in the visual cortex or if it can depend on the stimulation parameters or physical properties of the electrodes (such as their depth) as well. For example, there is no study that deals with the relationship between current amplitude and the location of the induced phosphene. Variation in the current stimulation parameters may activate neurons that encode a different location in the visual space than the closest neurons to the electrode site. This may be the reason for this difference between the phosphene map and the visuotopic map. Furthermore, the visuotopic map of the visual cortex varies from subject to subject, depending on innate variability and visual experience. Therefore, the success of a visual cortical prosthesis depends on the ability to selectively stimulate groups of neurons that control the appropriate

phosphene characteristics, the different neuronal ensembles that encode those characteristics, together with knowledge of individual differences in visual cortex organization.

At the same time, it is difficult to fully deliver phosphene stimulation in humans, as the anterior and medial parts of V1 are located deep within the calcarine sulcus, leaving some parts of the visuotopic map largely inaccessible. To overcome this limit, stimulation of area V2 could be used to elicit phosphenes in the remaining parts of the visual field because it is more accessible and complements the stimulation of inaccessible areas in the V1. In addition, recently a patent was presented that developed a surface electrode array for implantation within the human V1 Calcarine fissure [36]. However, no clinical stimulation result has been reported. A high-density 3D pyramid-shaped microelectrode array was also developed that has the ability to be used in various intracortical areas [76].

To create a percept, multiple phosphenes at different locations are required to be induced. As reported in [9], when multiple phosphenes were generated they appeared to have equal distances from the subject. In addition, train length affected the simultaneous appearance of phosphenes organized in a vertical line. It was also reported that increasing current from multiple stimulating electrodes can produce more complex shapes than single phosphenes such as ‘I’ or ‘M’. Limited object recognition and mobility were also reported with only 21 phosphenes, using surface electrodes in one of the subjects [2]. However, systematic control over phosphene organization has not been accomplished yet.

The effects of electrode depth, current amplitude, eccentricity, and train length on phosphene size have been studied. However, the effects of frequency and pulse duration have not to our knowledge been studied. Moreover, there has been no study of the sizes of phosphenes perceived during simultaneous stimulation at multiple sites.

There are still many unanswered questions regarding the modulation of colour with electrical stimulation. Since the perception of colour is different from subject to subject, it is difficult to determine what a subject has perceived. In addition, changes in perceived colour depend on the visual experience of the subject, as well as the duration of blindness. The effects of electrode size and depth are not known completely. The effect of stimulation parameters such as pulse duration, amplitude, and frequency, and the influence of stimulation parameters in other simultaneously

stimulating electrodes and their interaction also require further study. In addition, the brightness accommodation, when multiple electrodes are stimulated and have overlap in their stimulating current, is not known. More effort is required to study the effect of stimulation of multiple electrodes on phosphene brightness.

As discussed above in section 2, pulse duration is affected by train length and amplitude. However, there are still unanswered questions about the phosphene appearance and cessation. How do electrode size and depth influence the duration of phosphenes? If the stimulus is repeated several times will the phosphene duration change? How do the frequency and duration of pulses influence the duration of the phosphene? If we stimulate with more than one electrode, is there any correlation between the durations of the phosphenes? Will there be any change in the duration of phosphenes when more than one electrode is stimulated? These are all open questions to be studied.

2.1.4.2.1 Encoding of visual features in neuronal population activities

To generate a spatiotemporal pattern of electrical stimulation corresponding to a given visual scene and to transfer relevant information to the neural tissue, we need to know how visual features are represented in neuronal responses in different locations of V1. This is a key challenge in designing a cortical visual prosthesis [3]. In normal sight, when a visual input is presented, a set of neurons becomes active in the visual cortex. The responses of these cells encode one or more features of the image, such as colour, contrast, or location in space. Since the perception of phosphenes is similar to spots of light, it follows that knowledge of neural encoding of spatial locations, size, brightness, and colour would provide key constraints for the necessary spatial and temporal pattern of activation required for the production of a specific phosphenated percept. For example, to systematically control the brightness, we should know how changes in brightness influence neuronal activity in the primary visual cortex. Then, based on this information, we can electrically stimulate the neurons with an appropriate spatiotemporal pattern. Therefore, one of the main challenges of constructing a visual prosthesis is to design a system that mimics the transfer function of the corresponding biological module from visual input (e.g. data coming from a camera or a photosensor array) to the spatiotemporal pattern of electrical stimulation at the location of the electrodes [92].

A theoretical framework for generating a spatiotemporal electrical stimulation pattern from an arbitrary image is the bioinspired retina-like encoder/stimulator [93]. It is based on mimicking retinal function by considering how knowledge of the visual input is encoded into the spike trains of retinal cells. This framework performs spatiotemporal filtering to extract salient features of the visual scene and transforms them into electrical stimulation patterns [93]. To generate the electrical stimulation pattern, each electrode is associated with a pixel. The image input is transformed through a set of parameterized filters, and the ensemble of them is transformed into an output map called the 'information figure'. The filters are designed based on the distribution of photoreceptors in the human retina, so that in the central area, there is a higher density of pixels with smaller receptive field sizes than in the periphery. Each channel of an electrode then has a gain factor. The information figure array is reduced to the resolution of the electrode matrix, called an 'activity matrix', with the option to specify receptive field shapes and sizes. Finally, components of the activity matrix are converted into neuromorphic pulse-coded signals generated based on the function of retinal ganglion cells (Figure 2.15) [92].

The retina-like encoder has several problems. First, although V1 in blind people shows some plasticity, particularly in adapting to inputs from other sensory modalities, this level of plasticity is likely not sufficient [68] to learn a new code relating visual input to neuronal responses [26], and training sessions are required in order to be adapted. Second, visuotopic organization is different from subject to subject, depending on their visual experience. Thus, the same stimulation pattern cannot be applied for everyone [26]. Third, the retina-like encoder is designed based on retinal functions, without considering the architecture of the LGN, optic nerves, and V1. Fourth, the retina-like encoder can generate different percepts in different V1 locations or depths, and therefore it needs to be flexible depending on the location in the visual cortex. Fifth, trial-to-trial variability in neural responses [94] and the effects of neural adaptation [95] are ignored. A stimulation generator requires adaptive learning of stimulus-response patterns regarding response variability, while a retina-like encoder has a fixed encoding rule and does not generate an adaptive stimulation pattern. Sixth, the phosphene map only roughly follows the visuotopic organization of V1, and stimulating based on the visuotopic map is not enough to create the corresponding percept [28]. Seventh, the phosphene threshold changes over time [29], and accommodation in phosphene brightness results in a reduction of brightness in response to bouts of current stimulation. Eighth, because of

progression of disease and the effect of the plasticity and learning, new associations can be formed between perceived visual patterns and the electrical stimulation patterns, and thus modification in the stimulation parameters for each electrode would be required [92]. Ninth, limiting the receptive fields to a small region of the visual field covered by the implanted electrodes in the lateral occipital cortex limits the coverage area of the visual field [7]. Thus, an array with a higher number of electrodes is needed to cover a larger cortical area. Indeed, any encoder with a fixed rule for the generation of the stimulation pattern from the visual input will likely be unable to induce a phosphenated percept. Thus, adaptive algorithms are required to update the stimulation parameters and spatiotemporal pattern of activity for different situations.

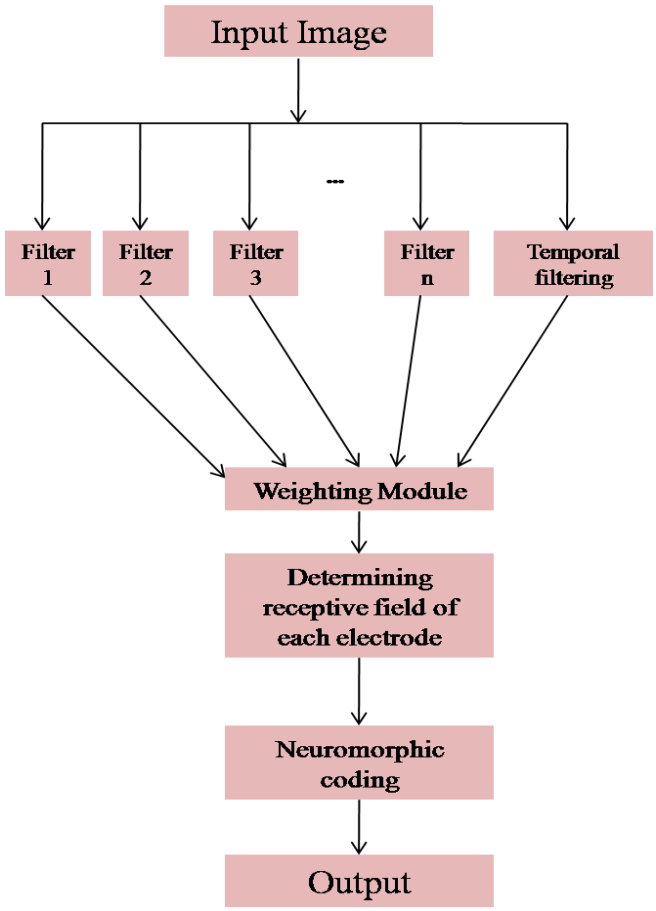

Figure 2.15 Function of a retina-like encoder to transform the visual information into a spatiotemporal pattern of electrical stimulation [93, 96].

2.1.4.2.2 Selective activation of neuronal population using microstimulation

Electrical microstimulation at different locations and depths and with different parameters perturbs the activity of subsets of neurons with high precision. To interpret the experimental results of microstimulation, we must understand the spatial and temporal distribution of neural activity resulting from microstimulation. Microstimulation can activate neurons directly or indirectly. Direct activation arises from changes in membrane potential when current flows from the electrode tips. This change in membrane potential depends on the distance between the electrode tip and the neuron as well as on the time derivative of stimulation intensity [97]. In direct activation, the stimulus depolarizes the neurons and make them spike [98, 99]. Microstimulation can also directly influence synaptic release in different ways. Microstimulation produces widespread subthreshold activity across the brain [100, 101] via synaptic transmission and therefore, indirectly affects neuronal activity through activation of many connected postsynaptic neurons [48]. Direct activation of a single action potential can produce many spikes indirectly that extend broadly in space and time. The behavioural consequences of microstimulation depend on the spread of indirect activity produced by direct activation of neurons. However, it can be said that any specific percept is produced by directly activated neurons [48].

In early studies it was considered that current stimulation activates neurons (soma and axons) directly in a sphere around the electrode tip such that an increase in the stimulating current increases the radius of the effective activation sphere. Excitation of neurons then depends on the effective activation sphere and the excitability of the neurons. Excitability of neurons varies between 100 and 4000 µA/mm^2 using 0.2 ms duration of cathodal stimulating pulse and for estimation of current spread in V1 usually 1000 µA/mm^2 is assumed [57]. Stimulation activates the initial segment of a neuron that has the lowest current threshold at the cell body [22]. The effective current spread is expressed as

$$r = \left(\frac{I}{K}\right)^{0.5} \qquad (2.1)$$

where I is current level [µA], r is the distance between the neuron and the electrode tip [mm], and K is the excitability constant [µA/mm^2] [102-106]. An increase in the excitability constant leads to a decrease in the conduction velocity of an axonal element [107].

Despite the conclusion in early studies that whole neurons in a sphere around the electrode tip (within 80-90 µm) are activated [22, 103, 108-110] with an amplitude of 10 µA, calcium imaging suggested that low-current microstimulation of 10 µA or lower activates populations of neurons around the electrodes sparsely (tens to hundreds) and sometimes activates neurons millimetres away [99]. Therefore, a much smaller volume of neural processes was activated by electrical stimulation compared to what was proposed earlier. The reason for this conclusion in early studies was the effect of stimulation current on the recording electrode in nearby sites and sampling of small number of neurons by a single electrode [99]. The observations indicated that increasing current instead of increasing the radius of the sphere of activated neurons fills in a large sphere of activated neurons, suggesting that a larger volume of neural processes (e.g. axons) around the tip are activated. Moving the electrode position by 15 µm yielded a different set of activated neurons (including common cells) and moving the position of electrode by 30 µm almost completely changed the pattern of activated cells. Thus, based on these results it is impossible to activate neurons in a restricted volume. By blocking synaptic transmission (to prevent indirect activation) and using calcium imaging it was shown that most of the directly activated neurons are located in the immediate vicinity of the stimulating electrodes (at a distance of hundreds of microns from the electrode tip), and those neurons that were activated directly millimetres away from the electrode tip were activated through direct activation of their axons passing in the vicinity of the electrode tip (tens of microns) [99]. Thus, the effect of microstimulation is dominated by activation of localized neurons immediately around the stimulating electrode tip. Similarly, microstimulation in middle temporal visual cortical area (MT) does not affect neurons that are located 1 mm away from the stimulation site [111]. It was experimentally shown that moving the electrode a few hundred microns to a location with a different direction preference had a different effect on direction discrimination [47, 112]. Functional Magnetic Resonance Imaging (fMRI) studies showed that microstimulation in macaque V1 can activate neurons indirectly in other functionally distant areas connected to the stimulated region including extrastriate visual areas [110]. Indirect effects can increase or suppress activity in distant downstream sites, depending on the number and frequency of stimulation pulses [113]. After the stimulation pulse immediately a short excitatory response occurs that is followed by a long-lasting inhibition.

This current spread beyond the electrodes perimeter that increase the activation area and activate indiscriminately neurons that encode different properties of the visual scene is one of the main reasons for underperformance of the visual prosthesis [114]. According to the above results, one of the challenges in selectively activating a neuronal population is the axons from distant neurons that pass near cell bodies that are the target of direct stimulation [115, 116]. Thus, microstimulation activates those axons extensively directly, while activating cell bodies through indirect activation. Thus, precise spatial control is difficult to achieve and it is important to study the contribution of different neural elements and indirect effects on the spatiotemporal spread of neural activity. By near-threshold single pulse stimulation in anaesthetized rat somatosensory cortex, the spatiotemporal extent of indirect activation of neurons was determined to be 1350 μm of horizontal spread; neural effects consisted of a sequence of fast excitatory response followed by an inhibitory response [116]. In this experiment, stimulation with frequencies of 20 and 40 Hz produced repetitive excitatory responses that persisted against a continuous inhibitory background, while stimulation with 5 and 10 Hz produced a complex interaction of inhibitory responses. In addition, stimulation with intensities of 1-4 μA with 0.1 ms pulses did not elicit visible responses, while higher intensities increased a fraction of responses and elicited excitatory and/or inhibitory responses.

Since the activation of a single neuron can change the activity of large networks [117, 118], it is important to have precise control over the activation of neural pools by microstimulation. However, such fine control is extremely difficult to achieve, given the abovementioned challenges of understanding the responses of neurons to electrical stimulation and controlling the spatial extent of stimulation. To address these challenges, some studies have used computer modeling to estimate how microstimulation activates neurons. Modeling of the electric potential field generated by stimulation, the response of a neuron to the field, and optimal electrode configuration for selective activation of neuronal pools near the stimulating electrode tip are reviewed in [119]. To identify spike initiation sites, a model was developed based on the densities of high-threshold sodium channels Nav1.2 in dendrites and soma and low-threshold sodium channels Nav1.6 in axons [120]. It was shown that axon initial segments, Ranvier nodes, and also thin axons and dendrites close to the electrodes are the most excitable sites for spike initiation. The cathodic excitation threshold of thin axons/dendrites depends on fibre diameter, distance from the electrode tip, and amplitude and

width of pulses. The results showed that the spike initiation site for dendrites for low current stimulation should be close to the electrode. A two-stage volume conductor model studied how cellular composition of tissue affects the electrical stimulation [121]. A modeling study showed that in somatosensory cortex the activation pattern of interneurons was dense around the electrodes, while in pyramidal cells the activation pattern was sparse near the electrode, extending up to several millimetres [122]. Compartmental neuron models of human motor cortex showed that anodal stimulation excites neuronal elements perpendicular to the surface of electrodes, while cathodal stimulation excites neuronal elements parallel to the surface of electrodes, and bipolar stimulation excites neuronal elements parallel to the dipole axis [123]. For a selectively targeted neuronal population, using cable modeling of mammalian motoneurons showed that monophasic cathodal or anodic first cathodic second asymmetric biphasic stimulation, selected fibres over cells, while anodal or cathodic first anodic second asymmetric biphasic stimulation selected cells over fibres [124]. However, stimulus with a symmetric balance of charge, i.e. the shape of cathode pulse is the same as the shape of anode pulse, was unselective and caused sparse and diffuse activation of neurons [99, 116]. Experimental results also showed that asymmetrical stimulation resulted in more spatially focused and controlled cortical activation than symmetric current pulses [125] but with higher current threshold than symmetric stimulation [126]. Methods proposed to increase the effective stimulation resolution by using local return electrode surrounding the stimulating electrode [127-131]. However, this solution can limit the penetration depth of the electric field and increase the phosphene threshold [132]. This issue could be overcome with a quasi-monopolar strategy [128, 130]. It was shown that electrodes with small diameters (9-15μm) can be used to activate individual ganglion cells [133, 134], and when multiple neurons were activated, current steering methods could be applied to target specific neuron preferentially [133].

Electrical stimulation usually consists of trains of constant current pulses delivered through extracellular electrodes [48]. However, with conventional pulsatile stimulation, activating specific neuronal elements with different activation thresholds may not be possible. Therefore, in a few studies the effects of other shapes of stimulation waveforms were investigated. Sinusoidal stimulation at specific frequencies was shown to activate certain types of retinal cells: at 5 Hz photoreceptor cells, at 25 Hz bipolar cells, and at 100 Hz ganglion cells were activated [115]. Low frequency stimulation ($\leq$ 25 Hz) did not activate axons nearby to the electrodes but produced

responses in ganglion cells throughout the synaptical transmission. In this work, sinusoidal stimulation of 10 Hz or 25 Hz elicited strong responses when the electrode was located near the soma, but produced no spike when it was located near distal axons, even at the highest amplitude. However, stimulation with 100 Hz frequency elicited strong responses when electrodes were located both near the soma or distal axons. Higher frequency sinusoidal stimulations required lower threshold compared to low frequency sinusoidal stimulation to elicit responses. Using pharmacological blockers, it was shown that response of neurons to 10 Hz, 25 Hz, and 100 Hz stimulation were affected through synaptic activity, direct and synaptic activation, and direct activation respectively [115]. In this way, it may be possible to control the spatial pattern of neural activity, to target individual classes of neurons, or even to replicate normal signalling. Using computer simulations it was shown that for all non-rectangular stimulation waveforms, the chronaxie time was longer than rectangular stimulation and linear decrease, exponential decrease, and Gaussian waveforms were the most efficient waveforms in maximizing charge injection capacity and minimizing the threshold for neural activation [135]. The optimal stimulation current waveform of excitable neural tissue to prevent tissue damage was determined using a computer simulation based on the Least-Action Principle [136]. In this work, it was shown that long stimulation pulses are more sensitive to the shape of the pulse, and a rectangular pulse is optimal for short stimulation pulses.

Microstimulation can also change plasticity in the brain. Using spike-triggered stimulation, plastic changes in rat and monkey sensorimotor cortex were induced [137, 138]. These changes were inferred using functional connectivity statistical measures, which depended on the latency between trigger spike and stimulation [137] or using mutual information measure [138].

In the future prosthesis a one-to-one electrode-neuron interface can provide the highest possible stimulation resolution with making any spatiotemporal pattern. It can be possible with penetrating electrodes having multiple stimulation sites and also using more complex stimulation paradigms to evoke specific group of cells [139]. For example, it was shown that using sinusoidal waves with different phases can activate ON and OFF retinal ganglion cells preferentially [140].

From the above review it can be concluded that current stimulation even at very low levels (1.9 μA according to [9]) can activate several dozen neurons, each of which encodes a different stimulus

feature and carries different information. Therefore, having control over the spatiotemporal pattern of activity induced by electrical stimulation of visual cortex, and presumably, reproducing neuronal population responses that match the responses evoked by a specific visual input, are important requirements for developing a cortical prosthesis. In addition, we should note that since V1 neurons naturally encode contrast, orientation, depth, and spatial frequency, restricting the stimulation strategy to a phosphenated bit-mapped images can limit the capability of a cortical visual prosthesis to induce meaningful percepts [6].

2.1.4.3 An initial experimental step: Learning population codes in the visual cortex of sighted animals and spatial stimulation

As discussed earlier [47] when animals are trained to detect microstimulation, neuronal circuitry changes so facilitate task performance. However, we still do not know what they perceive after training [48]. One way to solve this problem is to assume that we can reconstruct the natural pattern of activity induced by visual stimuli. In this way training is not required, because the spatiotemporal pattern of neuronal activity is known to the subject and we can recreate it. For this purpose, it required is to know the population coding of natural stimuli and to find a way to reconstruct the natural pattern of activity in the brain by targeting population of neurons using electrode arrays. So, sighted animal models should be used to initially circumvent the complexities resulting from changes in the organization of V1 after the onset of blindness and the challenges associated with human experiments.

Figure 2.16 shows an example framework for this study. A macaque monkey is implanted with microelectrode arrays in area V1, and after recovery from surgery it is ready to start experimental sessions. The monkey is trained to fixate on a point in the visual field and to receive a phosphenated-like stimulus (photic stimulus) made of multiple spots during the period of fixation. Different phosphenated stimuli should be presented and the resulting extracellular neural responses (made of spikes and LFP) would be recorded. A supervised learning algorithm such as a Deep Convolutional Neural Network is used as an encoder that learns the neuronal representation of different stimulus-response relations. Based on the learned encoding rule and according to the knowledge of targeting populations of neurons with current microstimulation in the primary visual cortex, a set of electrical stimulation spatial patterns are generated in order to generate a percept

corresponding to the induced population activity. Using psychophysical tests, the trained monkey provides information about what is perceived from the electrical stimulation. The difference between the expected and observed percepts from the psychophysical tests is then used to update learning rules of the encoder.

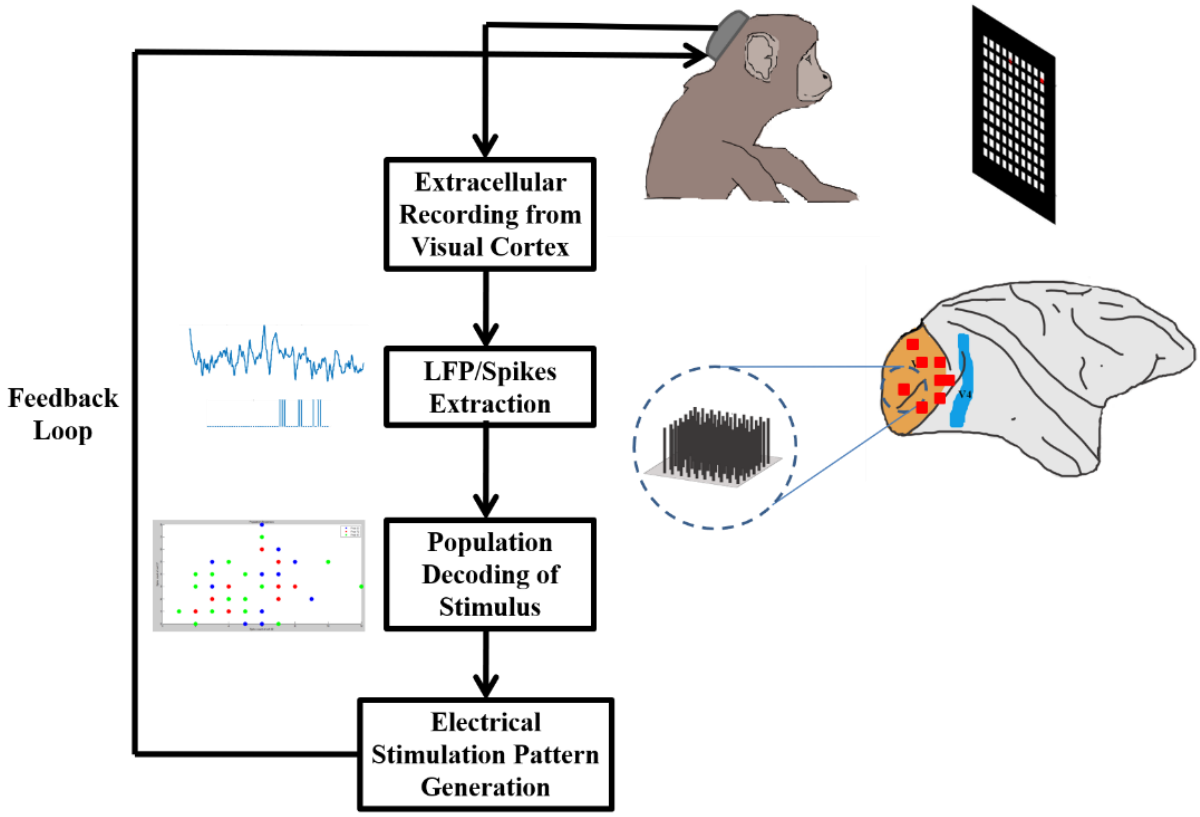

Figure 2.16 The basic framework for studying the adaptive generation of phosphenated image on sighted animals. In this framework a monkey that is implanted with intracortical microelectrode arrays receives visual stimuli in different phosphene-shaped patterns and the resulting large-scale activity of neurons is recorded. The responses are then decoded to generate the required pattern of electrical activity to produce the same percept as the visual stimulus.

2.1.4.4 Alternative solution: Stimulation of extrastriate cortical areas

To date, all existing visual prosthetic devices and prototypes have targeted the early visual system (the retina, LGN, or V1). The logic of targeting these areas is based on the apparent simplicity of encoding pixels as phosphenes in a visuotopic map and slightly lower current threshold in early visual system [14]. However, given the challenges summarized above, one might consider alternative possibilities. The human visual cortex contains many discrete regions beyond V1, each of which represents the visual input and can contribute to visual perception. Stimulation in these *extrastriate* cortical areas could serve as an alternative or complementary strategy to the V1 prosthetic, as typically conceived.

Although the properties of the extrastriate cortex have been reviewed elsewhere [141], we mention a few of its basic properties here. First, areas in the extrastriate cortex exhibit functional specialization; broadly speaking, each area is located along one of two pathways, dedicated to the encoding of either motion (the dorsal brain pathway) or shape (the ventral brain pathway) [142]. Second, individual neurons in these areas tend to be selective for complex stimulus patterns, with nearby neurons preferring similar stimuli. We consider here some of the advantages afforded by these properties.

1) *Selectivity*. Extrastriate neurons exhibit invariant selectivity similar to that of human visual perception. For example, within limits, our ability to recognize a face is unaffected by variations in distance, retinal position, rotation, and lighting, all of which dramatically affect the composition of the pixels in the input image. The same is true for recognizing other objects, and this perceptual invariance is even greater for interpreting motion signals during navigation. Indeed, it is now recognized that a fundamental function of high-level visual processing is to discard details about local features, such as pixels, in favour of a sparse representation of more complex image features [143]. Thus, it might not be necessary or even desirable to recreate the precise spatial arrangement of image pixels in the input image.

The fact that complex image features are represented locally in the extrastriate cortex provides a possible solution to the aforementioned problems of concurrent electrode activation. In essence, a feature that activates a large, distributed population of V1 neurons might activate a small, local cluster of neurons in extrastriate cortex [144]. In that case, the same visual percept could be

generated with far fewer electrodes. Indeed, previous work in the extrastriate cortex has shown that stimulation of even a single column is sufficient to yield complex stimulus percepts [145]. This could be quite important, as the number of V1 electrodes necessary to restore even modest vision is enormous: current estimates are that the restoration of 20/200 vision would require 15,000 electrodes in a 7 mm^2 area, and it is unclear whether such a transducer could be operated safely and effectively [5]. For full 20/20 vision, the number of necessary electrodes is estimated at 1.44 million [5].

2) *Plasticity*. Studies of perceptual learning in adult animals have shown greater plasticity in the extrastriate cortex than in V1 [146]. This suggests that the brain would more readily learn to interpret artificial stimulation that targeted higher-level cortical areas.

3) *Specialization*. Whereas the retina and area V1 are necessarily involved in representing all possible visual stimuli, extrastriate areas are functionally specialized. Consequently, an extrastriate prosthetic could be optimized according to the needs of the recipient: Patients with macular degeneration could receive ventral-stream devices, which would restore foveal vision for object recognition. Patients with peripheral vision loss due to glaucoma would receive dorsal-stream devices, which would restore peripheral vision for navigation. And those with traumatic injury or complete structural enucleation would receive both. Thus, an extrastriate prosthetic could be minimally invasive.

4) *Multimodality*. Neurons in the retina and V1 respond almost exclusively to visual signals. Consequently, in a blind patient, these neurons could only be activated with artificial stimulation, which would complicate the development and refinement of an encoder. In contrast, neurons in extrastriate areas receive weak but reliable non-visual inputs that have stimulus selectivity similar to that of the visual inputs. Thus, for example, extrastriate neurons in the dorsal stream respond to visual motion patterns but also to congruent vestibular inputs [147], so that neuronal selectivity could be estimated coarsely, but objectively, in a blind patient, by simply asking him to make head movements. However, the non-visual representations found in extrastriate cortex also carry the downside that the electrical stimulation would presumably cause some non-visual sensation.

Although such effects are likely quite small [148], they might complicate the transduction of sensory signals.

Of course, there is a cost associated with this approach, in the form of increased complexity of visual encoding. In general, there appears to be a trade-off between the complexity of encoding and the complexity of stimulating in the brain. While an encoding system based on pixels is simple, it requires stimulating in complex and dense patterns, which complicates the transduction process. On the other hand, an encoding system based on the properties of the extrastriate cortex is more complex [149], but would likely simplify the transduction of the signals by reducing the number of electrodes necessary to create a meaningful percept. An analogous approach in the motor system has recently shown great promise, by using cortical areas outside of the primary motor cortex to decode movement goals [150].

2.1.5 Conclusion

Although the idea of a phosphenated image generated with a cortical visual prosthesis has an appealing simplicity, it has not yet been achieved. Phosphene characteristics are affected by different stimulation parameters, such as the frequency of stimulation, pulse duration, pulse amplitude, etc. However, the perception of a phosphenated image requires activation of multiple phosphenes with specific spatial topography and brightness. This requires activation of different neuronal ensembles with a predefined pattern. Reaching this goal requires a deeper understanding of various issues including the encoding of location, size, brightness, and colour of multiple spots of light in populations of V1 neurons; electrical current spread in V1 neural circuits at different spatial and temporal scales; and dynamic changes of the visuotopic map after the onset of the blindness and sensory deprivation in the visual system. The advent of machine learning techniques might provide a means of optimizing the transformation of visual images into stimulation patterns. They may be used to create a phosphene map that represents not only phosphene topographical features but also other non-topographical attributes such as size, brightness, and colour of phosphenes. Stimulation of higher level (extrastriate) cortical areas is an alternative scheme for cortical visual prosthesis that can be considered in future research.

Acknowledgements

The authors acknowledge the financial support from the Natural Sciences and Engineering Research Council of Canada (NSERC) and the Canada Research Chairs in Smart Medical Devices.

2.2 Opinion on a recently published paper

In this section we present our opinion about a recently published paper [151] in May 2020 in the field of cortical visual prosthesis.

This is the first report presenting a meaningful relationship between the spatiotemporal microstimulation pattern and induced visual percept. Shape generation via applying a pre-designed stimulation pattern was a challenge for years. So, it is a significant scientific achievement. Although still preliminary, it will pave the road for future clinical applications to provide sight for the blind individuals. Future efforts can focus on transforming more complex shapes and even videos into dynamic and real time stimulation patterns. Needless to say that to test the generalizability of their findings, in the future works, larger population of patients should be used. This will confirm the scalability and reliability of their technique.

Although this is a great leap in the development of visual cortical prosthesis, the neural mechanisms underlying their findings are not explained well in the paper. We know that V1 has a clear retinotopic map and the position of the receptive field is correlated with the induced phosphene position. In line with that, they reported that a stimulation pattern following the "z" shape in the visual cortex generates a visual percept with the same shape. However, a single microstimulation pulse can activate neurons in an uncontrolled manner. These neurons encode different visual features. In addition, microstimulation can significantly affect the subthreshold activity which carries visual information. It should be clarified that how perturbing neurons and subthreshold activity have produced this level of similarity in the percept.

CHAPTER 3 METHODOLOGY

In this chapter, we describe the methodology and experimental procedures used in this thesis.

3.1 Electrophysiological recordings

We used recorded data from two adult rhesus macaque monkeys. A standard sterile surgical procedure was performed under general anesthesia to implant a headpost (Hybex Innovations, Montreal, Canada) and a 10×10 Utah Microelectrode Array (Utah array; Blackrock Microsystems) with 1 mm electrodes and 400 µm inter-electrode spacing into the dorsal V4 of macaque monkeys. After recovery, they were familiarized with the laboratory environment and the behavioral task.

The wideband extracellular signals were recorded simultaneously from the arrays using a standard data acquisition system with sampling rate of 10 kHz. LFPs and MUA were extracted offline in MATLAB (The MathWorks, Natick, USA) using fourth-order two-pass Butterworth filter. MUA was extracted by high-pass filtering the wideband signals and thresholding the results. LFPs were extracted by low-pass filtering the raw wideband signals and down-sampling the results.

3.2 Experimental paradigm

Visual stimuli were back-projected at a 78 cm viewing distance onto a semi-transparent screen, by a cathode ray tube video projector, with refresh frequency 75 Hz. The screen covered 80×50° of visual angle. All visual stimuli were white square probes with 2° width and luminance of 22.5 cd m^{-2} presented on a dark background with less than 0.01 cd m^{-2} luminance. Each probe was chosen among 100 locations on a 10×10 grid, with 4° center-to-center distance from each probe to its neighbours in both vertical and horizontal directions.

In each trial, the monkey fixed its gaze on a small red dot of 0.5° diameter on the top right of the grid. After 500 ms of fixation, a probe stimulus was flashed at a randomly chosen location on the grid for 25 ms separated by a 500 ms blank screen. After a variable delay (500-1000 ms), the fixation point jumped to a new position at the top middle of the grid and the monkey was required to make a visually guided saccade to the new fixation point and fixate there for another 500 ms. Another probe stimulus was then flashed for 25 ms, and the monkey was required to maintain its

fixation for another 500-1000 ms delay. Each successful trial ended with a liquid reward to the monkey. If the monkey could not maintain its gaze within 2.5° of the fixation point, the trial was aborted. In each session, each probe location on the grid was repeated at least 10-15 trials for each fixation point in a pseudorandom order. For each monkey, at least 10-20 sessions were performed. The data were recorded on non-consecutive days.

3.3 Data analysis

All of the analyses were performed in Python 3.6.

3.3.1 LFP and MUA responses

In each trial, LFP and MUA data were evaluated following the stimulus onset. The LFP response of each electrode on each trial was calculated as the mean amplitude of the broadband LFP signal over a specific time-window bin. The evoked MUA response was also calculated as the spike count over the same window bin. For each time-window, we created independent response datasets for LFP and MUA. Then for each dataset, we z-scored the data across all the trials for each electrode, to ensure that the decoding algorithm would be influenced by all electrodes rather than those with high response values. We concatenated the responses of all electrodes together to create the response datasets.

3.3.2 Spatial receptive field map

A spatial receptive field map of each recording site was determined over the probe grid by averaging the z-scored responses of trials with the same probe positions. We fitted a two-dimensional Gaussian model to the receptive field maps separately through least-squares minimization:

$$G(A, \mu_X, \mu_Y, \sigma_X, \sigma_Y, d) \sim G(X, Y) = Ae^{-\left(\frac{(X-\mu_X)^2}{2\sigma_X^2}+\frac{(Y-\mu_Y)^2}{2\sigma_Y^2}\right)} + d \qquad (3.1)$$

The Gaussian model had six parameters: maximum response A, centre position (μ_X, μ_Y), SD (σ_X, σ_Y), and bias d. We used the X-Y positions of each probe on the grid (taking the fixation point position as the reference) as the input to the model and the mean response to each probe as the

output. The Gaussian model was then fitted, and the receptive fields were presented as the ellipses of full width at half height of the fitted Gaussians. The diameter of each receptive field was reported as the average of D_X and D_Y:

$$D_X = 2\sigma_X\sqrt{-2\ln(\frac{1}{2}-\frac{d}{2A})} \qquad (3.2)$$

and

$$D_Y = 2\sigma_Y\sqrt{-2\ln(\frac{1}{2}-\frac{d}{2A})}\ . \qquad (3.3)$$

The center of each receptive field was calculated as the center of its fitted Gaussian (μ_X, μ_Y). We defined the eccentricity of each receptive field as the Euclidean distance between the center of the receptive field and the position of the fixation point.

3.3.3 Selecting informative electrodes

To interpret discrimination performance for pairs of positions and to have an unbiased sample for the subsequent analysis, we removed recording electrodes that were not informative about the probe positions on the grid. We applied univariate feature selection to each dataset (MUA or LFP and for each window) by computing ANOVA F-values. Electrodes showing $p<0.05$ were considered informative and were selected for the subsequent analyses. Separate analyses including all the electrodes resulted in poorer discrimination performance (not shown).

3.3.4 Discrimination analysis

We used population decoding tools to estimate discrimination performance by combining responses of multiple electrodes [152-154]. Discrimination analysis was performed by classifying responses corresponding to pairs of stimuli. In each discrimination, we used Support vector machines (SVMs) for the MUA and LFP responses containing all the trials in which one of the two stimuli were presented.

SVM builds a classification hyperplane by maximizing the distance (margin) to the nearest data points of any class (called support vectors). Given training vectors $x_i \in \mathbb{R}^p, i = 1, \dots, n$ and targets $y \in \{1, -1\}^n$, SVM solves:

$$\min_{w,b,\xi} \frac{1}{2} w^T w + \frac{C}{2} \sum_{i=1}^{n} \xi_i^2 \qquad (3.4)$$

$$\text{Subject to } y_i(w^T \varphi(x_i) + b) \geq 1 - \xi_i,\ \xi_i \geq 0, i = 1, \dots, n$$

where, $C > 0$ is the upper bound, function φ maps the training samples into a higher dimensional space [155], and $K(x_i, x_j) = \varphi(x_i)^T \varphi(x_j)$ is the kernel function. We separately applied linear SVM and SVM with Radial Basis Function (RBF) kernel. RBF kernel is defined as $K(x_i, x_j) = e^{-\gamma \|x_i - x_j\|^2}$. In this setting, the hyperparameter C trades off correct classification of training samples against maximization of the margin (i.e. complexity of the decision function) and thus, it behaves as a regularization parameter. Hyperparameter γ in the RBF kernel, determines the influence of a single training sample.

We randomly changed the order of trials in the training set to make sure that the resulting set was representative of the overall distribution of the data. We used a stratified 5-fold cross validation procedure which preserved the relative class frequencies in each training and validation fold [156]. Validation score was determined as the mean of the 5 scores. We also applied Grid Search [157] to tune hyperparameters. The highest stratified 5-fold cross validation score was reported as the validation performance for the discrimination of a pair. Because of an imbalance in the number of trials with the same stimulus, we used the area under the Receiver Operating Characteristic (ROC) curve to measure the decoding performance [158]. ROC curve shows the true positive rate (TPR) or sensitivity versus a false positive rate (FPR) or one minus specificity for all possible threshold values. It plots cumulative distribution function (of discrimination threshold) for TPR on y-axis versus cumulative distribution function for FPR on x-axis. In scikit-learn roc_curve takes as input y_true and y_score and calculates TPRs and FPRs of the ROC curve for varying threshold values. In binary classification which is our case, y_true are true labels (0 or 1) for each test sample and y_score are the probabilities calculated by the classifier for assigning a sample to class 1. For each value of the threshold, probabilities in y_score that are smaller than the threshold are assigned to

label 0 and those bigger than it will be assigned to 1. Therefore, each threshold produces a pair of TPR and FPR which is represented as a point in the ROC curve. The ROC curve is depicted by decreasing the threshold from values where no instances being predicted to small values when all instances being predicted. TPR defines the number of correctly predicted samples to be in class 1 among all test samples with label 1. FPR defines the number of incorrectly predicted samples to be in class 1 among all test samples with label 0. So, ROC curve shows relative trade-off between TPR (benefits) and FPR (costs). The best possible prediction is when TPR = 1 and FPR = 0 which is a point in upper left corner. A random guess is a point along a 45° diagonal line. For the best classification, the area under the curve is 1 while for the random guess it is 0.5. Wrong classification will give a point under the diagonal and for ROC curve under this diagonal, the area under the curve is between 0 and 0.5.

The meaning of area under ROC curve (ROC AUC) is how well positive classes are predicted as positive and at the same time how well the negative classes are predicted as negative. Since the effect of both positive and negative classes are regarded in ROC AUC, it can be interpreted as how well two classes are discriminated (distinguished). Therefore, it represents the degree of separability. On the other hand, since ROC considers multiple threshold values it handles imbalance in the classes. Thus, it is applicable for discriminating imbalanced data.

3.3.5 Analysis of decoding weights

In each discrimination, the decoder assigns a weight to each electrode based on its importance. Positive weights support the hypothesis that the classification label is 1, while negative weights support the hypothesis that the label is 0. We independently normalized the weights corresponding to each discrimination. We defined the importance of each electrode in each discrimination as the square of its weights. The overall importance of each electrode was then calculated as the mean importance over certain discriminations. We sorted the electrodes based on their overall importance to find the best and the worst electrodes (overall). This algorithm selects the best k electrodes available in *combination* and in a non-greedy fashion.

3.3.6 Probes separation distances, eccentricity, and cortical magnification factor

As the probes are placed at different eccentricities, discrimination of pairs with the same separation distance on the grid will not lead to the same level of performance. Therefore, it is important to present discrimination performance in the context of the retinal eccentricity of the probes, taking into account cortical the magnification factor. Cortical magnification factor is the ratio of distance between two points on the cortex (in millimeters) divided by distance between their corresponding points in the visual field (in degrees) [159]. As previously shown by Gattass et al., cortical magnification in cortical area V4 (M) is related to eccentricity (E) in the visual field by $M = 3.01E^{-0.9}$ [160]. We used this equation to estimate the cortical magnification factor at specific eccentricities and then used its results to convert the separation distance on the grid to their corresponding distances on the cortex.

Separation distance for a pair of probes was calculated as their Euclidean distance on the grid in degrees of visual angle. The retinal eccentricity of a probe was calculated as the Euclidean distance between its position and the position of the fixation point (in degrees of visual angle). For every pair of probes, eccentricity was calculated as their mean eccentricity. The magnification factor for each eccentricity (of the pair) was then multiplied by their separation distance to give the cortical distance in mm.

We plotted the discrimination performance as a function of cortical distance. To make these plots, we sorted and grouped cortical distance values into 0.5 mm bins, and averaged performance values for the pairs whose cortical distances were within a bin. Similarly, discrimination performance was presented as a function of probe pair eccentricity for a fixed separation distance. Values of the probe pair eccentricities were sorted and divided into 3° bins and the discrimination performance values were averaged for eccentricities within a bin.

3.3.7 Selecting similar receptive fields

Inspection of the receptive fields indicated a level of similarity. We applied k-means clustering to systematically group similar receptive fields. k-means algorithm clusters n samples into k disjoint

clusters C, each described by a mean μ_j for the samples in the cluster (called the centroid). The centroids are chosen to minimize the within-cluster sum of squared criterion:

$$\sum_{i=0}^{n} \min_{\mu_j \in C} \left(\left\| x_i - \mu_j \right\|^2 \right) \qquad (3.5)$$

The algorithm has three steps: 1) initializing the centroids (e.g. by choosing k samples from the dataset). 2) assigning each sample to its nearest centroid, and 3) updating the location of the centroids by taking mean value of all the samples assigned to their previous locations. The algorithm repeats the second and third steps until the difference between the old and the updated location of a centroid becomes less than a threshold.

We selected 1-3 representative electrodes from each group and repeated the discrimination analysis using the total representatives from all of the groups.

3.3.8 Influence of noise correlations

The magnitude of response to presentations of the same stimulus differs from trial to trial. These trial-to-trial fluctuations are correlated between pairs of neuronal elements (henceforth noise correlations) [161, 162]. In order to determine the effect of noise correlations on decoding, we destroyed their structure in the training set by shuffling the order of trials corresponding to the same stimulus for each electrode site separately. The decoder was trained on the correlation-free training set, but was evaluated on the left-out unshuffled test set (henceforth correlation-blind decoding). The performance of the correlation-blind decoder was compared with the previous decoding results (henceforth correlation-aware decoding). Differences between the performance of these two decoding schemes reflects the impact of noise correlations from a decoding perspective. Then, we followed encoding perspective and trained the decoder on the uncorrelated data and evaluated its performance on the uncorrelated data.

The detailed procedure for removing the noise correlation in the data is as follows:

We collected the response data from all the trials associated to a particular probe and randomly shuffled the order of these values for each electrode. This breaks the inter-electrode correlations. For example, if a probe position on the visual field has been presented 15 times, we will have a matrix of size 15 × (number of recording electrodes). So, for each column, i.e. each electrode, the

order of values is randomly shuffled. We repeated the same procedure for all the probes to make correlation-free responses.

In our study, the number of electrodes was bigger than the number of trials with the same probe. This led the correlation-free dataset to be actually partially correlation-free. In other words, the average of Pearson's correlation for all electrode pairs was not perfectly $r = 0$. The consequence will be that a lower effect of correlation might be observed on decoding. The only solution for this problem is to have many more trials in each session for each probe. However, it will be hard because of the experimental limit in performing very long sessions with monkey.

We also calculated pair-wise correlated variability (noise correlation), as the Pearson correlation coefficient for the responses of two electrodes to repeated presentation of a particular stimulus [161]. We removed trials in which the response of either electrode was >3SD [163].

CHAPTER 4 ARTICLE 2 : SPATIAL RESOLUTION OF LOCAL FIELD POTENTIAL SIGNALS IN MACAQUE V4

This manuscript has been published in Journal of Neural Engineering – IOPscience on March 2020, Volume 17, Pages 026003.

Title: Spatial Resolution of Local Field Potential Signals in Macaque V4

DOI: https://doi.org/10.1088/1741-2552/ab7321

Authors: Armin Najarpour Foroushani[1,8], Sujaya Neupane[2,5], Pablo De Heredia Pastor[6], Christopher C. Pack[2,7] and Mohamad Sawan[1,3,4,7]

Affiliations:

[1] Polystim Neurotechnology Lab., Institute of Biomedical Engineering, Polytechnique Montreal, Montreal, QC, Canada

[2] Montreal Neurological Institute and Hospital, McGill University, Montreal, Canada

[3] School of Engineering, Westlake University, Hangzhou 310024, People's Republic of China

[4] Institute of Advanced Study, Westlake Institute for Advanced Study, Hangzhou 310024, People's Republic of China

[5] McGovern Institute for Brain Research, Massachusetts Institute of Technology (MIT), Cambridge MA, United States of America

[6] Escuela T´ecnica de Ingenieros Industriales, Universidad Polit´ecnica de Madrid 28040, Madrid, Spain

[7] Christopher C. Pack and Mohamad Sawan contributed equally to this work.

[8] Author to whom any correspondence should be addressed.

4.1 Abstract

Objective. An important challenge for the development of cortical visual prostheses is to generate spatially localized percepts of light, using artificial stimulation. Such percepts are called phosphenes, and the goal of prosthetic applications is to generate a pattern of phosphenes that matches the structure of the retinal image. A preliminary step in this process is to understand how the spatial positions of phosphene-like visual stimuli are encoded in the distributed activity of

cortical neurons. The spatial resolution with which the distributed responses discriminate positions puts a limit on the capability of visual prosthesis devices to induce phosphenes at multiple positions. While most previous prosthetic devices have targeted the primary visual cortex, the extrastriate cortex has the advantage of covering a large part of the visual field with a smaller amount of cortical tissue, providing the possibility of a more compact implant. Here, we studied how well ensembles of Local Field Potentials (LFPs) and Multiunit activity (MUA) responses from extrastriate cortical visual area V4 of a behaving macaque monkey can discriminate between two-dimensional spatial positions. *Approach.* We used support vector machines (SVM) to determine the capabilities of LFPs and MUA to discriminate responses to phosphene-like stimuli (probes) at different spatial separations. We proposed a selection strategy based on the combined responses of multiple electrodes and used the linear learning weights to find the minimum number of electrodes for fine and coarse discriminations. We also measured the contribution of correlated trial-to-trial variability in the responses to the discrimination performance for MUA and LFP. *Main results.* We found that despite the large receptive field sizes in V4, the combined responses from multiple sites, whether MUA or LFP, are capable of fine and coarse discrimination of positions. Our electrode selection procedure significantly increased discrimination performance while reducing the required number of electrodes. Analysis of noise correlations in MUA and LFP responses showed that noise correlations in LFPs carry more information about spatial positions. *Significance.* This study determined the coding strategy for fine discrimination, suggesting that spatial positions could be well localized with patterned stimulation in extrastriate area V4. It also provides a novel approach to build a compact prosthesis with relatively few electrodes, which has the potential advantage of reducing tissue damage in real applications.

Keywords: spatial discrimination, local field potential, V4, neural coding, support vector machines, correlation, cortical visual prosthesis

4.2 Introduction

A significant challenge for the development of cortical visual prostheses is to generate spatially localized spots of light, called phosphenes, to restore perception of visual scenes [13, 164, 165]. In practice, the spatial position of these phosphenes depend on the location and stimulation parameters of the implanted electrodes in the visual cortex [166-171]. Although much progress has been made

in generating and modulating individual phosphenes, no experimental study has reported systematic control over the spatial positions of multiple phosphenes to restore a visual scene. Previous studies however, showed that the phosphene positions are correlated with the receptive field positions of the electrodes at the microstimulated site [170, 172-174]. However, dealing with multiple phosphenes requires involvement of multiple electrodes, each contributing partly to the generation of spatial positions. This suggests that controlling the spatial position of phosphenes requires patterns of microstimulation sufficient to reconstruct the responses that encode the positions of phosphene-like visual stimuli. Determining this microstimulation strategy requires knowing how the spatial positions of phosphene-like visual stimuli are encoded in the distributed activity over the electrodes. The key characteristic of such a system is to be able to discriminate between these positions. Therefore, the spatial resolution with which the distributed responses discriminate positions puts a limit on the capability of visual prosthetic devices to induce phosphenes at multiple positions.

Multielectrode recordings are necessary to obtain both the spatial and temporal sampling properties of distributed activity required for the representation of position [175, 176]. However, the majority of previous multielectrode recordings and stimulation studies in the visual cortex of monkeys have been performed in V1 [168, 170, 177-185], which is quite large relative to standard recording arrays. Therefore, a multielectrode array in V1 can often sample only a tiny region of visual space. In contrast, extrastriate visual areas generally contain retinotopic maps that are physically smaller, while the receptive fields are much larger than those in the primary visual cortex (V1) [15-17]. This provides the opportunity to sample a larger region of visual space, albeit with reduced spatial resolution, using standard devices such as Utah arrays [18, 19]. In particular, extrastriate area V4 offers an opportunity to recover the location of static visual stimuli, as it contains a retinotopic map of visual space [19, 160] and responds well to stimuli of low to moderate complexity [186, 187]. However, the potential capability of V4 in discrimination of different positions in the visual space is remained to be discovered.

While chronically implanted recording arrays could provide the necessary information for stimulus localization, it is well known that the ability to resolve individual neurons with these devices declines over time [188]. However, local field potentials (LFPs) are more durable and can often be measured reliably for years after the implantation of multi-electrode arrays [189, 190]. They are

low frequency fluctuations [191, 192] generated by the synaptic current flow in neural ensembles [193-195]. They reflect subthreshold activity at larger spatial and temporal scales than single unit recording [196, 197], and they can be modulated by microstimulation [198-201]. Importantly, previous work has shown that the LFPs represent neural activity over a scale of about 400 microns [19], which is comparable to the spread of microstimulation effects in cortex, for reasonable parameter choices.

Since the receptive fields in V4 are large and have extensive spatial overlap, each position in visual space projects onto a large population of neurons. The capability of these receptive fields in discriminating fixed positions in the visual space, however, has not been addressed. Chen et al. showed that overlapping receptive fields provide sufficient spatial precision in area MT [18]. However, these results were obtained using the multiunit spiking activity (MUA). Here, we chronically implanted Utah electrode arrays with 96 electrodes to study the spatial discrimination in area V4. We recorded both LFP and MUA activity from area V4 while individual probe stimuli were presented to the macaque monkey. The probes were squares of 2° visual angle with similar characteristics to the phosphenes [166, 202-205]. We determined the spatial precision with which these signals could discriminate fixed positions in the visual field. We proposed and compared two selection strategies to reduce the number of electrodes used for fine and coarse discriminations. Then, we characterized the coding strategy by which the decoder discriminated positions with different spatial separations. We also examined the spatial resolution of band passed LFPs compared to that of the broad band LFPs. As a source of information about the spatial positions, we identified the structure of noise correlations, and showed their strengths as a function of cortical distances.

4.3 Materials and Methods

4.3.1 Electrophysiological recordings and signal pre-processing

All aspects of the experiment were approved by the Animal Care Committee of the Montreal Neurological Institute and were conducted in agreement with regulations of Canadian Council of Animal Care. The recording procedure has been described before [19, 206]. Briefly, a sterile surgical procedure was performed under general anesthesia to implant a headpost and a 10×10 Utah

Microelectrode Array (Utah array; Blackrock Microsystems) with 1 mm electrodes and 400 µm inter-electrode spacing into dorsal V4 of two macaque monkeys (*Macaca fascicularis*; monkey N: female, 8 years old and monkey C: male 10 years old). The impedance of the electrodes was in the range of 100 KΩ-800 KΩ. The arrays were placed to cover sizeable portion of the parafoveal visual representation. Area V4 was identified based on its anatomical landmarks and stereotactic coordinates [207] and the physiological properties of the neurons [160]. After recovering from the surgery, the monkey was seated in a primate chair (Crist Instruments) and trained to maintain fixation and to make visually guided saccades.

The data were collected by simultaneously recording wideband extracellular signals using a standard data acquisition system (Plexon Multichannel Acquisition Processor System) with a sampling rate of 10 kHz over all 96 channels of Utah Microelectrode Array. Preliminary signal-processing and custom setting of preamplifier were performed as explained previously [206]. The same recording equipment was used for both monkeys with the electrical ground being embedded on the skull 2-3 cm away from the array. The power of the wideband signals was monitored daily to minimize line noise and other artifacts. The remaining 60 Hz power noise was removed using a method introduced previously [208]. LFP and MUA were extracted offline in MATLAB (Mathworks). The raw signals were band-pass filtered between 500 and 4000 Hz and then the spikes were detected using established methods [209] to form the MUA activity. LFP signals were obtained by removing action potential signals from the raw signal using a Bayesian spike removal algorithm [208], band-pass filtering of the resulting signal between 0.2-150 Hz, and then down-sampling it to 500 Hz [210]. All the digital filtering was performed with a fourth-order two-pass Butterworth filter.

4.3.2 Experimental paradigm

The experimental procedure has been described previously [210]. Briefly, visual stimuli were back-projected at a 78 cm viewing distance onto a semi-transparent screen, by a cathode ray tube video projector, with refresh frequency 75 Hz. The screen covered 80×50° of visual angle. All visual stimuli were white square probes with 2° width and luminance of 22.5 cd m^{-2} presented on a dark background with less than 0.01 cd m^{-2} luminance. Each probe was chosen from among 100 locations on a 10×10 grid, with 4° center-to-center distance from each probe to its neighbours in

both vertical and horizontal directions. The grid was placed in the lower left quadrant of the visual field and its size and location were determined to cover the retinal eccentricity of the receptive fields of all the recorded neurons; these were centered within the central 40° of the lower left visual hemifield (see Figure 4.1 (a)).

On each trial, the monkey fixated its gaze on a small red dot of 0.5° diameter on the top right of the grid. After 500 ms of fixation, a probe stimulus was flashed at a randomly chosen location on the grid for 25 ms separated by a 500 ms blank screen. After a variable delay (500-1000 ms), the fixation point jumped to a new position at the top middle of the grid and the monkey was required to make a visually guided saccade to the new fixation point and fixate there for another 500 ms (see Figure 4.1 (a)). Another probe stimulus was then flashed for 25 ms, and the monkey was required to keep its fixation for another delay 500-1000 ms. Each successful trial ended with a liquid reward to the monkey. If the monkey could not maintain its gaze within 2.5° of the dot, the trial was aborted. In each session, each probe location on the grid was repeated at least 10-15 trials for each fixation point in a pseudorandom order. For each monkey at least 10-20 sessions were performed. The data were recorded on non-consecutive days.

Eye movements were monitored at 1000 Hz using an infrared eye tracker (Eyelink; SR Research). Trials that contained blink, double step, or catch-up saccades were discarded.

4.3.3 LFP and MUA analysis

All the analyses were performed in Python 3.6. The recorded activity for presentation of each probe was analyzed starting 350 ms before and ending 350 ms after probe onset. All of the analyses here and in the subsequent sections were performed separately for each fixation point. Multiunit activity (MUA) data at each electrode site was presented as spike counts computed in nonoverlapping time windows of width 25 ms. The evoked MUA response of each electrode to the presentation of each probe was defined as the total spike count over a certain time window. We defined three time windows, all beginning 50 ms after the stimulus onset; wide (150 ms), medium (50 ms), and narrow (25 ms). We created separate response datasets based on each measure for each window. For each dataset, the responses then were z-scored across all the trials, for each electrode independently.

Given previous results [19], we assume that the broadband LFP amplitude (0.2-150 Hz) has better localization than the instantaneous LFP power in area V4. Therefore, we defined the LFP response as the mean amplitude of the broadband LFP signal over the same time windows as those defined for MUA. As in the MUA analysis, the responses for each dataset were z-scored across all the trials and for each electrode separately.

To confirm that the information about the position was not restricted to certain frequency band, we applied fourth order Butterworth FIR filter to the broadband LFPs recorded 350 ms before to 350 ms after the probe onset. We filtered these signals over five frequency bands: theta (4-8 Hz), alpha (8-12 Hz), beta (12-30 Hz), gamma (30-50 Hz), and high gamma (50-80 Hz) independently. The delta frequency band (0.5-4 Hz) was not considered in the analysis, as it could not capture the responses over each of the three windows. We then calculated the responses and created datasets for each band passed LFP signal.

4.3.4 Spatial receptive field map

The spatial receptive field map of each recording site was determined over the probe grid by averaging the z-scored responses of trials with the same probe positions. We fitted a two-dimensional Gaussian model to the receptive field maps separately through least-squares minimization:

$$G(A, \mu_X, \mu_Y, \sigma_X, \sigma_Y, d) \sim G(X, Y) = Ae^{-\left(\frac{(X-\mu_X)^2}{2\sigma_X^2}+\frac{(Y-\mu_Y)^2}{2\sigma_Y^2}\right)} + d \qquad (4.1)$$

The Gaussian model had six parameters: maximum response A, centre position (μ_X, μ_Y), SD (σ_X, σ_Y), and bias d. We used the X-Y positions of each probe on the grid (taking the fixation point position as the reference) as the input to the model and the mean response to each probe as the output. The Gaussian model was then fitted, and the receptive fields were presented as the ellipses of full width at half height of the fitted Gaussians, where the diameter of each receptive field was reported as the average of D_X and D_Y, for which

$$D_X = 2\sigma_X\sqrt{-2\ln\left(\frac{1}{2}-\frac{d}{2A}\right)} \qquad (4.2)$$

and

$$D_Y = 2\sigma_Y\sqrt{-2\ln(\frac{1}{2} - \frac{d}{2A})}\ . \qquad (4.3)$$

The center of each receptive field was calculated as the center of its fitted Gaussian (μ_X, μ_Y). We defined the eccentricity of each receptive field as the Euclidean distance between the center of the receptive field and the position of the fixation point.

4.3.5 Selecting informative electrodes

To interpret the discrimination performance between pairs of positions and have an unbiased sample for the subsequent analysis, we removed recording electrodes that were not informative about the probe positions on the grid. We applied univariate feature selection to each dataset (MUA or LFP and for each window) by computing ANOVA F-values. Electrodes showing $p<0.05$, were considered informative and were selected for the subsequent analyses. Separate analyses including all the electrodes resulted in poorer discrimination performances (not shown).

4.3.6 Discrimination analysis

Discrimination analysis was performed by classifying ensemble responses for every pairs of probe positions on the grid. Discrimination between pairs of probes when at least one was not within the receptive field of the responsive electrodes was difficult to interpret. Thus, to collect probes that elicited responses, we calculated the mean z-score across electrodes and trials at each probe position [18]. For MUA, positions for which this value was positive and for LFP, positions for which it was negative were included in the discrimination analysis.

Support vector machines (SVMs) have frequently been used in previous studies to quantify the discriminability of population activity for pairs of stimuli [18, 152, 211, 212]. SVMs are effective in high dimensional spaces and in cases where the number of dimensions is greater than the number of samples. In addition, compared to other algorithms such as logistic regression, they are less sensitive to outliers. We therefore used SVMs on the MUA and LFP responses separately to discriminate pairs of probe positions. In each analysis (i.e. in each figure), we used all the trials of

a single session with a single fixation point. The dataset used for the discrimination of each pair contained all the trials in which one of the two probes were presented. Support vector machines build a classification hyperplane by maximizing the distance (margin) to the nearest data points of any class (called support vectors). Given training vectors $x_i \in \mathbb{R}^p, i = 1, \dots, n$ and targets $y \in \{1, -1\}^n$, SVM solves:

$$\min_{w,b,\xi} \frac{1}{2} w^T w + \frac{C}{2} \sum_{i=1}^{n} \xi_i^2 \qquad (4.4)$$

$$\text{Subject to } y_i(w^T \varphi(x_i) + b) \geq 1 - \xi_i,\ \xi_i \geq 0, i = 1, \dots, n$$

where, $C > 0$ is the upper bound, function φ maps the training samples into higher dimensional space [155], and $K(x_i, x_j) = \varphi(x_i)^T \varphi(x_j)$ is the kernel function. We separately applied linear SVM and SVM with Radial Basis Function (RBF) kernel defined as $K(x_i, x_j) = e^{-\gamma \|x_i - x_j\|^2}$. In this setting, the hyperparameter C trades off correct classification of training samples against maximization of the margin (i.e. complexity of the decision function) and thus, behaves as a regularization parameter. The hyperparameter γ in the RBF kernel, determines the influence of a single training sample.

We randomly changed the order of the trials in the training set to make sure that the training set was representative of the overall distribution of the data. Since the number of repetitions differed across the probe positions, we adjusted the SVM weights in inverse proportion to the class frequencies in the input data to keep the balance of the learned weights. We used a 5-fold cross validation procedure to prevent overfitting: all the trials were divided into 5 groups of trials, called folds, of equal sizes (if possible). The training was performed using 4 folds, and the remaining fold was used for validation. This procedure was repeated 5 times by using each of the folds once as the left-out fold. The validation score was determined as the mean of the 5 scores. Because of the imbalance in the number of repetitions of probes, we used stratified mode of 5-fold cross validation which preserved the relative class frequencies in each training and validation fold [156]. Similar results were obtained with 10-fold stratified cross validation (not shown).

Not every pair of probes can be discriminated with the same values of the hyperparameters. Discrimination between each pair of probes required a new adjustment in the hyperparameters to

prevent overfitting. To this end, we applied Grid Search [157] over C and γ to determine values with the highest stratified 5-fold cross-validation score. This score was reported as the validation performance for discrimination of each probe pair.

Because of the imbalance in the number of repetitions of the probes and also because two probes (negative and positive targets) were equally important in each single discrimination, we used the area under the Receiver Operating Characteristic (ROC) curve to measure the classification performance [158]. ROC curve plots true positive rate (TPR) or sensitivity versus false positive rate (FPR) or one minus specificity. Each prediction result represents one point in the ROC space. The area under this curve (AUC) is a measure of performance (in classification) that ranges in value from 0 to 1.

In discrimination of two positions, Linear SVM assigns a weight to each electrode based on its importance. The positive weights support the hypothesis that the stimulus is at a target position, while the negative weights support the hypothesis that the stimulus is at another position. We independently normalized the SVM weights corresponding to each discrimination. Since the L2 norm was used in the formulation of the SVM here, we defined the importance of each site in each discrimination as the square of its weight [213]. The overall importance of each electrode was calculated as the mean of the importance values over all the discriminations (here, we only considered probe pairs with separations <15°). We sorted the recording sites based on their importance to find the most and least important sites over all the discriminations. We also calculated the mean of the importance values over discriminations whose probes were separated by 4° and positioned at ≤8° eccentricity. Sorting electrodes over these importance values helped us to select only those electrodes that played a key role in discriminating close spatial positions at small eccentricities.

4.3.7 Probes separation distances, eccentricity, and cortical magnification factor

As the probes are placed at different eccentricities, discrimination of pairs with the same separation distance on the grid will not have the same level of performance. Therefore, it is important to present discrimination performance in the context of the retinal eccentricity of the probes, taking into account cortical magnification factor. Cortical magnification factor is the ratio of distance

between two points on the cortex (in millimeters) divided by distance between their corresponding points in the visual field (in degrees) [159]. As previously shown by Gattass et al., cortical magnification in cortical area V4 (M) is related to eccentricity (E) in the visual field by $M = 3.01E^{-0.9}$ [160]. We used this equation to estimate cortical magnification factor in V4 and applied it to convert the probes separation to their corresponding distances on the cortex.

Separation distance for a pair of probes was calculated as their Euclidean distance on the grid in degrees of visual angle. The retinal eccentricity of a probe was calculated as the Euclidean distance between its position on the grid and the position of the fixation point (in degrees of visual angle). For every pair of probes, the magnification factor was calculated using the above equation by Gattass et al., where the eccentricity was calculated as the mean eccentricity of the pair of probes (we call it probe pair eccentricity). The magnification factor for each pair was then multiplied by their separation distance to give the cortical distance in mm.

We plotted the discrimination performance as a function of cortical distance. To make these plots, we sorted and divided the cortical distance values into 0.5 mm bins, and then averaged performance of pairs with cortical distance values within each bin. Similarly, discrimination performance was presented as a function of probe pair eccentricities for those with the same separation distances. The values of probe pairs eccentricities were sorted and divided into 3° bins and the discrimination performances for pairs with eccentricity within each bin were averaged. To investigate the relationship between eccentricity and performance, we calculated the Pearson correlation.

4.3.8 Selecting similar receptive fields

Inspection of the receptive fields, indicated a level of similarity to stimuli at different positions. These electrodes had receptive fields with similar shape, location, or diameter. We applied k-means clustering to systematically group these similar receptive fields. The k-means algorithm clusters n samples into k disjoint clusters C, each described by a mean μ_j for the samples in the cluster (called the centroid). The centroids are chosen to minimize the within-cluster sum of squared criterion:

$$\sum_{i=0}^{n} \min_{\mu_j \in C} \left(\left\| x_i - \mu_j \right\|^2 \right) \qquad (4.5)$$

The algorithm has three steps: 1) it initializes the centroids (e.g. by choosing k samples from the dataset). 2) assigns each sample to its nearest centroid, and 3) updates the location of the centroid by taking the mean value of all the samples assigned to its previous location. The algorithm repeats the second and third steps until the difference between the old and the updated location of the centroid is less than a threshold. In this implementation we used the k-means++ initialization in scikit-learn to initialize the centroids to be distant from each other, and prevent convergence to a local minimum [214].

When similar receptive fields were identified, we selected 1-3 representative electrodes from each group and repeated the discrimination analysis using the total representative electrodes obtained from all the groups.

4.3.9 Influence of noise correlations on spatial discrimination

Most of the recording sites have correlated trial-to-trial variability in response to the same stimulus (called noise correlation). To determine whether these correlations have an impact on discrimination performance, we repeated the analyses above but after destroying the noise correlations in the training set. As before, the SVM cross validation score was computed on the left-out raw unshuffled data (one- fold), but for each electrode site, the order of trials with the same stimulus in the training set was shuffled and the SVM was trained on a correlation-free training set. This procedure destroyed the correlation between pairs of recording sites without changing the response statistics at site. Training on a shuffled dataset made the decoder blind to noise correlations, so that changes in discrimination performance then reflected the contribution of noise correlation to the subsequent computations.

We then calculated the noise correlation values as the Pearson correlation coefficient of the responses of two electrodes to repeated presentations of a particular stimulus [161]. This value is -1 for perfect negative correlation, +1 for perfect positive correlation, and 0 for no correlation. For each probe position, we standardized (z-score) the responses of each electrode independently and then calculated the noise correlation. We removed trials on which the response of either electrode was >3SD different from its mean [163]. The noise correlation was computed for all the electrode pairs and for all the probes included in the analysis.

4.3.10 Correcting the probe positions for the eye movement

Since the eye position can vary from trial to trial, we corrected the probe positions by subtracting the amount of eye dispersion from the fixation point. The correction was made by determining a new position for each probe presentation using the eye movement data and then we calculating the closest probe position on the grid to that new position. In this way the impact of eye movement will be reduced to lower than 1°.

4.4 Results

In this section, we first characterized the precision of spatial discrimination in area V4. Indeed, we analyzed LFPs and MUA recorded thorough a 96-channel multielectrode array implanted into behaving macaque monkeys. Then, we proposed two procedures to significantly reduce the number of electrodes for discrimination. Next, we presented the decoding strategy used by the decoder to discriminate positions at smaller and larger distances. Later, we investigated the capability of band-passed LFPs in discriminating positions. Finally, we identified the structure of noise correlations as a source of information about spatial position.

The results presented in Figure 4.1 to 4.9 are based on the recorded data from monkey N in a single session. Further results using the data from other sessions or from another monkey are presented in the Supplementary information.

4.4.1 Preliminary analysis

Neural responses were studied with white square probes presented for 25 ms at random locations on a 10×10 grid while the monkey maintained its fixation on the red point (Figure 4.1 (a); Methods). Figure 4.1 (a, left) shows a representative signal's sample. Figure 4.1 (c) left shows five example probes presented at different positions on the grid for the fixation point in the upper right of the grid. Presentation of each probe started at time 0 and lasted for 25 ms. We selected a group of 28 electrodes that responded well to the probe presentation for both LFP and MUA data (see Material and Methods – Selecting informative electrodes). The trial-averaged MUA and LFP signals from these electrodes, for each probe position (on its left) has been illustrated in Figure 4.1 (c), middle. The traces of neural activity are plotted from 100 ms before until 300 ms after stimulus onset. The red traces represent the MUA spike counts obtained over 25 ms time bins. The blue

traces are the corresponding LFP signals. The modulation of neural activity is observable in a period of 50 to 125 ms after stimulus onset for both the MUA and LFP traces. MUA modulation appeared in the form of an increase in the spike counts, while modulation in the LFP occurred in the form of biphasic or triphasic fluctuations, often with a clear increase in the signal's negative amplitude. The modulation intensities depended on the position of the stimulus on the grid and differed across recording sites.

We calculated the evoked responses using narrow, medium, and wide windows separately, transformed them into z-scores, and averaged them for each probe position. These values were then color-coded separately and displayed at the location of the recording electrodes within the electrode array. We then visually compared the results for the three time-windows (Figure 4.1 (c), right). From the graphs, different spatial patterns of electrodes activation can be observed for LFP versus MUA in response to the same probe positions. This suggests that MUA and LFP may encode the positions with different strategies and by involvement of different set of electrodes. These results also show a difference in the spatial pattern of responses between different time windows for presentation of the same probes. This difference suggests that the amount of information about the spatial positions may differ over time windows and latency after stimulus onset. In the next section we compare the precision of spatial discrimination, for these three response windows, using LFPs and MUA activities.

The MUA (red) and LFP (blue) receptive fields of the same group of electrodes (28 selected electrodes) are presented for each time window in Figure 4.1 (b). These receptive fields were extensively overlapping and many of them were similar in size and position for the LFP and MUA except for a number of MUA receptive fields that appeared around the upper left area of the grid. Further analysis showed that these few receptive fields had small response peaks. Using the medium time window, the estimated MUA receptive field diameter (the mean of x-diameter and y-diameter of an ellipse) ranged from 4.64º to 29.53º (13.1º±7.1º), while for the LFPs it ranged from 12.06º to 31.73º (20.7º±4.4º). Using the wide time window, it changed to range 4.64º to 36.30º (12.3º±7.7º) for MUA and 6.15º to 35.00º (21.2º±6.9º) for the LFP.

We presented the receptive fields mean diameters as a function of receptive fields eccentricity for the three response windows (for both MUA and LFP activity) (Figure 4.2-scatter plots). As expected, by increasing the eccentricity, receptive fields sizes increased, except for the narrow

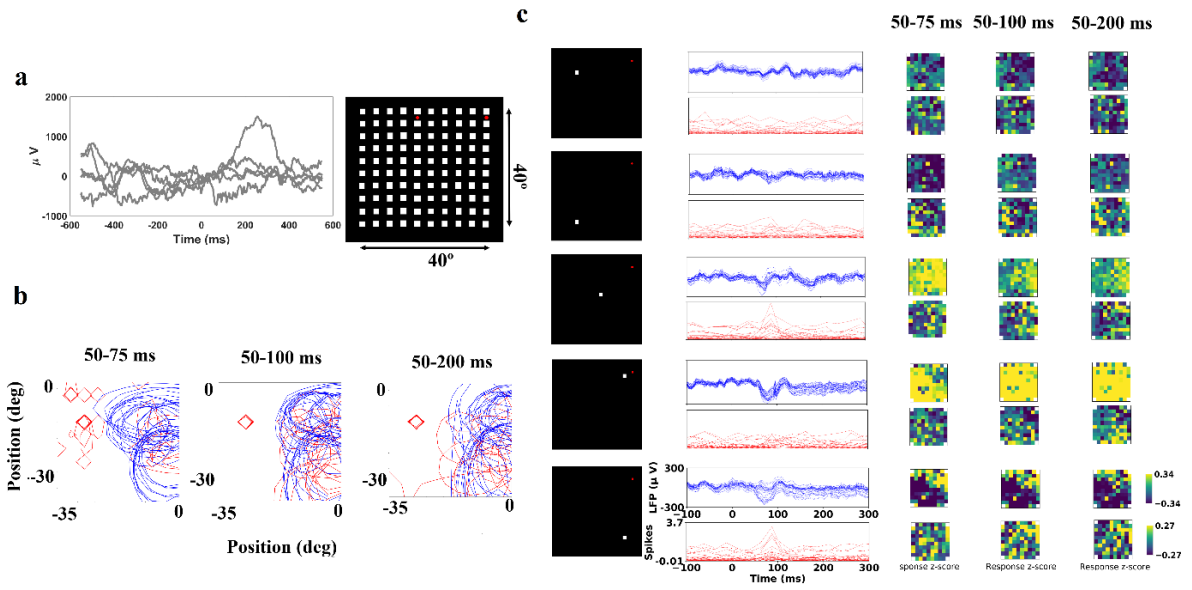

Figure 4.1 Responses of neural ensemble to different stimulus positions in visual cortical area V4. (a) (left) Samples of recorded activity with time in ms and signal amplitude in micro-volts (right) all possible probe positions on the 10×10 grid spanning 40°×40° of visual space. The red dots show the fixation points used in this experiment. One was in the upper right of the grid and the other in the upper middle of the grid. (b) Estimated receptive fields of a selected group of 28 recording sites in V4 obtained during fixation on the upper right red dot. MUA (red) and LFP (blue). Receptive fields were determined for three different time windows as labeled on their top. The x-y positions in (visual degrees) with the upper right red dot as the reference. (c) (left) Presentation of probes at five different positions on the grid and the fixation point at the upper right. (middle) time course of MUA and LFP activity from multiple sites. The blue traces are LFP activity and the red traces are the MUA spike counts (sampled over 25 ms bins). Each trace is the trial-averaged activity of an electrode over trials with the same probe positions. The traces of activity are illustrated between 100 ms before to 300 ms after the stimulus onset. (right) Responses of electrodes on the array to probe positions illustrated on the left. For the LFP, since the responses mostly appeared as negative values, we changed the polarity of responses to present more negative values as the higher responses. The responses are calculated for each window separately. Values on the array are color-coded between -0.27 to 0.27 for MUA and -0.34 to 0.34 for the LFP. The blue color corresponds to small response values and yellow color represent higher values. The white cells on the array show electrically grounded sites.

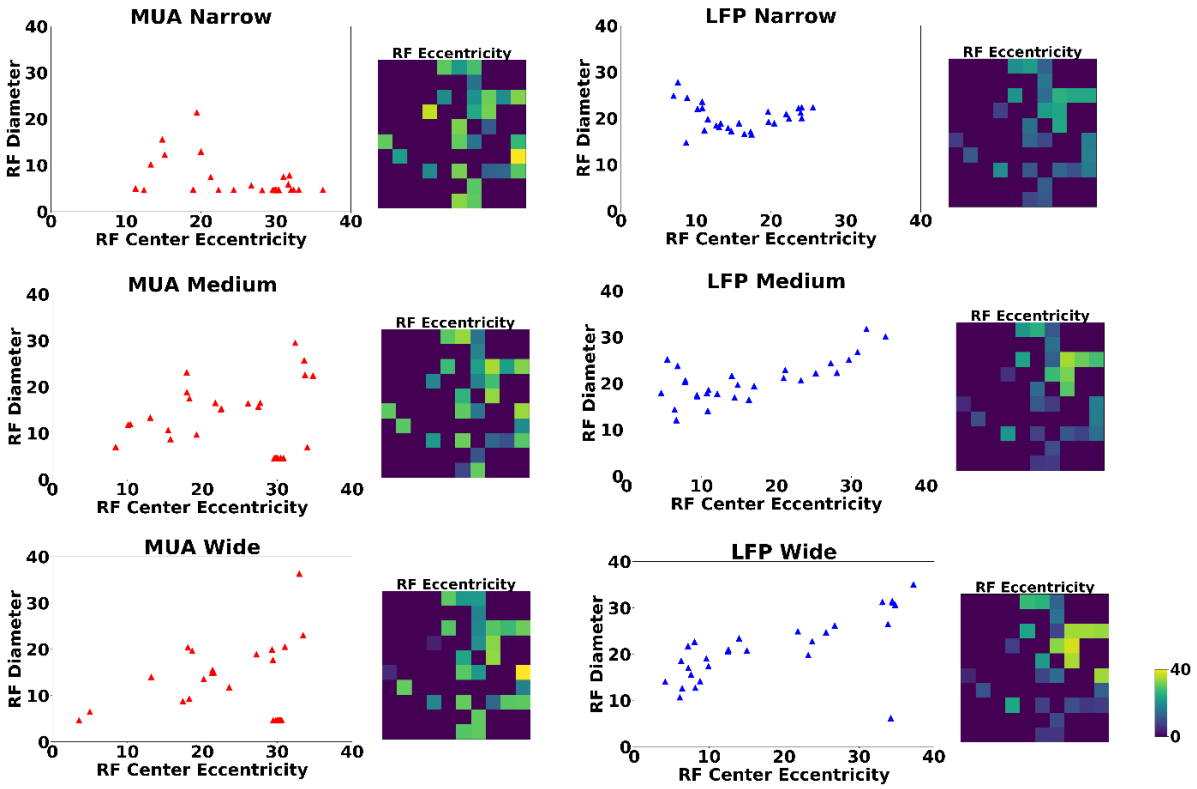

Figure 4.2 Relationship between receptive fields and their eccentricity. The scatter plots show the relationship between mean diameter of the receptive fields and the eccentricity of their centers for three response windows narrow (top), medium (middle), and wide (bottom) for the MUA (red) and LFP (blue) activities. On the right side of each scatter plot, the eccentricity values are presented for each of the selected 28 electrodes at their location on the array. Yellower values indicate higher eccentricities while the darker values show closer electrodes to the foveal presentation on the cortex. The color bar shows values between 0-40° eccentricity.

windows. This suggests that the content of information in the neural responses in V4 has not been captured using the narrow window. We also presented the receptive fields' eccentricities for each electrode at its location on the electrode array (right side of each scatter plot). The results demonstrated that upper and middle right of the array were corresponding to the peripheral representations while the bottom left included electrodes that recorded from foveal representations. These observations suggest that as individual stimulus is presented across the grid, it evokes

reliable responses in multiple recording sites, at each spatial position. This distributed response is a potentially rich source of information for position judgements when it is measured over a right window.

4.4.2 Spatial precision of MUA and LFP in area V4

In this subsection we characterized the spatial precision of the MUA and LFP responses in V4. To have an unbiased sample, for each time window independently, we excluded electrodes that were not informative about the stimulus positions on the grid (see Methods). This left 28 electrodes for MUA and 91 electrodes for the LFP, using the wide response window. For the medium window, for MUA, 29 electrodes were left, and for the LFP, 87 electrodes. Using the narrow window, left 4 electrodes for MUA and 82 electrodes for the LFP. We included these electrodes in the discrimination analysis.

We separately trained linear SVMs and Radial Basis Function (RBF) SVMs on MUA and LFP response datasets to discriminate differences in spatial position of the probes presented on the grid. For each response window then, we selected a separate set of probes that elicited responses in the electrodes. Since the electrodes' receptive fields were mostly located in the closer eccentricities, most of the probes in far eccentricities (>35°) were removed. Application of the linear and RBF SVMs showed that both MUA and LFP responses were capable of discriminating the positions of individual probes (Figure 4.3). The results showed that the discrimination performances (cross validation score) depended on the separation distances and eccentricities of the probe pairs.

As the probes were not all placed in the same eccentricities, discriminating probe positions with the same separation distances on the grid did not give the same level of performance. Therefore, we used the cortical magnification factor in V4 and converted their visual distances on the grid to distances on the cortex (see Methods). The discrimination performances of pairs of probes versus their cortical distances are presented in Figure 4.3 (a), (c) for each window ((a) linear SVM and (c) RBF SVM). In most of the cases, performance increased with cortical distance. For example, using the responses for fixation on the upper right dot, applying linear SVM, at 0.75 mm cortical distance, the average MUA performance for the narrow, medium, and wide windows were 64.7%, 65.2%, and 67.5%, which were increased to 73.4%, 84.1%, and 93.8% for 3.75 mm distance respectively (Figure 4.3 (a), left). For LFP with 0.75 mm cortical distance, for narrow, medium, and wide

windows, the discrimination performances were 56.5%, 60.8%, and 59.6% that reached 81.5%, 87.0%, and 87.0% for 3.75 mm distance (Figure 4.3 (a), right). These results were predictive for eccentricities and separation distances that were not used in the experiment. Assuming two probe positions with a 1° separation distance at 1° eccentricity, their V4 cortical distance (using $M = 3.01E^{-0.9}$) is 3.01 mm. At this cortical distance, the MUA discrimination performance with a wide window is around 92% and for LFP it is around 82%.

We performed additional analyses to determine the effect of eccentricity on discrimination performance for probes with the same separation distances. We selected probe pairs with 4° and 8° separations and plotted their performance versus their eccentricity. Figure 4.3 (b) shows the results of MUA and LFP, for each distance, and for each window. The results demonstrated that eccentricity plays an important role in the spatial resolution: the performance was higher for probe pairs located near the fovea and decreased by increasing the eccentricity. Exceptions occurred ($p>0.05$) when we used MUA with medium and narrow windows to discriminate 4° separation and a narrow window to discriminate 8° separation and also for LFP with narrow window for the both separations (Figure A.1 (b)). This indicated that the content of information in time windows shorter than 50 ms for MUA and 25 ms for LFP were not sufficient to discriminate between the positions. Using the wide window, with MUA, at 4.5° eccentricity and for 4° separation, the performance was 83.1%, while using medium and wide windows with LFP, this performance was 82.6% and 76.8% respectively. For 8° separation, at the same eccentricity, performance with both MUA and LFP were much higher: 95.5% for MUA with the wide window and 85.7% and 95% for LFP with medium and wide windows respectively.

Similar results were obtained using the data recorded on the other sessions (Figure A.5) and using the data recorded from the other monkey (Figure A.10 (a)). We repeated the above analysis with a RBF SVM (Figure 4.3 (c), (d)). The results of using the RBF SVM were similar to the linear SVM, with slightly higher performance (1-4% higher). Although the RBF SVM yields slightly better discrimination performances, it does not directly assign weights to the recording sites. Instead it transforms the data into a new space and classifies the transformed data. In contrast, linear SVM assigns linear weights to each electrode in the discrimination of each pair of positions, which provides more interpretability. Furthermore, linear SVM is faster than RBF SVM, which makes it

more practical when the number of discriminations is high. Taken the above factors into considerations, subsequent analyses were performed using linear SVM.

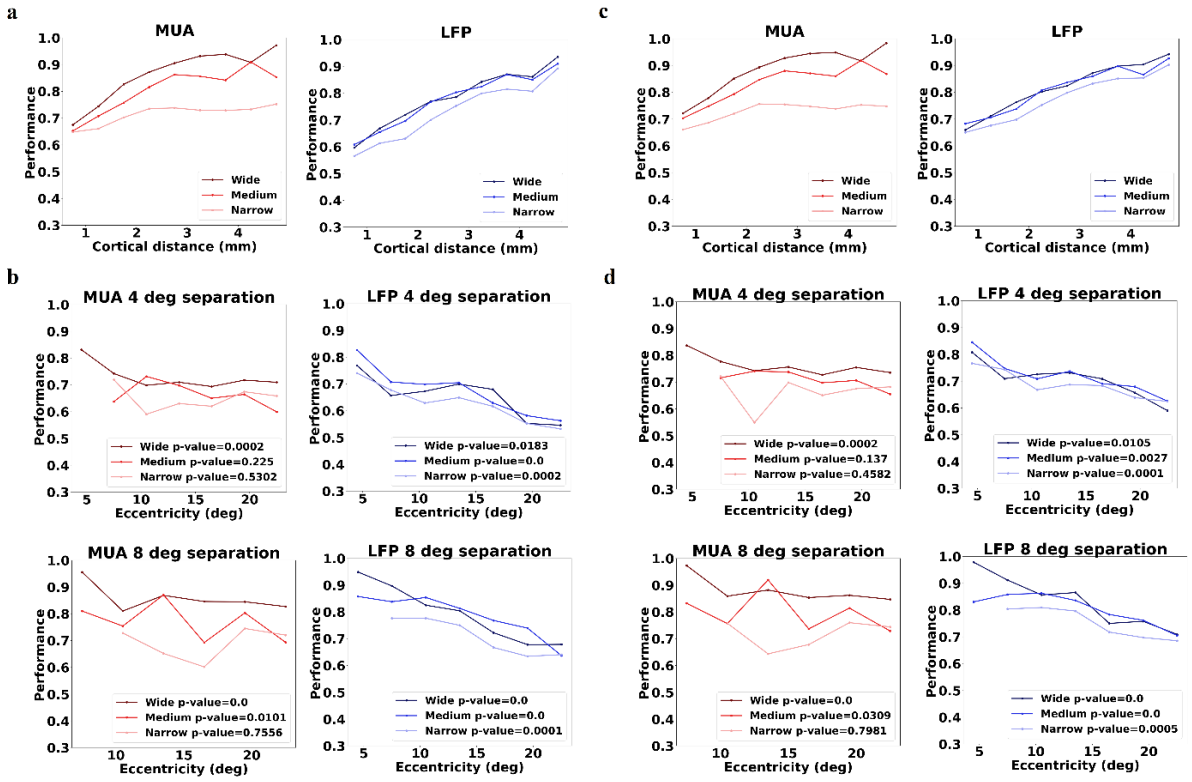

Figure 4.3 V4 ensemble response allows spatial discrimination. Darker colors correspond to the wider response windows. The performances are validation scores of 5-fold cross validation measured as the area under the ROC curve. (a) Discrimination performance versus cortical distance (in mm) for MUA (left) and LFP (right) using wide, medium, and narrow windows. The cortical distance values are divided into 0.5 mm bins and the discrimination performances of pairs with cortical distances within each bin were averaged. (b) Discrimination performances of pairs with 4° and 8° separation distances as a function of eccentricity (in deg) of the pairs for both MUA (left) and LFP (right) for responses defined over wide, medium, and narrow windows. Significance (p-values) of correlations between performance and eccentricity for each response window is presented for each plot. Eccentricity values are divided into 3° bins and the discrimination performances of pairs with eccentricities within each bin were averaged. (c) Same analysis as section (a), applying RBF SVM. (d) Same analysis as section b, applying RBF SVM.

Comparing the discrimination performance of response windows showed that for both MUA and LFP, narrow time window led to lower performance, while medium and wide windows resulted in much higher performances. These results suggest that capturing the content of information about the spatial precision requires response window of at least 50 ms. For MUA, the wide window obtained better performance over the medium window. For LFP, medium and wide windows had close performances with a mean difference of only 3.1% for the wide versus the medium window. This suggests that the information content for the spatial discrimination is mainly accumulated between 50-100 ms after the stimulus onset. This property makes the medium size window more practical for the use of LFP when temporal resolution is important. Therefore, for the subsequent analysis we used medium response window for LFPs and the wide window for MUA.

Although the animals were required to maintain fixation within 2.5°, in the experiment, for 92% of the trials, dispersion from the fixation point was less than 2° with a mean of 1.32° and standard deviation of 0.43° over all the trials. The distribution of eye positions was not different for different probe positions, so the eye movements just add variability to the neural responses. To determine the effect of this dispersion, we repeated our analysis after correcting for changes in fixation on each probe presentation. Results before and after the correction were almost similar. A reason is that, since the distribution of eye positions were not different, and since we averaged the discriminations for cortical distances within the same range, final results fell around the same level. Dispersion increases separation distance of some probe pairs while decreases it for the others. Therefore, it makes some pairs easier while some harder to discriminate. However, the overall result would stay around the same value. We have presented the discrimination performance versus cortical distance before correction in Figure A.11 (a) and after correction in Figure A.11 (b) for MUA and LFP. As we can see, the results are very close and the same conclusion can be reached.

In practical applications, we are interested in smaller probe separations with high spatial precision. As we showed above, if we present the probes in smaller eccentricities, the discrimination performance will be much higher. This is the result of larger area of the visual cortex that is dedicated to the fovea representation. Therefore, if we implant the same array in the foveal region of V4, it will yield far better resolution. In the next subsection, we present new strategies to select a smaller population of electrodes systematically while at the same time increases the performance for a particular value of the separation distance.

4.4.3 Minimizing the number of electrodes

In this subsection we proposed and compared two strategies to reduce the number of electrodes in the discrimination analysis. In the first method, we clustered the electrodes whose receptive fields were similar while in the second method we used linear SVM weights to select minimum number of the best electrodes.

4.4.3.1 Clustering electrodes with similar receptive fields

Comparing the receptive fields of individual electrodes showed some level of similarity in their shapes and locations that made it possible to group them into a few classes. Using k-means clustering we grouped the receptive fields of the informative electrodes, and found that 3 clusters gave the best results for both MUA and LFP. Figure 4.4 (b), bottom, shows the receptive fields that fell into the same group. To select a smaller population for discrimination, from each group, we selected 1-3 representative electrodes with the highest receptive fields peak and repeated the above analysis. Figure 4.4 (a) compares the performance as a function of cortical distance using representative versus using all the informative electrodes. The performances were calculated with the 8 representative electrodes for MUA and with 9 electrodes for LFP. Using the representative electrodes, the average MUA performance decreased by 3.2% while for LFP it decreased by 3.9%. These results suggest that performance was marginally affected by removing redundant electrodes from the analysis.

Next, we presented the discrimination performance of MUA and LFP as a function of eccentricity for 4° and 8° separations (Figure 4.4 (b)). With 4° separation and <8° eccentricities, for MUA, using the representative electrodes, the performance was increased by 6% compared to using all the electrodes while in LFP, it decreased by 0.8%. For the 8° separation, the average performance of MUA and LFP decreased by 4.6% and 4.7% respectively. Moreover, in all cases, the correlation between performance and eccentricity was significant ($p<0.05$). Clustering of similar electrodes, thus could help to reduce the number of electrodes used in the analysis to less than 10 while reasonable spatial precision is still maintained.

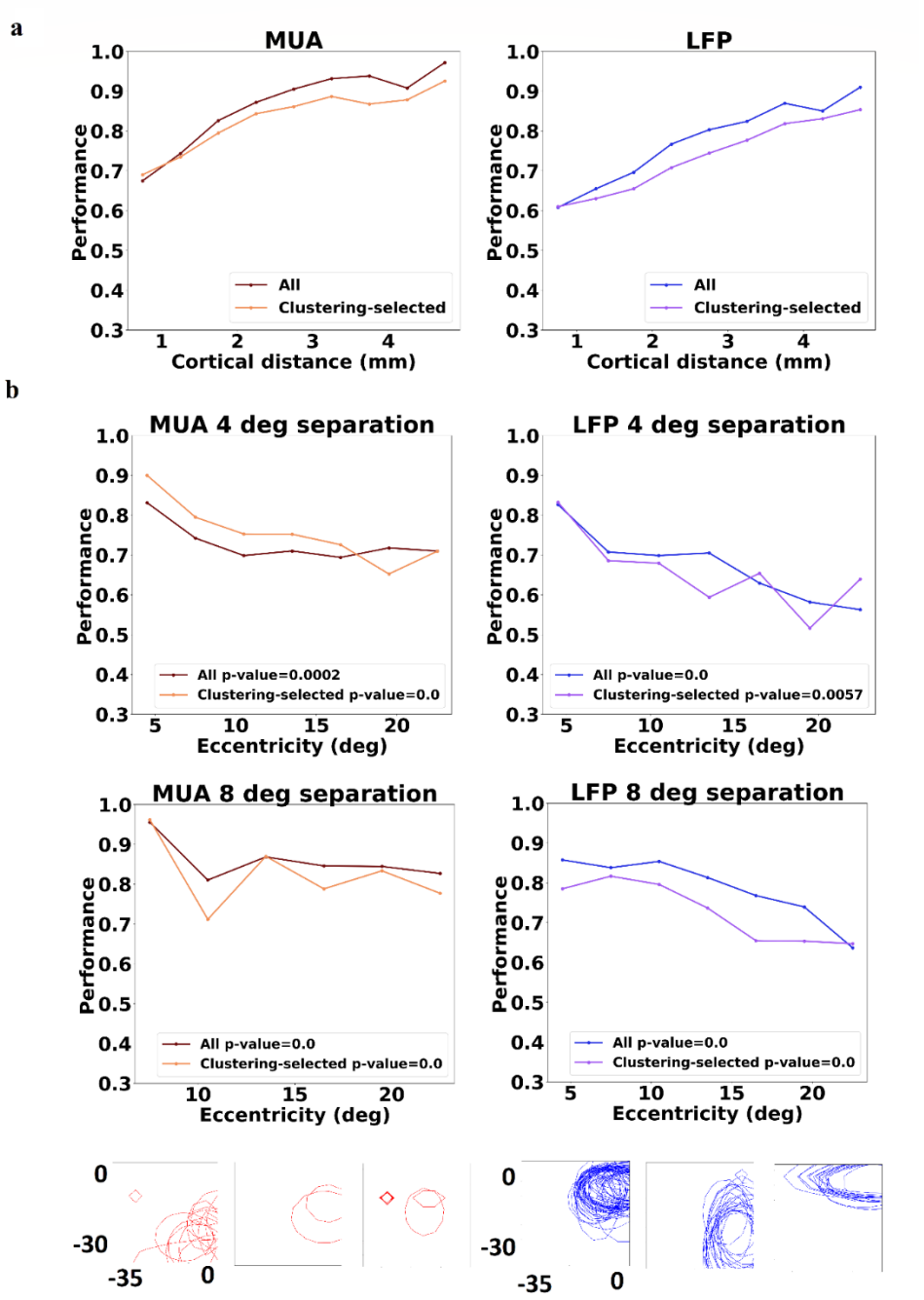

Figure 4.4 Spatial discrimination with a smaller subset of electrodes selected using clustering. Similar receptive fields were clustered into 3 groups and 1-3 representative electrodes with the highest receptive field peaks were selected from each group for use in the discrimination analysis. Three (k=3) groups for MUA (left) and three for LFP (right) were obtained (bottom contours). Dark red and blue colors show the results for MUA and LFP respectively, when all the

informative electrodes were used. Orange and purple colors show MUA and LFP when only representative electrodes were used. (a) Spatial discrimination as a function of cortical distance when all the informative electrodes were used versus when only representative electrodes were used. The cortical distance values are divided into 0.5 mm bins and the discrimination performances of pairs with cortical distances within each bin were averaged. (b) Spatial discrimination versus eccentricity for probes with 4° and 8° separations. Significance of Pearson correlation (p-values) are presented on the plots for each curve. Eccentricity values are divided into 3° bins and the discrimination performances of pairs with eccentricity within each bin were averaged. (bottom) The contours of similar receptive fields over the grid coordinate system with fovea location as the reference.

4.4.3.2 Selecting electrodes with the highest importance values

We sorted the electrodes based on their overall importance and selected the 4, 6, 8, 10, and 12 most important (best) electrodes, and for each set separately we performed the discrimination analysis as above. Figure 4.5 (a) and Figure A.2 (a) illustrates discrimination performance versus cortical distance for each set of the selected electrodes, as compared to the performance when the full set of the informative electrodes were used. For both MUA and LFP, the full set of electrodes (black curves), gave slightly higher or lower performances over all the discriminations, compared to using the other smaller sets of electrodes. The exception was with 4 electrodes that gave the lowest performances of all. As before we also illustrated discrimination performance versus eccentricity for 4° and 8° separations (Figure 4.5 (b) and Figure A.2 (b)). For the MUA, for 4° separation in closer eccentricities, with 4 and 6 electrodes, performance was in average 3.5% higher than with the full set of electrodes. For LFP also, 1.8% lower performance was obtained with 8 electrodes, for 4° separation in the closer eccentricities. Overall, in all cases, the averaged performance differences did not exceed 10%. Comparing the overall performance of MUA and LFP, we concluded that the minimum number of electrodes for fine discriminations (4°) without impairing performance (and also achieving $p<0.05$) for LFP was 10, while for MUA was 6. Similar results were obtained using the data recorded on the other sessions (Figure A.6) and using the data recorded from the other monkey (Figure A.10 (b)).

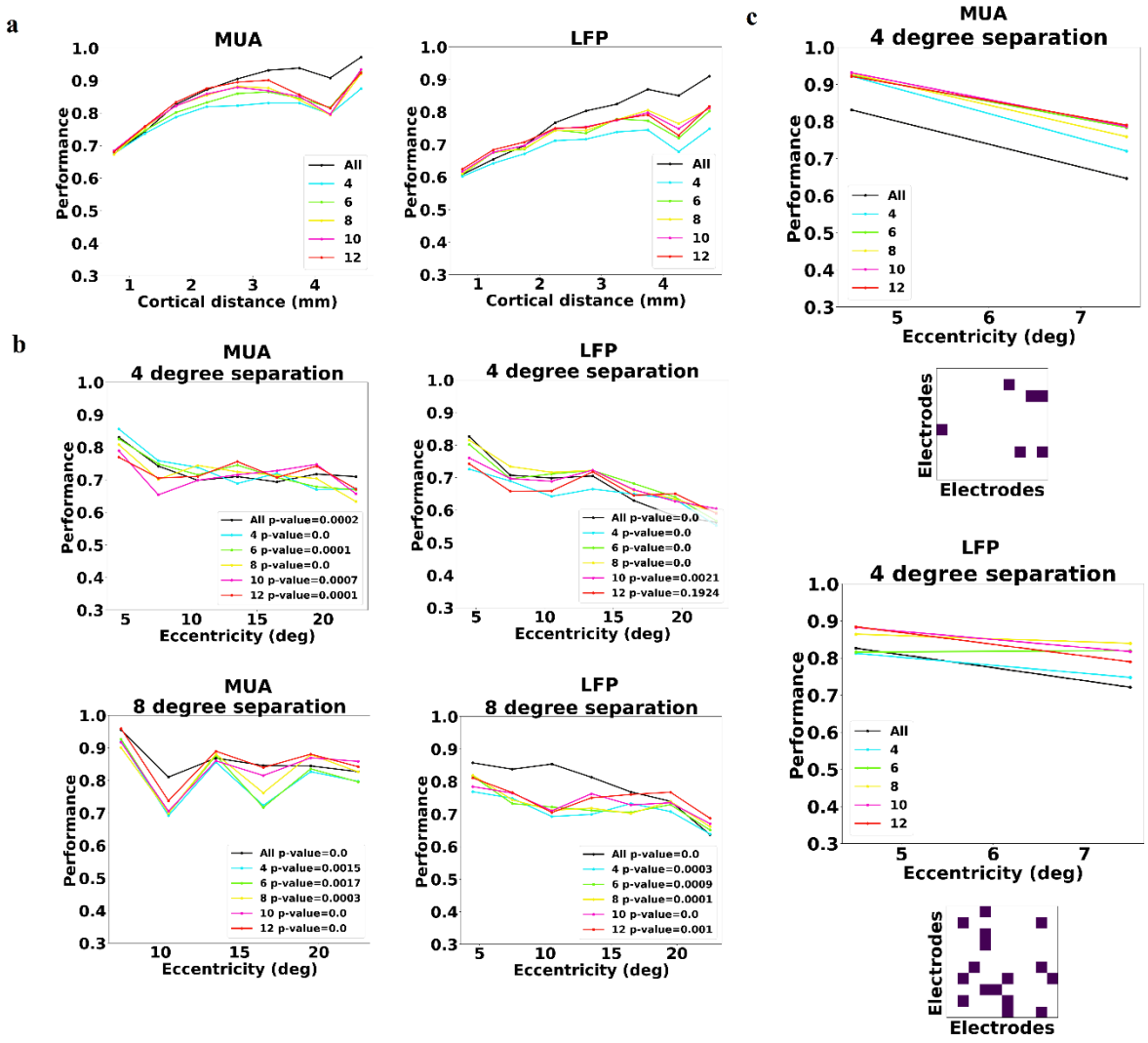

Figure 4.5 Results of discrimination analysis with the best (most important) 4 (blue), 6 (green), 8 (yellow), 10 (purple), and 12 (red) electrodes. Discrimination using all the electrodes is shown in black. (a) Discrimination performance versus cortical distance (in millimeters) for MUA (left) and LFP (right) with different sets of the best electrodes. The cortical distance values are divided into 0.5 mm bins and the discrimination performances of pairs with cortical distances within each bin were averaged. (b) Discrimination of probes with 4° (top) and 8° (bottom) separation versus the mean eccentricity of the pairs in visual degrees using the same sets of the best electrodes as (a). MUA results are presented on the left and LFP on the right. Pearson correlation significance (p-values) are presented on each plot associated to the results obtained with each electrode set. Eccentricity values are divided into 3° bins and the discrimination performances of pairs with

eccentricity within each bin were averaged. (c) Selecting the best electrodes using importance values obtained by averaging over discriminations with 4° probe separation and <8° pairs eccentricity. The electrodes were sorted by these new importance values. As only the closer eccentricities were important, the plots are illustrated for smaller range of eccentricities. At the bottom of each plot the locations of the best electrodes are presented on the electrode array. These best 6 electrodes for MUA and 16 electrodes for LFP can achieve better performance than using all the electrodes for 4° probe separations.

Although the above results showed that systematic selection of electrodes could significantly reduce the number of electrodes without damaging the discrimination performance, the selection strategy was based on all the discriminations with <15° separations. Since the goal of cortical visual prosthetic devices is to discriminate stimuli of small separations (high spatial resolution), and in closer eccentricities, we repeated the above analysis only for the probe pairs with 4° separation and eccentricities closer than 8°. We sorted the electrodes based on these new importance values and again selected the best 4, 6, 8, 10, and 12 electrodes. We repeated the discrimination analysis as before and illustrated the performance as the function of eccentricity for the 4° separation (Figure 4.5 (c) and Figure A.2 (c)). For MUA, at 4.5° eccentricities, with all the smaller groups of electrodes, the performance was more than 10% higher than the performance obtained with all the informative electrodes. For LFP, at 4.5° eccentricities, using 8, 10, and 12 electrodes, performance were in average 12%, 13.5%, and 13.7% higher than the performance obtained with all the electrodes. Further analysis (not shown) on LFP with more than 12 electrodes showed that performance reached its maximum value (>90%) with 16 electrodes. However, this maximum was slightly (<1%) better than using 10 electrodes. To obtain insight about the distribution of these best electrodes on the cortex, we plotted the location of the 6 best electrodes for MUA and 16 best electrodes for LFP (Figure 4.5 (c), at the bottom of the curves).

According to the cortical magnification factor in V4 [160], 4° separation at 4.5° eccentricity subtends a distance of 3.11 mm on the cortex. This amount of distance in a square (3.11×3.11 mm^2) can cover 64 electrodes of the Utah array. However, the results of this analysis showed that precise discrimination can be made with a much sparser distribution of electrodes. This result would be

useful for the prosthetic applications, as it suggests that a lower number of electrodes can be used, thereby limiting damage to the cortex without considerable reduction in performance.

We used two different methods to minimize the number of the electrodes for discrimination of spatial positions. Comparing the two methods showed that selecting electrodes based on their importance values provided a more systematic strategy and at the same time minimized the number of electrodes and increased the performance for both MUA and LFP. For the subsequent analysis in which we need to select the best electrodes, we use the second method.

4.4.4 Coding strategies

We next analyzed the coding strategy for position discrimination by examining the weights recovered by the SVM. This analysis shows the utility of the assigned weights in discriminating positions at a specific distance and their relation to the spatial tuning of the underlying electrodes. To determine this information, the weights were first normalized for each discrimination. For each probe position included in the analysis, we selected discriminations made between that probe and the other probes located at a particular separation distance from it and averaged the weights for these discriminations. We then presented these values for all the probes at their location on the grid. We investigated the coding strategy for 4°, 8°, and 12° separations for MUA and LFP independently. Examining individual electrodes suggested that, for small separations (4°) the peak of the receptive fields of more informative sites was offset from the target, such that the target position was situated on the flanks of the receptive field (Figure 4.6 and Figure A.3). In contrast, for large position separations (12°), sites were more likely to be informative if one of the targets was near the centre of the receptive fields. We observed a transition in the distribution of the weights between the two coding schemes over a range of target separations (8°). This pattern was observed for both MUA and LFP. As MUA responds by positive increase in the spike count, from 4° to 12° separation, the more yellow regions move from the flank of receptive fields to the centre of receptive fields. However, since LFP responses appeared in the negative amplitude of the signal, negative weight values followed this pattern (Figure 4.6 (b), right). These results are in agreement with the coding schemes for spatial position discrimination previously reported in area MT [18]. Similar results were obtained using the data recorded on the other sessions (Figure A.7).

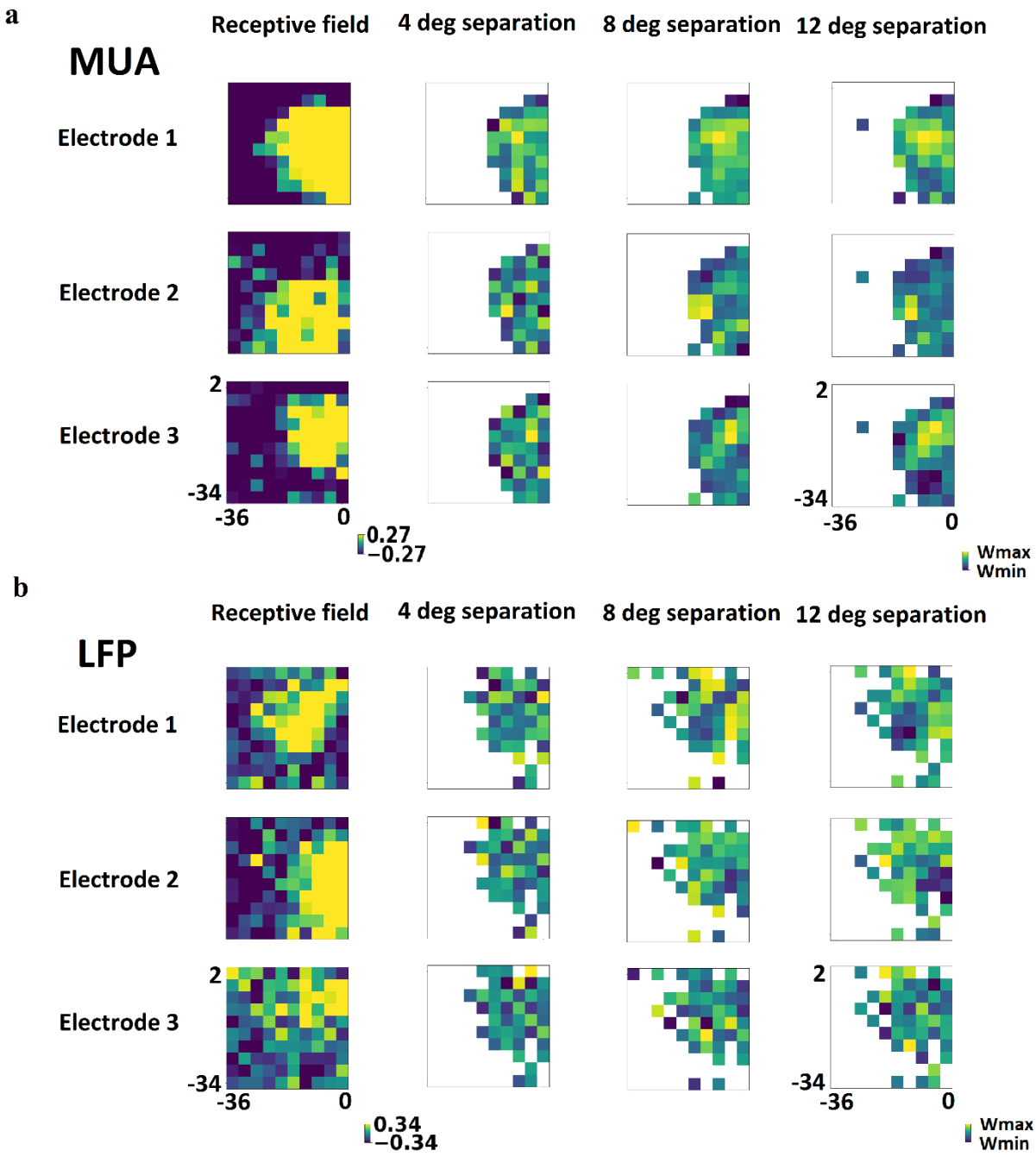

Figure 4.6 The coding strategy of individual sites for position discrimination of small and large separations. The degree of color lightness indicates polarity of values; lighter colors show more positive and darker blue colors show more negative values. Spatial receptive field profile is shown for each electrode on the left. The spatial distribution of the weights assigned to each site for discrimination of a probe from the other ones with a fixed distance. This value is calculated

for each probe and is presented at its location on the grid. The change in the coding strategy can be observed from 4° to 12° separation in the visual field (left to right). The values of the discrimination weights are visualized over the ranges between their maximum and minimum to capture the weight variations specific to each separation distance. (a) MUA results: The range of response values for the receptive fields are set to -0.27 to 0.27. The best three electrodes for MUA are selected for this analysis. (b) LFP results: The range of response values for the receptive fields are set to -0.34 to 0.34. The best three electrodes for LFP are selected for this analysis. As the LFP respond by negative peaks, the darker colors indicate the higher values of the weights.

We then assessed the relationship between the weights and the cortical distances. Using the Pearson's correlation we found that there was no significant correlation between the weights assigned to a particular electrode and the cortical distances of the included pairs of probes for both MUA and LFP ($p>0.05$). The same analysis on the averaged importance values for the four best electrodes and the cortical distances showed similar results.

4.4.5 Spatial precision of LFP at different frequency bands

We next sought to determine whether specific LFP frequency bands carry different amounts of information about stimulus positions. For each band-limited LFP, we calculated the responses using the medium time window. We used the same full set of responsive electrodes, as used for the broadband LFP with the medium window, and repeated the SVM discrimination analysis.

Figure 4.7 compared the discrimination performances obtained for each frequency band. Plotting performance versus cortical distance (Figure 4.7 (a)) showed that for no frequency band the performances exceeded 70%. This suggests that the information about stimulus position is distributed across frequencies. To study the relationship between band limited performance and eccentricity, we repeated the above analysis for 4° and 8° separations (Figure 4.7 (b)). Although there was a correlation between performance and eccentricity, with 4° separation using theta frequency bands and with 8° separations using the gamma frequency band, no overall significant relation to eccentricity was found as a source of information about spatial position. These findings

a

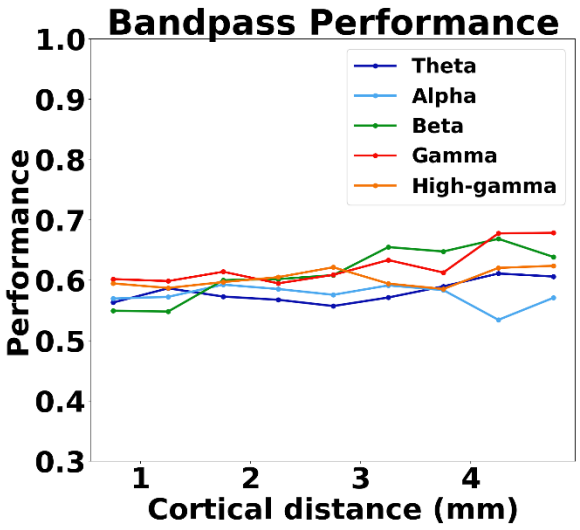
Bandpass Performance
Theta
Alpha
Beta
Gamma
High-gamma
Performance
1.0
0.9
0.8
0.7
0.6
0.5
0.4
0.3
1
2
3
4
Cortical distance (mm)

b

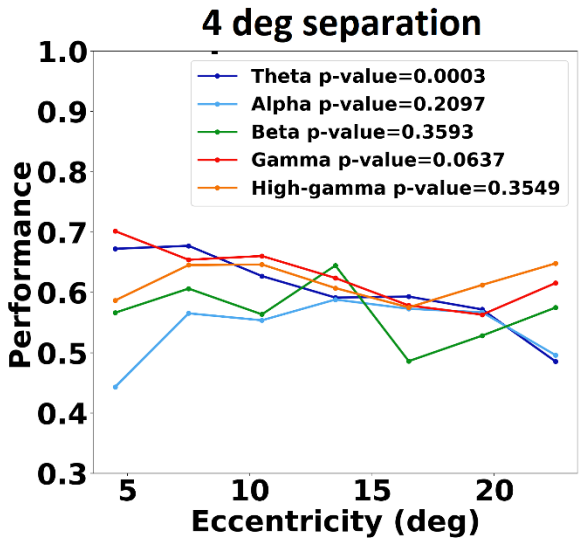
4 deg separation
Theta p-value=0.0003
Alpha p-value=0.2097
Beta p-value=0.3593
Gamma p-value=0.0637
High-gamma p-value=0.3549
Performance
1.0
0.9
0.8
0.7
0.6
0.5
0.4
0.3
5
10
15
20
Eccentricity (deg)

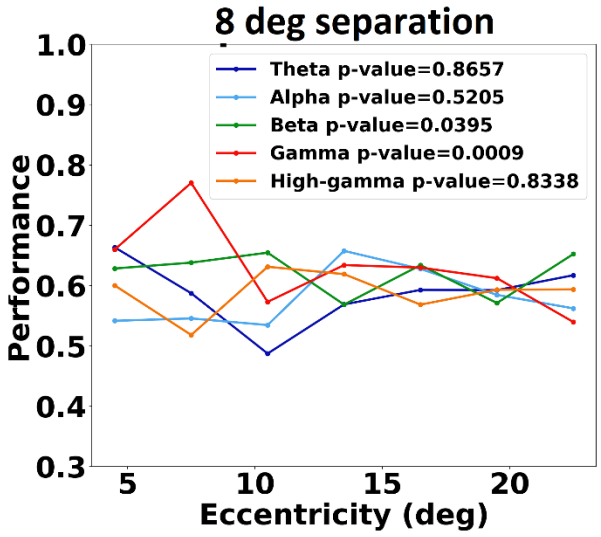
8 deg separation
Theta p-value=0.8657
Alpha p-value=0.5205
Beta p-value=0.0395
Gamma p-value=0.0009
High-gamma p-value=0.8338
Performance
1.0
0.9
0.8
0.7
0.6
0.5
0.4
0.3
5
10
15
20
Eccentricity (deg)

Figure 4.7 Discrimination performance of band passed LFPs. Responses for each band passed signal were calculated using the medium window. (a) The band passed LFP performance versus cortical distance for theta (4-8 Hz), alpha (8-12 Hz), beta (12-30 Hz), gamma (30-50 Hz), and high gamma (50-80 Hz) frequency bands. The cortical distance values are divided into 0.5 mm bins and the discrimination performances of pairs with cortical distances within each bin were averaged. (b) Discrimination performances of the same band passed LFPs (as A) as a function of eccentricity for 4° and 8° separations. The significance (p-values) of each band is presented on the plots. Eccentricity values are divided into 3° bins and the discrimination performances of pairs with eccentricity within each bin were averaged.

indicated the necessity of using broadband LFP in extracting information about the spatial positions. Similar results were obtained using the data recorded on the other sessions (Figure A.9).

4.4.6 Influence of noise correlations on spatial discriminations

The receptive fields in V4 are highly overlapping, and therefore the neurons are likely to receive input from similar groups of afferent neurons. Thus, some of their responses will be shared with other neurons and consequently, correlated [162, 177]. These interneuronal correlations in the responses might be used by decoding algorithms [152]. Noise correlations, which are the shared trial-to-trial variability in responses, are critical for understanding the representation of stimuli in neural ensembles [215] and have been shown to be related to the amount of information in a neuronal population [163].

To assess whether in our analyses, SVM uses noise correlations, we trained it on datasets in which the correlation structure was destroyed and cross validated it on the real unshuffled data (Figure 4.8 (a)). The removal of noise correlations from the training set impaired the ability of the decoder to interpret real neural activity and reduced the decoder performance (Figure 4.8 (b) and Figure A.4 (a)). Averaging the performance over all the discriminations showed that this reduction was around 4.3% for MUA and 14.0% for the LFP. This reduction was around the same level over all cortical distances. This suggest that the change in the computational performance was independent of cortical distances. We also illustrated the performance as a function of eccentricity for 4° and 8°

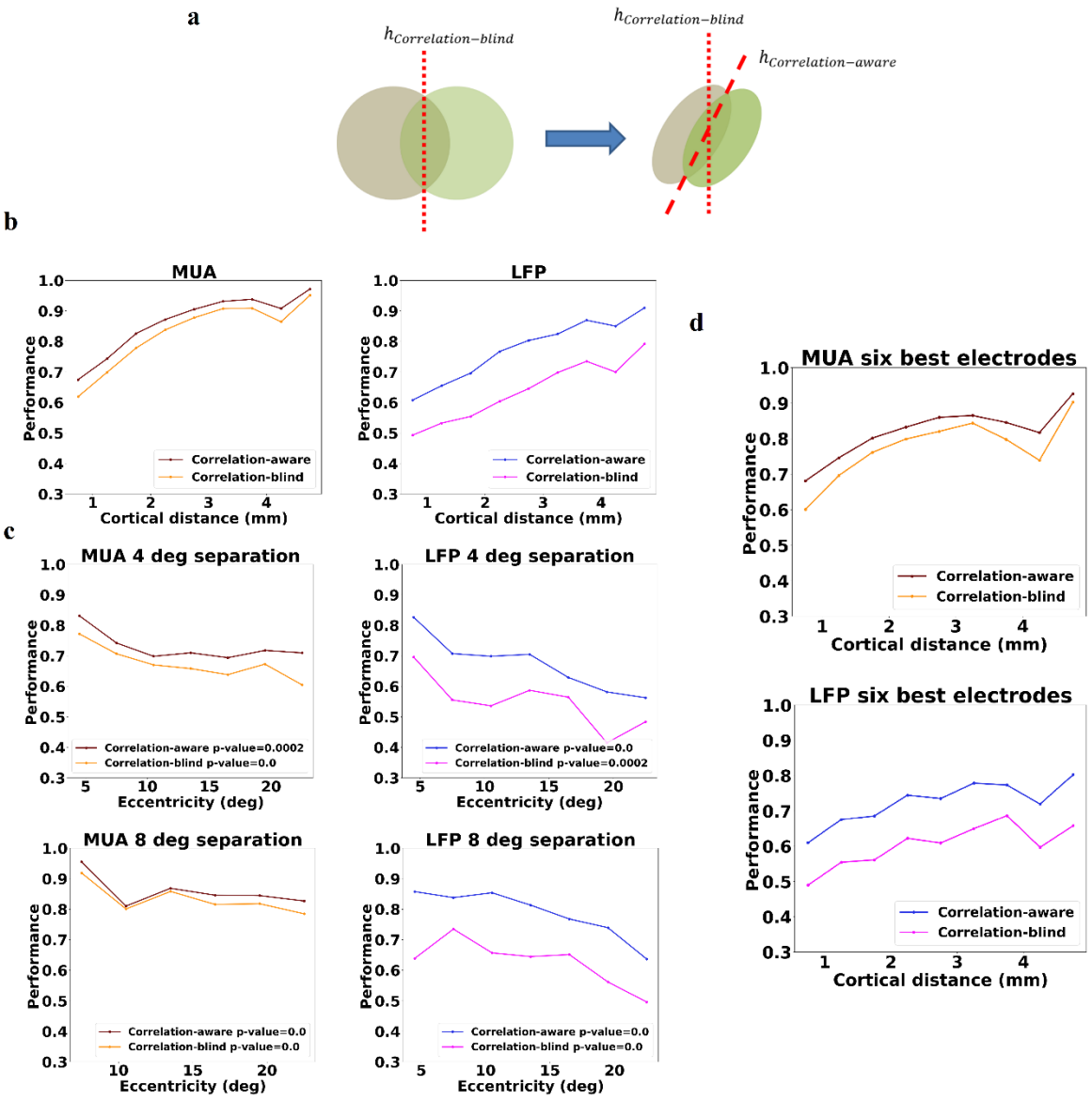

Figure 4.8 Effect of noise correlations on spatial discrimination. Dark red and orange colors represent correlation-aware and correlation-blind performances of MUA respectively, while blue and purple colors are representative of the same measures in the LFP. The correlation-blind performances are the cross-validation scores when SVM is trained on the shuffled data but validated on the unshuffled data. (a) (left) Training decoder on shuffled data with noise correlations removed. $\boldsymbol{h_{Correlation-blind}}$ shows the hyperplane optimized on the correlation-blind data. (right) original unshuffled data are discriminated with $\boldsymbol{h_{Correlation-blind}}$ and compared to

the discrimination with $\boldsymbol{h_{Correlation-aware}}$ that is optimized on the original unshuffled data. (b) Discrimination performance versus cortical distance for correlation-blind versus correlation-aware responses. (left) MUA (right) LFP. The cortical distance values are divided into 0.5 mm bins and the discrimination performances of pairs with cortical distances within each bin were averaged. (c) Discrimination performance as a function of eccentricity for 4° (top) and 8° (bottom) separations comparing correlation-blind and correlation-aware response data (left) MUA (right) LFP. Pearson correlation p-values are shown on each plot indicating the significance of the relationship. Eccentricity values are divided into 3° bins and the discrimination performances of pairs with eccentricity within each bin were averaged. (d) Same as (a) when the best six electrodes for MUA and the best six electrodes for LFP are selected for the discrimination.

separations (Figure 4.8 (c) and Figure A.4 (b)). With MUA, the effect of noise correlation was more pronounced in discriminations with 4° separation with 5.6% reduction compared to 8° separation with 2.7% reduction in the performance. This pattern was different for LFP with 12.2% reduction for 4° separation and 14.65% reduction for 8° separation. These results indicate the importance of noise correlations in finer discriminations when MUA is used and in coarser discriminations when LFP is used. In addition, it suggests that LFP performance highly depends on the noise correlations. Altogether, findings suggest that the interneuronal correlations contain information that could in principle be extracted by downstream regions.

To study the effect of noise correlation in smaller population of electrodes with comparable results, we selected the best six electrodes over all the discriminations for both MUA and LFP separately. Repeating the analysis for this population showed that the average reduction in the MUA performance was 4.6% and for LFP it was 12.1% (Figure 4.8 (d)). In other word, by reducing the number of electrodes, the effect of noise correlation on performance stayed around the same level. This suggests that using smaller number of electrodes still requires the same considerations about the noise correlation. Similar results were obtained using the data recorded on the other sessions (Figure A.8) and using the data recorded from the other monkey (Figure A.10 (c)). Repeating the noise correlation analysis after correcting for the eye movement during probe presentation showed

no particular difference in the results (Figure A.12). This confirms that the results are robust to small eye dispersions.

We next measured the noise correlations. To understand the dependence of noise correlation on the stimulus position, we selected the best two electrodes for LFP and MUA separately and calculated their noise correlation for the probes included in the analysis. We then plotted the resulting values at the location of probes on the grid (Figure 4.9 (a)). Comparing the results to the response profiles of the electrodes indicated that the stimulus can induce higher or lower levels of correlation depending on the receptive field location. For both MUA and LFP, the magnitudes of noise correlations were increased when the probe was in the receptive field of both sites or in the receptive field of neither of the sites. This pattern has been observed before for spiking activity [161, 177, 216, 217]. Correlations were relatively low when the stimulus was in the receptive field of one site and not in the receptive field of the other site. This pattern has also been observed in area MT [18].

To understand how noise correlations change over cortical distances, we calculated the noise correlations for all the electrode pairs included in the analysis and sorted the values by the inter-electrode distances on the cortex. Figure 4.9 (b) shows noise correlation values versus inter-electrode distances for six different probes for both MUA and LFP. These six probes were selected from three independent ranges of eccentricities with two probes in each range that were presented with the same colors. The results showed that for MUA, overall noise correlation dropped slightly (<0.1) with increasing the inter-electrode distances, which was in agreement with [215]. This decline in the noise correlations for LFP was much bigger and for some probe locations it was >0.2 for 4 mm increase in inter-electrode distances. This level of dependence of LFP on the noise correlation can explain the high drop in discrimination performance of the correlation-blind versus the correlation-aware responses. As we found before, discrimination performance increases with increasing cortical distance. The results here suggest that more distant points on the cortex have lower levels of noise correlation, and thus will be easier for the decoder to discriminate. In addition, since LFP produces highly correlated responses, even in more distant points on the cortex, responses will be more difficult than MUA to discriminate. Success in discrimination with LFP signals then, can be achieved by selecting electrodes optimally and as far as possible on the cortex and presenting stimuli at smaller eccentricities. The curves for probes at different eccentricities

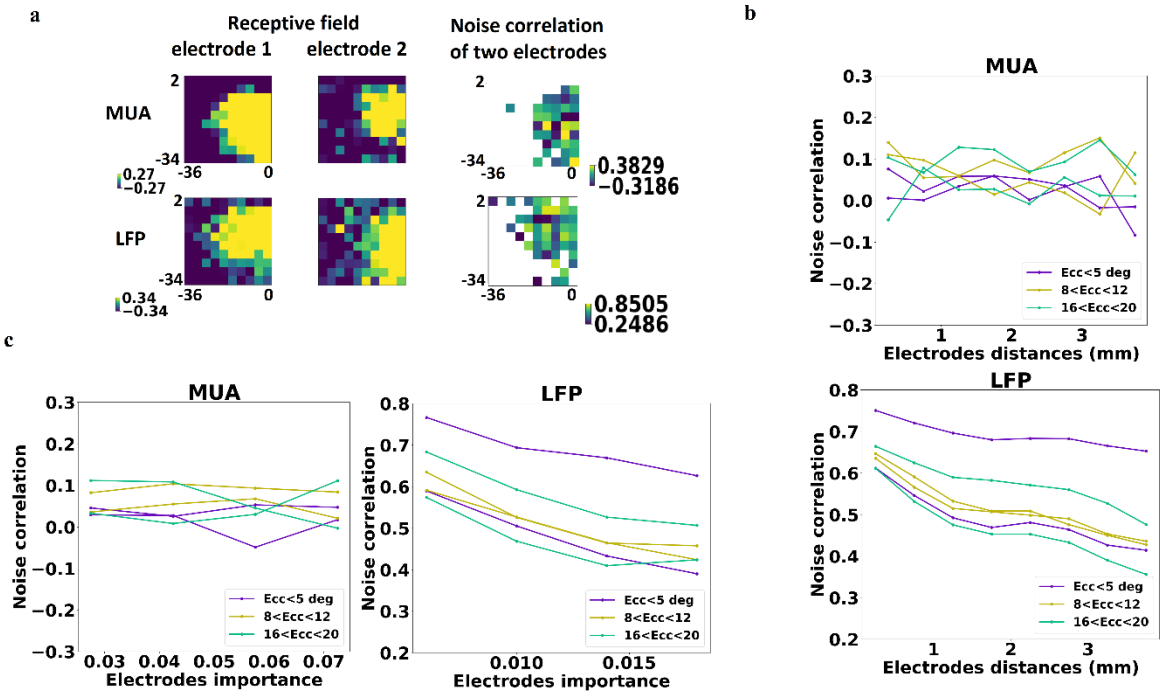

Figure 4.9 Dependence of noise correlation on probe position, electrodes distances, and electrodes importance. Noise correlation values are the Pearson correlation coefficients and are between -1 to 1. (a) Noise correlation of the best two electrodes (independently for MUA and LFP) in response to different probe positions on the grid. The range of noise correlation values is presented on the grid (on the right) and compared to the receptive fields of the two electrodes (on the left). We limited the range of the receptive field values on the graph between -0.27 to 0.27 for MUA and -0.34 to 0.34 for the LFP. The noise correlation values for both MUA (top) and LFP (bottom) are limited between Mean±1.5SD of the values on the graph. The degree of color lightness indicates polarity of values; lighter colors show more positive and darker blue colors show lower (more negative) values. The positions on the graphs are shown with the fovea center as the reference. (b) Noise correlation versus distances of the electrode pairs for responses to six different probe positions placed at three separate eccentricity ranges- with two probes in each range. Purple color for the eccentricities less than 5° from the fovea, brown color for eccentricities between 8° and 12°, and green color for eccentricities between 16° and 20°. (top) MUA (bottom) LFP. (c) Noise correlation versus mean importance of the electrode pairs. The importance value of each electrode is obtained as the mean of the squared weights calculated over

all the discriminations (with <15° probe pair separations). The same probe positions and color codes as b are used. (left) MUA (right) LFP.

also showed no particular relationship between eccentricities and noise correlation. As we can see in the figures, the correlations for probes at the same eccentricity ranges had different levels of noise correlation for both MUA and LFP signals.

We also investigated the relationship between the mean importance of pairs of electrodes and their noise correlations (Figure 4.9 (c)). The results showed that noise correlation drops with increased overall importance of the electrodes, and this drop is more pronounced in LFP. This suggests that electrodes that are important in discrimination of two positions are less correlated. In addition, no significant relationship was observed between the eccentricity of probes and their noise correlation as a function of electrodes importance. As we could select the minimum number of electrodes optimally, we actually selected less correlated electrodes in the discrimination analysis. Therefore, we minimized the redundant information but still kept important information that exists in the noise correlations for the discrimination.

4.5 Discussion

While most of the previous cortical visual prosthesis studies have been performed in V1, extrastriate visual areas offer sampling of a much larger region of visual space with the same coverage of electrode implants. Receptive fields in extrastriate areas are large and have extensive spatial overlap and therefore, spatial precision is unlikely to match the maximum precision in area V1. However, previous analysis have shown that the interaction between multiple receptive fields can provide relatively high precision that is behaviorally relevant [18]. Here, we studied the two-dimensional spatial precision of V4 as an intermediate extrastriate region in the visual processing hierarchy. We chronically implanted Utah electrode arrays in area V4 of macaque monkeys and recorded LFP and MUA activity, while individual stimuli at different positions were presented. The MUA and LFP receptive fields were highly overlapping, but differed in size and spatial position of their centers across different electrodes. Discrimination of visual features has been previously shown to rely on ensembles of neurons with broad tuning curves [18, 152, 218]. Our

results used a similar representation for the spatial positions in two dimensions. We found that despite wide difference in the receptive fields of the electrodes, both LFP and MUA were able to discriminate spatial positions.

4.5.1 Spatial discrimination of MUA and LFP

We found that both MUA and LFP responses were capable of precisely discriminating spatial positions and that this precision increased with increasing the distance between the corresponding representation of the positions on the cortex. The performance levels for MUA and LFP were comparable with that for MUA being an average of 6.3% higher. The results showed that the discrimination performance was highest at smaller eccentricities <°8. Probes that were presented closer to the fovea location then, had more distant positions on the cortex and could be discriminated more easily. Therefore, for prosthetic applications in which high spatial resolution is required, implanting electrodes in the fovea representation on the V4 cortex would give higher performances even for very small spatial separations.

Comparing linear and RBF decoders showed that neural responses in V4 corresponding to spatial different positions were linearly separable. SVMs are appropriate when the number of samples is less than the number of features. Here, we had at least 10-15 samples for each probe while the number of features was a subpopulation of electrodes and most of the times, it was larger than the number of samples. If the number of trials that a probe position was presented, was more than 50 times we could use even simpler decoders such as a Linear Discriminant analysis (LDA) [219]. An increase in the number of trials then, can provide a better estimate of the linear decision boundary for discriminating spatial positions. For cortical visual prosthesis applications in which a precise use of current stimulation is needed, having an accurate estimation of the decision boundary will be important.

There are two advantages of using LFP instead of MUA: 1) LFPs are more durable: they can often be measured reliably for years after the implantation of the multi-electrode arrays [189, 190]. Therefore, for the prosthesis applications in which both recording and microstimulation are important, they are more applicable. 2) LFP responses can be captured over the medium window 50-100 ms while for MUA the wide window 50-200 ms is required to achieve maximum performance. For real-time applications where the system needs to maintain temporal resolution,

using the LFP will be more applicable. However, to have a good precision with LFPs, implantation of the electrode arrays needs to be made in the fovea representation.

4.5.2 Minimizing the number of electrodes

One of the main challenges in the development of clinical prosthesis is the potential tissue damages. This damage can result from the insertion and chronic presence of the intracortical electrode [220-223], excess charge delivery [224, 225], chronic electrical stimulation [226-228], or thermal effect [229]. In all these cases, reducing the number of electrodes can reduce the risk of tissue injury. Reduction in the number of electrodes is obtained by selecting V4 instead of V1 as fewer electrodes are needed to cover the same extent of the visual field. For V4 itself, we also showed that we can further reduce the number of required electrodes without impairing the performance. We found that the minimum number of electrodes required for high spatial precision for both MUA and LFP was much lower than all the electrodes on the array (6-10 for MUA and 8-12 for LFP). Although previous literature has shown that using fewer randomly selected electrodes for decoding decreases the performance [18], we showed that if those electrodes are selected systematically, we can obtain higher performance for fine discriminations. For applications in which multiple cortical areas are implanted with electrodes, this could significantly reduce the number of recording (or stimulating) electrodes.

We proposed and compared two methods for selecting the best electrodes: clustering of electrodes with similar tuning and selecting electrodes based on the linear SVM weights. There are several advantages of using SVM weights over clustering analysis: 1) In applications where finding the receptive field map of the electrodes is difficult or impossible, SVM weights can be used. 2) Calculation of the performance and weights are integrated within the same algorithm, while clustering is a separate procedure for the electrode selection. 3) Using SVM weights is a systematic procedure, as we can sort the electrodes for an arbitrary set of discriminations. 4) Using SVM weights yielded significantly better discrimination for both MUA and LFP. 5) Depending on the nature of experiment, k-means clustering may not always give the best grouping of electrodes and more complicated clustering algorithms will be required to overcome complexities in the responses. But, SVM weights are computed linearly as part of the discrimination process.

Furthermore, selection of the electrodes based on the weights considers the effect of electrodes in combination and not separately.

4.5.3 Preprocessing steps

Preparing LFP signals for use in spatial discrimination analysis requires a number of preprocessing steps. The initial and the most important one is to extract the stimulus-modulated responses from the neural activity. The appropriate response measure is found under some assumptions about the signal and verification of the ability of the response in discriminating fine or coarse differences in the visual features. Defining the response measure is a features extraction step that has been obtained partly through trial-and-error. Such approaches can bias the results, as they entail assumptions on the response measures. For example, in the LFP analysis, we defined the responses as the mean amplitude over a specific time window. One assumption is that the information about the stimulus is encoded in the LFP amplitude. The other one is that the relevant information about the stimulus are accumulated, for example between 50-100 ms after the stimulus onset. Although these assumptions provide relatively precise discrimination results, they are not used as part of the classification algorithm (here SVM). There are set of techniques called feature learning that can replace manual selection of features by learning them to perform specific tasks [230]. For examples convolutional neural networks [231] can be used to learn response features and classify the LFP signals directly without the need to define the responses manually. However, using these techniques require many training examples (trials) to work accurately.

In our analyses, we investigated the need for filtering the LFP signals to specific frequency bands in order to extract more precise spatial information. Our analysis then showed that the information about the position was encoded in the broadband LFP. The performance thus dropped significantly by limiting the LFPs to specific frequency bands. This suggests that for spatial discrimination in V4, there would be no need for additional preprocessing step to filter LFP.

4.5.4 Microstimulation pattern to generate a phosphenated percept

Cortical visual prostheses offer the promise of restoring vision in patients with acquired blindness resulting from damaged eyes or optic nerves [13, 37]. The functionality of these devices relies on the hope to localize multiple phosphenes in the visual field by electrically stimulating multiple

implanted electrodes in the visual cortex [166-171]. Most previous studies have used concurrent electrical pulse stimulations from single or multiple electrodes to generate phosphenes and control their characteristics. However, there is no report of restoring a visual scene by localizing multiple phosphenes experimentally. One explanation for these failures is that the neural activity patterns induced by current pulses are not similar to the natural patterns, and so the downstream circuits cannot easily interpret them. In contrast to visual stimuli that activate neurons selectively, electrical stimulations activate random set of neurons in a close vicinity of the stimulating electrodes [99]. Electrical stimulation of early visual areas (V1/V2/V3) can generate simple percepts, but non-selective activation of neurons may not effectively propagate to higher visual areas to produce natural vision [48]. This explains the observation that electrical stimulation of late visual areas (e.g. IT) sometimes fails to induces a percept [232], as they require generation of complex activation patterns. This also explains the need for extensive training sessions before patients are able to detect percepts induced by electrical stimulation in both early and higher visual areas [232]. With training, as a result of brain plasticity in the adult brain, new activity patterns can be learned and electrical stimulation of any part of the cortex can be detectable [48]. However, the induced perception is still distinct from the natural activation patterns.

Imitating natural activity patterns generated in response to phosphene-like stimuli, provides a systematic way to control the positions of multiple phosphenes. Since those activity patterns are familiar to the cortex, they may easily become detectable and be interpreted by downstream circuits. To imitate a natural activity pattern, a novel stimulation paradigm, called dynamic current steering, was suggested [233]. However, this paradigm still did not imitate natural responses but instead was *inspired* by the V1 responses.

To be able to localize multiple percepts at different positions, their corresponding imitated activity patterns should be discriminable. As our results showed, spatial positions were discriminable using both MUA and LFP responses in V4. The precision of this discrimination depends on the distance between their representations on the cortex. As the magnification factor increases with decreases in eccentricity, the positions located at smaller eccentricities will be placed at farther distances on the cortex, and thus can be discriminated more precisely. By implanting electrodes in the foveal representation of V4, we can precisely discriminate probes that are located at very small distances. As we calculated earlier in the results section, probes with 1° separation at 1° eccentricity are

located with 3.01 mm distance from each other on the cortex. At this cortical distance, 7-8 electrodes of Utah electrode array, similar to what was used in this study, can be embedded. We can conclude that for prosthetic applications, electrodes should be implanted in the foveal representation and the spatiotemporal patterns of electrical stimulations should be able to reconstruct discriminable natural responses to stimuli at different positions.

To generate such patterns of electrical stimulation, the stimulation parameters need to be tuned. As we found in our results, discrimination of spatial positions in V4 requires the recruitment of multiple receptive fields that each contribute to varying degree in each discrimination. This contribution was determined by the weights that the decoder assigned to each electrode. The weighting strategy (coding strategy at Figure 4.6) used by the decoder determines how the stimulation parameters can be tuned. In the prosthetic applications with the need for higher precision, a coding strategy for fine discriminations should be applied: Localizing phosphenes at specific position requires stimulating electrodes whose receptive fields' flanks are at the position of the phosphene. The stimulating electrodes should be weighted according to the weight values obtained for each spatial position in the coding strategy.

In addition to the coding strategy, tuning the stimulation parameters depends on the responses of local and non-local brain circuits to the electrical stimulation patterns. As we found in our results, noise correlation carries information about the stimulus. Noise correlations are the result of shared trial-to-trial variability in response whose structure and extent depends on the distances on the cortex [161]. Correlations arise from shared inhibitory and excitatory inputs [234, 235], either from ongoing activity or from other neurons that were activated by stimulus [236-238]. When we are performing electrical stimulation, these sources of correlations may affect the induced activity pattern, especially when LFP signals are used. This may happen by altering the natural contribution of these sources or interrupting their influence on the stimulated ensemble. On way to solve this issue is to build statistical model of the implanted area using injected current as the input and the induced ensemble activity as the output. Then, this model can be used to determine current stimulation for a specific neural activity pattern.

To apply these results to real visual prosthesis (i.e. blind people), the above analyses need to be tested on human subjects. Our results here, are based on the responses of macaque V4 neurons. However, to be applicable to human, the SVM decoder needs to be trained on data recorded from

several human subjects and be tested on data from new unseen subjects. This will be a subject-wise classification problem to generalize the results over the subjects (and not over the samples). As for blind people there is no way to measure the receptive fields, area V4 should be identified based on its anatomical landmarks and stereotactic coordinates. The implantation should be performed as soon as possible after the onset of blindness to prevent cross-modality adaptation. Human verbal reports then should be used to evaluate the performances of the stimulation strategy that is trained on the sighted subjects but is tested on the blind subjects.

4.6 Conclusion

Our findings showed that the combined responses from multiple sites, whether MUA or LFP, has the capability for fine and coarse discrimination of positions. Moreover, we presented the decoding schemes used by the decoder for discriminating the spatial positions. This is appropriate for cortical visual prostheses applications in extrastriate cortical areas to localize phosphenes accurately. Building this kind of prostheses, however, require future investigation to design electrical stimulation pattern that reconstructs specific natural patterns of responses in neural ensembles. We proposed a procedure for electrode selection that can be used in similar decoding studies to reduce the number of electrodes while increasing the discrimination performance. This is crucial for prosthetic applications to minimize the amount of physical, electrical, and thermal damages to the brain tissues. Future work is needed to shed a light on the nature of input connections to the implanted area. This will help to design an appropriate pattern of electrical stimulation to reconstruct natural neural responses.

Acknowledgement

The authors acknowledge financial support from Canadian Institutes of Health Research (to C.C.P., PJT-148488) and the *Natural Sciences and Engineering Research Council* of Canada (*NSERC*) (RGPIN-2017-05738 to M.S.) and the Canada Research Chairs in Smart Medical Devices.

CHAPTER 5 THE EFFECT OF NOISE CORRELATIONS FROM ENCODING PERSPECTIVE

5.1 Introduction

The idea that the correlated noise impacts decoding performance has been shown in several studies [18, 239, 240]. However, all of our analyses in the previous chapter about the effect of noise correlations were focused on the decoding perspective. In this chapter, we focus on the encoding perspective and compare it to our previous results.

Neural responses are noisy, meaning that even when the same stimulus is presented, the same pattern of activity never occurs. So, the brain must compute an estimate of a stimulus. According to [239], two questions are raised related to the impact of correlated noise on the population coding: How accurately can stimulus variables be represented in population responses? What is the effect of noise on computations? To answer these questions, two complementary perspectives have been studied: 1) Encoding perspective: will adding correlation to a population of neurons without modifying single neuron responses increase or decrease the population coding performance? 2) Decoding perspective: how well can decoding strategies that ignore correlations compare with optimal strategies that take into account the correlations? In other words, how much do downstream neurons have to know about correlations to extract all of the available information? [3].

It should be noted that there is a difference between 1) the value of noise correlations (also called correlated variability) and 2) the effect of removing noise correlations on population coding. For example, spatial noise correlation is reduced by half after stimulus onset compared to spontaneous activity [161]. However, it does not mean that removing noise correlations reduces the decoding performance.

5.2 Methods

In the encoding perspective, the effect of noise correlations on coding is measured by subtracting the decoding performance obtained using the uncorrelated responses from decoding performance obtained using the correlated responses (both train and test). There are three possibilities for the

outcome in this perspective: 1) performance with correlated responses is lower than uncorrelated responses, 2) performance with correlated responses is bigger than uncorrelated responses, or 3) both performance values are the same. So, if we know only the individual responses of neurons and not their correlational structure, we cannot say how much the real performance is.

In the decoding perspective, we measure the effect of correlations by calculating the difference between the decoding performance obtained with the original correlated responses, and the decoding performance of a decoder optimized on the uncorrelated data but evaluated on the raw correlated data. In this perspective there are two possibilities: 1) removing correlations does not cause change in the decoding performance 2) removing correlations leads to a sub-optimal decoder with lower performance.

Trials/Electrodes	Electrode 1	Electrode 2	…	Electrode 96	Label
1	0.67	0.45	…	0.77	6
4	1.12	0.78	…	1.50	6
5	2.40	3.60	…	1.13	6
8	0.23	1.20	…	0.41	6
9	0.98	0.56	…	2.7	6
10	2.90	2.30	…	1.8	6
3	3.4	1.7	…	0.8	6

Trials/Electrodes	Electrode 1	Electrode 2	…	Electrode 96	Label
-	0.23	1.7	…	0.8	6
-	1.12	3.60	…	0.41	6
-	3.4	0.78	…	2.7	6
-	0.67	2.30	…	1.8	6
-	2.90	0.45	…	1.50	6
-	0.98	1.20	…	1.13	6
-	2.40	0.56	…	0.77	6

Trials/Electrodes	Electrode 1	Electrode 2	…	Electrode 96	Label
-	1.3	1.00	…	1.2	6
-	0.55	3.9	…	2.3	6
-	2.6	1.3	…	0.69	6

Trials/Electrodes	Electrode 1	Electrode 2	…	Electrode 96	Label
2	0.55	1.3	…	0.69	6
6	1.3	3.9	…	2.3	6
7	2.6	1.00	…	1.2	6

Figure 5.1 Training and test sets related to encoding and decoding perspectives. In the encoding perspective, a model which is trained on the correlation-blind (shuffled) set is tested on a test set which is also uncorrelated. In the decoding perspective, the model is instead tested on unseen

correlated original data. Correlation-aware training set which contains original correlated data is converted to uncorrelated set by randomly shuffling the order of trials in each column.

Figure 5.1, shows the method used in each perspective. In this diagram, single-label data is shown, but in practice, the training and test sets contain data from other labels, too. This shuffling procedure is performed separately for each stimulus (label). Each column in the resulting uncorrelated training/test set will have the same mean and variance as the correlated set, but only the order of trails differs for each electrode. Therefore, it will remove the trial-to-trial variability or noise correlations. In both perspectives, the model is built on the uncorrelated set. In the encoding perspective, it is tested on the uncorrelated data while in the decoding perspective it is tested on the original correlated data.

5.3 Results

We repeated our analyses according to the encoding perspective and compared the results with the correlation-aware and correlation-blind results. According to Figure 5.2, performance reduced by removing the correlations in all the data related to the LFPs. Thus, for any value of cortical distance or eccentricity, removing correlations yields a reduction in performance with the LFPs. The level of this reduction, however, is bigger for lower cortical distances (20-30%).

For MUA, the effect of removing noise correlations depends on the cortical distance or eccentricity. For cortical distances less than 3 mm, performance is slightly lower, while for bigger distances it is slightly higher than correlated-aware performance. With 8° separation, performance increases for lower eccentricities and decreases for bigger eccentricities.

5.4 Discussion

Although encoding and decoding perspectives are related [240], they are not tightly coupled. For example, the difference between correlation-aware and correlation-blind performance (ΔI_{diag}) can be zero, while the difference between correlation-aware and correlation-shuffled performance ($\Delta I_{shuffled}$) is non-zero. The opposite is also possible: $\Delta I_{shuffled}=0$ and $\Delta I_{diag}>0$.

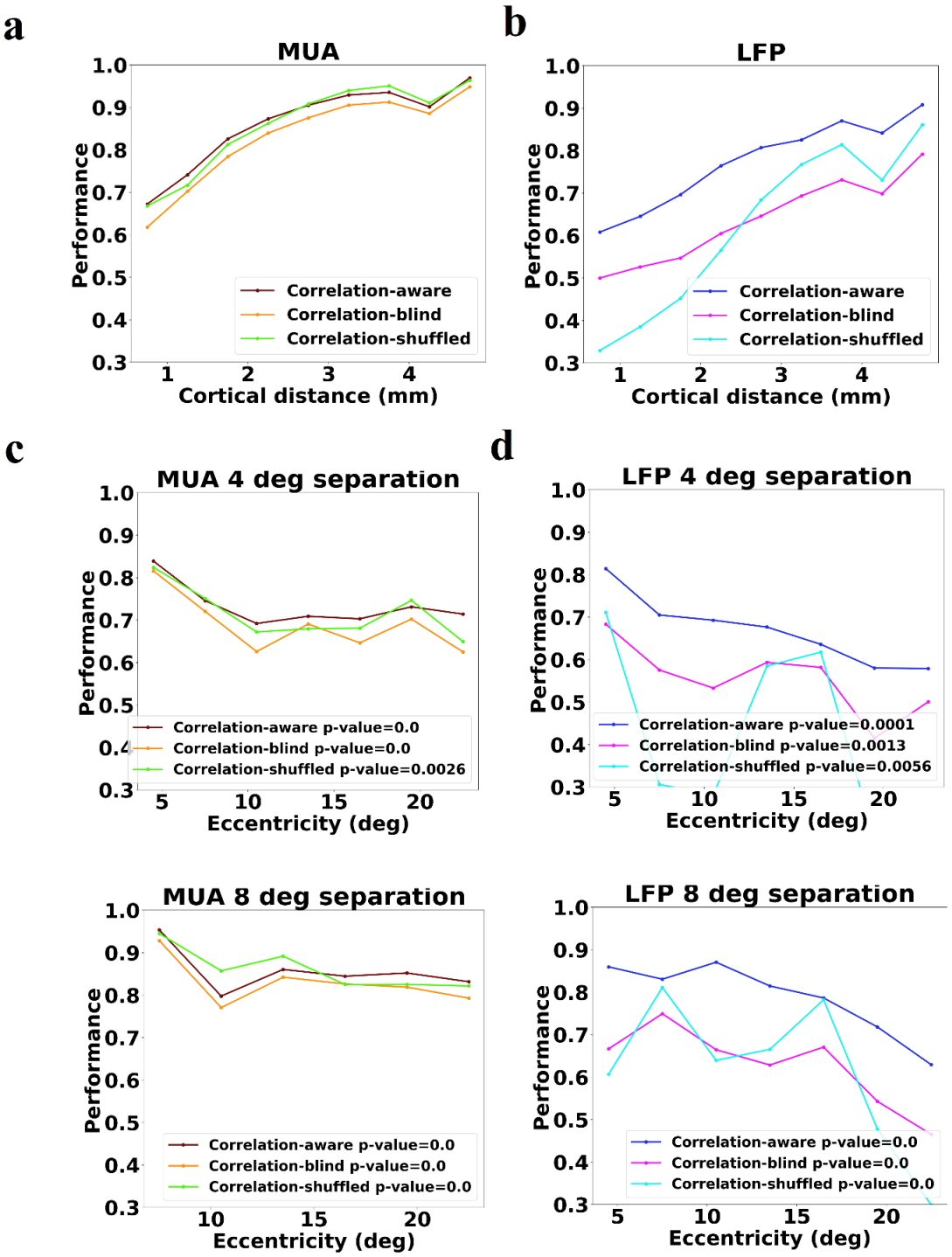

Figure 5.2 Discrimination performance results from the encoding perspective (correlation-shuffled). These results are compared with our previous results of correlation-aware and

correlation-blind performance. For the MUA data, brown, orange, and light green colors and for the LFP data, dark blue, purple, and light blue represent correlation-aware, correlation-blind, and correlation-shuffled performance respectively. Discrimination performance versus cortical distance for (a) MUA and (b) LFP. Discrimination performance versus mean eccentricity for (c) MUA and (d) LFP.

In the decoding perspective, correlation-blind decoder can never obtain higher level of performance than correlation-aware decoder. In other words, ΔI_{diag} can never be negative, because no decoder can extract more knowledge than a decoder with full knowledge of correlations. If performance of correlation-blind decoder is equal to the performance of correlation-aware decoder, knowledge of the noise correlations is not important for the decoding. But if we observe reduction in the performance, knowledge of correlations is important for the decoding.

In summary, these two quantities/perspectives address different questions, but together, both provide deeper knowledge about population codes.

CHAPTER 6 GENERAL DISCUSSION

The idea of generating a meaningful phosphenated image with cortical visual prosthetic devices has not yet truly been achieved. The main difficulty is in the activation of multiple phosphenes with specific properties. Designing a correct electrical stimulation strategy requires knowledge of how visual features are encoded in the combined neural activity.

Although most previous cortical visual prosthesis experiments have been performed in the primary visual cortex (V1), extrastriate visual areas offer sampling of a much larger region of visual space with the same coverage of the electrodes. In this project, we studied the discrimination capability of MUA and LFPs recorded from extrastriate cortical areas as key knowledge for the development of prosthetic devices.

We found that the combined responses from multiple sites in area V4, as an intermediate region in the visual processing hierarchy, has the capability for fine and coarse discrimination of positions. As we expected, cortical representation of spatial positions closer to the fovea were easier to discriminate. Therefore, for the prosthetic applications, electrodes must be implanted in the fovea representation of V4. The coding schemes used by the decoder have the potential to be used in extrastriate visual prostheses to localize phosphenes. Our electrode selection strategy was able to minimize the number of electrodes for the discrimination, and at the same time, could increase performance. The reason for this increase in the performance is that the electrode selection reduces the noise from the data by selecting the most useful features for training. This helps the model to become less overfit to the noises from the training data and to have a better generalization ability when tested with unseen data points. An interesting point about the distribution of the most important electrodes on the array is that they are not concentrated in a particular area (**Error! Reference source not found.**) of the array. It makes sense because closer electrodes have more correlated responses and the electrode selection algorithm removes redundant information by keeping one or few electrodes among a group of the close electrodes.

Reducing the number of implanted electrodes can reduce the risk of tissue injury and can help design minimally invasive prosthesis with lower physical, electrical, and thermal damage to the brain. In clinical applications with the prosthetic devices, if minimizing the number of electrodes

for microstimulation would first need information from full extent of the electrodes, we can not prevent the damage resulting from the insertion and chronic presence of the intracortical electrodes [220, 221]. However, we can prevent the damages resulting from excess charge delivery [224], chronic electrical stimulation [227, 228], and thermal effect [229] by stimulating through a much smaller set of electrodes. The set of the best electrodes may vary depending on the complexity of the task. For example, discrimination of spatial positions and discrimination of orientations might require a different set of (the best) electrodes. Therefore, we need to consider a bigger set to have a device that is applicable in various levels of perceptual complexity. We can use the same technique for stimuli of categorical nature with low to moderate complexity. For example, V4 encodes contour-based shapes [241]. Given visual stimuli with different shapes we can select electrodes that are more important in discriminating shapes. As we found from further analysis of our data, a set of 96 electrodes carries a considerable amount of redundant information. In other words, if we remove the set of the best electrodes and repeat the decoding/discrimination analysis using the remaining electrodes, the performance will still be larger than 50% (Figure A.13). An important conclusion about this result is that even if we randomly select a smaller set of electrodes, we can discriminate with an acceptable level of performance. This conclusion can help in clinical application for late blind people (acquired blindness) when determining the receptive fields is not possible.

If we can further find the set the best electrodes ahead of implantation without need to access to all electrodes, we will significantly reduce the damage resulting from the insertion and chronic presence of the intracortical electrodes. However, this needs further study, which possibly will be an unsupervised approach, to find a specific pattern in the anatomical location of the best electrodes on the cortex. Moreover, a general conclusion requires testing on several subjects. For visual prosthetic devices specifically, foveal representation is an acceptable target. Further reduction in the number of electrodes is made through the choice of implantation in the extrastriate areas.

We also found that information about position is encoded in the broadband LFP, suggesting that no band-pass filtering of LFP is required as a preprocessing step to extract spatial information.

Although several challenges need to be solved in order to build practical cortical visual prostheses, these results suggest that the discrimination capability of the implanted brain area should be considered a limiting factor. This limit differs for MUA and LFP and also for fine versus coarse

discriminations. This is specifically important when electrodes are implanted into the extrastriate cortical areas, as they introduce more restricted upper bounds in the discrimination.

Given the neural activation pattern corresponding to a percept, the development of a basic visual prosthesis also requires the following challenges to be addressed:

1) Finding mapping between microstimulation pattern and activity pattern. In other words, we need to find a function that takes as input the activity pattern and returns as output the electrical stimulation pattern. Several factors may be involved in the operation of this mapping, such as local circuitry of the implanted area, as well as feedback connections.
2) Stimulation patterns would reach larger subsets of relevant sources than natural pattern of neural signals.
3) Challenges related to blindness, such as cross-modality adaptation, change in the plasticity of visual cortex, and inability to find receptive fields.

Some suggested solutions are:

1) Preparing a comprehensive dataset by giving many different microstimulation patterns and recording induced output activity from local and distant brain regions on many subjects. Predictive models (e.g. deep neural networks) can be developed using this dataset to learn the input-output relationship.
2) As microstimulation may activate relevant and several irrelevant sources, one might need to implant electrodes in the other brain areas to control the activation pattern or might use complementary non-invasive brain stimulation such as tDCS.

CHAPTER 7 CONCLUSION AND RECOMMENDATIONS

In this PhD project, we first reviewed the challenges in creating a meaningful functional percept using cortical visual prosthetic devices and mentioned the advantages of targeting extrastriate cortical areas. Our published paper entitled, "Cortical visual prostheses: from microstimulation to functional percept" [13] covered this part. Next, we determined the spatial resolution of extrastriate cortical area V4 to find resolution limits that this area introduces for phosphene induction. This work was published as a paper entitled, “Spatial resolution of local field potential signals in macaque V4” [20].

7.1 Summary of the contributions

Our achievements in this PhD project are summarized as follows.

The capability of V4 will be higher in discriminating a pair of visual positions whose representations on the cortex is more separated. Thus, for the prosthetic devices where small separations is desirable, if close enough to the fovea center, even positions with 1° distance can be discriminated precisely. Whether we use MUA or LFP, with a small number of electrodes <10 we can achieve the same level of spatial resolution as using the whole set of the electrodes. If they are selected correctly, higher level of resolution can also be achieved. Analysis of the decoding weights showed that each electrode can precisely discriminate positions located on its receptive field flank. We found that wide band LFPs contain more information about spatial positions than the band-passed LFPs. For noise correlations, we showed that their effect was higher for LFPs than MUA. We also found that for the LFPs with uncorrelated responses, a lower level of performance is obtained. The value of noise correlations in LFPs was higher than MUA, and in both cases, decreased by increasing the distance between the electrodes.

7.2 Recommendations

The final use of visual prosthesis products is for human subjects with visual impairments. This requires comprehensive recording from human subjects, developing predictive models, and testing the model on many samples from new unseen subjects. This scheme will be a subject-wise classification that can generalize the results across the subjects. For blind people, there is no way to measure the receptive fields. Therefore, visual cortical areas should be identified based on their

anatomical landmarks and stereotactic coordinates. If the onset of blindness is after the critical period, implantation must be performed as soon as possible to prevent cross-modality adaptation. And finally, a human verbal report is needed to evaluate the performance.

An important point to be noted is that decoding frameworks usually involves determining the response from the evoked neural activity. A response measure is obtained under some assumptions about the signal and the verification of the response's ability to discriminate. However, this can introduce bias to the results, as they entail assumptions on the response measures. One way to overcome this challenge is to use all of the temporal samples of neural activity to train the decoder instead of only a single response value. This will be a more accurate approach, but needs more data and complicated models (e.g. convolutional neural networks) to accurately determine the decision boundary.

In almost all of the cortical visual prosthetic reports, the generation of phosphenated percepts is made by electrical current pulse stimulations regardless of whether an expected neural activity pattern is generated. These stimulation waveforms introduce unfamiliar neural activity to the brain that might not be processed by the subsequent brain circuits, and consequently extensive training sessions will be required to detect these unnatural activity patterns. Therefore, a significant effort is required to invent stimulation strategies that can generate pre-designed neural activity patterns corresponding to meaningful percepts.

7.3 Limitations and recommendations for improving the approach

Limitations of this work together with their recommended solutions are listed below:

- Although LFPs are more durable than MUA, they have lower spatial resolution which makes them less applicable when electrodes are implanted in the peripheral and even parafoveal areas. To obtain precise resolution with LFPs, the electrodes must be implanted in the foveal representation.
- To have a precise prediction with minimum level of overfitting many more trials must be recorded for each probe in each session. However, this is difficult for monkey to perform many more than 2000 trials (of this kind) in a session. A solution to this is to put together trials from multiple sessions. However, it will produce unreliable results with MUA as they

are not stable over sessions with a long time between them (e.g. sessions recorded in different weeks). As LFPs are more durable, trials from multiple sessions can be merged to produce better results.

- The strategy to minimize the number of electrodes was particularly reported for probe stimuli. However, for other stimuli, a different set of electrodes may be selected. Thus, for each task and stimulus type we need to repeat our analysis and select a new set. But it still can benefit from minimizing the excessive charge, thermal, and electrical damages to the tissue in microstimulation tasks. The coding strategy presented here was for the discrimination purpose. For localization, weights should be calculated by discriminating each probe from the rest of the positions.
- Existence of noise correlations improves the discrimination performance. For the prosthesis applications, some electrode arrays might be required to be implanted in other brain areas to control the effect of noise correlations. These electrodes can also be used to provide information for converting retinal coordinate to body-centered coordinate.

7.4 Future works

In this work we determined spatial resolution of MUA and LFPs in V4 and presented strategies to use less electrodes with potential benefit for microstimulation applications. However, creating a real cortical visual prosthesis still requires several further studies. The future of this work should first focus on the probe localization by discriminating each probe from the rest of probes. This provides an important knowledge for inducing a phosphene at a particular position in the visual fields. Next, a new experimental paradigm should be designed for simultaneous presentation of multiple probes each time. For example, a visual stimulus can be a pair of probes shown together and the whole experiment is designed to present every possible pair (e.g. $\binom{100}{2} = 4950$) several times in random order. This will elucidate spatiotemporal pattern of recorded neural activity required for simultaneous presentation of multiple probes which helps for creating a phosphenated image using the future prosthetic devices. Since the number of trials is big, LFPs will be more applicable because they allow combining data from many sessions each including part of the trials.

In addition to the above, generating a specific pattern of neural activity by applying a spatiotemporal pattern of microstimulation is not an easy task because activation of neurons can be distributed in an uncontrolled manner. This activation pattern depends on multiple factors such as the structure of neural circuits in the implanted brain area. Therefore, the future of this project will also need to focus on creating a predictive model to estimate microstimulation pattern for a given neural activity pattern. However, this itself requires an experimental paradigm for collecting a lot of data.

REFERENCES

[1] D. Pascolini and S. P. Mariotti, "Global estimates of visual impairment: 2010," *British Journal of Ophthalmology,* pp. 614-618, 2011.

[2] W. H. Dobelle, "Artificial vision for the blind by connecting a television camera to the visual cortex," *ASAIO J,* vol. 46, pp. 3-9, Jan-Feb 2000.

[3] L. B. Merabet, J. F. Rizzo, A. Amedi, D. C. Somers, and A. Pascual-Leone, "What blindness can tell us about seeing again: merging neuroplasticity and neuroprostheses," *Nature Reviews Neuroscience,* vol. 6, pp. 71-77, Jan 2005.

[4] D. Purves, G. J. Augustine, D. Fitzpatrick, L. C. Katz, A.-S. LaMantia, J. O. McNamara, *et al.*, "Neuroscience," *Sunderland, MA: Sinauer Associates,* vol. 3, 2001.

[5] R. K. Shepherd, M. N. Shivdasani, D. A. Nayagam, C. E. Williams, and P. J. Blamey, "Visual prostheses for the blind," *Trends Biotechnol,* vol. 31, pp. 562-571, Oct 2013.

[6] P. Troyk, M. Bak, J. Berg, D. Bradley, S. Cogan, R. Erickson, *et al.*, "A model for intracortical visual prosthesis research," *Artif Organs,* vol. 27, pp. 1005-1015, Nov 2003.

[7] D. C. Bradley, P. R. Troyk, J. A. Berg, M. Bak, S. Cogan, R. Erickson, *et al.*, "Visuotopic mapping through a multichannel stimulating implant in primate V1," *Journal of Neurophysiology,* vol. 93, pp. 1659-1670, Mar 2005.

[8] W. H. Dobelle, M. G. Mladejovsky, and J. P. Girvin., "Artificial vision for the blind: electrical stimulation of visual cortex offers hope for a functional prosthesis.," *Science,* vol. 183, pp. 440-444, 1974.

[9] E. M. Schmidt, M. J. Bak, F. T. Hambrecht, C. V. Kufta, D. K. O'rourke, and P. Vallabhanath, "Feasibility of a visual prosthesis for the blind based on intracortical micro stimulation of the visual cortex.," *Brain,* vol. 119, pp. 507-522, 1996.

[10] W. H. Dobelle and M. G. Mladejovsky, "Phosphenes produced by electrical stimulation of human occipital cortex, and their application to the development of a prosthesis for the blind.," *The Journal of physiology,* vol. 243, pp. 553-576, 1974.

[11] G. S. Brindley and W. S. Lewin, "The sensations produced by electrical stimulation of the visual cortex," *The Journal of physiology,* vol. 196, pp. 479-493, 1968.

[12] W. H. Dobelle, M. G. Mladejovsky, J. R. Evans, T. S. Roberts, and J. P. Girvin, "Braille'reading by a blind volunteer by visual cortex stimulation.," *Nature,* pp. 111-112, 1976.

[13] A. N. Foroushani, C. C. Pack, and M. Sawan, "Cortical visual prostheses: from microstimulation to functional percept," *Journal of neural engineering,* vol. 15, p. 021005, 2018.

[14] D. K. Murphey, J. H. Maunsell, M. S. Beauchamp, and D. Yoshor, "Perceiving electrical stimulation of identified human visual areas," *Proceedings of the National Academy of Sciences,* vol. 106, pp. 5389-5393, 2009.

[15] R. T. Born and D. C. Bradley, "Structure and function of visual area MT," *Annu. Rev. Neurosci.*, vol. 28, pp. 157-189, 2005.

[16] K. Britten, "The middle temporal area: Motion processing and the link to perception," *The visual neurosciences*, 2003.

[17] P. Lennie, "Single units and visual cortical organization," *Perception*, vol. 27, pp. 889-935, 1998.

[18] S. C. Chen, J. W. Morley, and S. G. Solomon, "Spatial precision of population activity in primate area MT," *Journal of neurophysiology*, vol. 114, pp. 869-878, 2015.

[19] P. J. Mineault, T. P. Zanos, and C. C. Pack, "Local field potentials reflect multiple spatial scales in V4," *Frontiers in computational neuroscience*, vol. 7, p. 21, 2013.

[20] A. N. Foroushani, S. Neupane, P. D. H. Pastor, C. Pack, and M. Sawan, "Spatial resolution of local field potential signals in macaque V4," *Journal of Neural Engineering*, 2020.

[21] K. Cha, K. Horch, and R. A. Normann, "Simulation of a phosphene-based visual field: visual acuity in a pixelized vision system," *Ann Biomed Eng*, vol. 20, pp. 439-449, 1992.

[22] E. J. Tehovnik, "Electrical stimulation of neural tissue to evoke behavioral responses," *J Neurosci Methods*, vol. 65, pp. 1-17, Mar 1996.

[23] D. J. Felleman and D. C. Van Essen, "Distributed hierarchical processing in the primate cerebral cortex," *Cereb Cortex*, vol. 1, pp. 1-47, Jan-Feb 1991.

[24] B. M. Harvey and S. O. Dumoulin, "The Relationship between Cortical Magnification Factor and Population Receptive Field Size in Human Visual Cortex: Constancies in Cortical Architecture," *Journal of Neuroscience*, vol. 31, pp. 13604-13612, Sep 21 2011.

[25] P. M. Daniel and D. Whitteridge, "The representation of the visual field on the cerebral cortex in monkeys," *J Physiol*, vol. 159, pp. 203-221, Dec 1961.

[26] R. T. Born, A. R. Trott, and T. S. Hartmann, "Cortical magnification plus cortical plasticity equals vision?," *Vision Res*, vol. 111, pp. 161-169, Jun 2015.

[27] M. Bak, J. P. Girvin, F. T. Hambrecht, C. V. Kufta, G. E. Loeb, and E. M. Schmidt, "Visual sensations produced by intracortical microstimulation of the human occipital cortex," *Med Biol Eng Comput*, vol. 28, pp. 257-259, May 1990.

[28] K. Torab, T. S. Davis, D. J. Warren, P. A. House, R. A. Normann, and B. Greger, "Multiple factors may influence the performance of a visual prosthesis based on intracortical microstimulation: nonhuman primate behavioural experimentation," *Journal of Neural Engineering*, vol. 8, Jun 2011.

[29] T. S. Davis, R. A. Parker, P. A. House, E. Bagley, S. Wendelken, R. A. Normann, *et al.*, "Spatial and temporal characteristics of V1 microstimulation during chronic implantation of a microelectrode array in a behaving macaque," *J Neural Eng*, vol. 9, Dec 2012.

[30] P. H. Schiller, W. M. Slocum, M. C. Kwak, G. L. Kendall, and E. J. Tehovnik, "New methods devised specify the size and color of the spots monkeys see when striate cortex (area V1) is electrically stimulated," *Proceedings of the National Academy of Sciences of the United States of America*, vol. 108, pp. 17809-17814, Oct 25 2011.

[31] J. Coulombe, M. Sawan, and J.-F. Gervais, "A highly flexible system for microstimulation of the visual cortex: Design and implementation," *IEEE Transactions on Biomedical Circuits and Systems,* vol. 1, pp. 258-269, 2007.

[32] M. Ghovanloo and K. Najafi, "A modular 32-site wireless neural stimulation microsystem," *IEEE Journal of Solid-State Circuits,* vol. 39, pp. 2457-2466, 2004.

[33] M. Sawan, Y. Hu, and J. Coulombe, "Wireless smart implants dedicated to multichannel monitoring and microstimulation," *IEEE Circuits and systems magazine,* vol. 5, pp. 21-39, 2005.

[34] T. Sugiura, A. U. Khan, J. Yu, Y. Takeuchi, S. Kameda, T. Kamata, *et al.*, "A programmable controller for spatio-temporal pattern stimulation of cortical visual prosthesis," in *Biomedical Circuits and Systems Conference (BioCAS)*, 2016, pp. 432-435.

[35] R. J. Greenberg, N. Talbot, P. Datta, D. Tobey, D. M. Zhou, and J. Dorn, "Cortical Visual Prosthesis," ed: Google Patents, 2016, U.S. Patent No. 8,000,000.

[36] T. Lauritzen, J. D. Dorn, R. J. Greenberg, J. M. Neysmith, N. H. Talbot, and D. D. Zhou, "Cortical visual prosthesis," ed: Google Patents, 2016, U.S. Patent No. 9,302,107.

[37] P. M. Lewis, H. M. Ackland, A. J. Lowery, and J. V. Rosenfeld, "Restoration of vision in blind individuals using bionic devices: A review with a focus on cortical visual prostheses," *Brain Research,* vol. 1595, pp. 51-73, Jan 21 2015.

[38] P. M. Lewis and J. V. Rosenfeld, "Electrical stimulation of the brain and the development of cortical visual prostheses: an historical perspective," *Brain research,* vol. 1630, pp. 208-224, 2016.

[39] E. A. DeYoe, J. D. Lewine, and R. W. Doty, "Laminar variation in threshold for detection of electrical excitation of striate cortex by macaques," *J Neurophysiol,* vol. 94, pp. 3443-3450, Nov 2005.

[40] E. J. Tehovnik, Warren M. Slocum, and Peter H. Schiller, "Saccadic eye movements evoked by microstimulation of striate cortex.," *European Journal of Neuroscience,* vol. 17, pp. 870-878, 2003.

[41] J. R. Bartlett, E. A. DeYoe, R. W. Doty, B. B. Lee, J. D. Lewine, N. Negrao, *et al.*, "Psychophysics of electrical stimulation of striate cortex in macaques," *J Neurophysiol,* vol. 94, pp. 3430-3442, Nov 2005.

[42] D. N. Rushton and G. S. Brindley, "Properties of cortical electrical phosphenes.," *Frontiers in visual science,* pp. 574-593, 1978.

[43] R. W. Doty, "Electrical stimulation of the brain in behavioral context," *Annual review of psychology,* vol. 20, pp. 289-320, 1969.

[44] D. K. Murphey and J. H. Maunsell, "Behavioral detection of electrical microstimulation in different cortical visual areas," *Current biology,* vol. 17, pp. 862-867, 2007.

[45] A. M. Ni and J. H. Maunsell, "Microstimulation reveals limits in detecting different signals from a local cortical region," *Current Biology,* vol. 20, pp. 824-828, 2010.

[46] L. D. Liu and C. C. Pack, "The contribution of area MT to visual motion perception depends on training," *Neuron,* vol. 95, pp. 436-446. e3, 2017.

[47] C. D. Salzman, C. M. Murasugi, K. H. Britten, and W. T. Newsome, "Microstimulation in visual area MT: effects on direction discrimination performance," *Journal of Neuroscience,* vol. 12, pp. 2331-2355, 1992.

[48] M. H. Histed, A. M. Ni, and J. H. Maunsell, "Insights into cortical mechanisms of behavior from microstimulation experiments," *Progress in neurobiology,* vol. 103, pp. 115-130, 2013.

[49] E. J. Tehovnik and W. M. Slocum, "What delay fields tell us about striate cortex," *Journal of Neurophysiology,* vol. 98, pp. 559-576, Aug 2007.

[50] G. S. Brindley, "Sensory Effects of Electrical Stimulation of the Visual and Paravisual Cortex in Man," *Visual Centers in the Brain. Springer Berlin Heidelberg,* pp. 583-594, 1973.

[51] A. J. Lowery, "Introducing the monash vision group's cortical prosthesis," in *Image Processing (ICIP)*, 2013, pp. 1536-1539.

[52] N. Srivastava, P. Troyk, V. Towle, D. Curry, E. Schmidt, C. Kufta, *et al.*, "Estimating phosphene maps for psychophysical experiments used in testing a cortical visual prosthesis device," in *Neural Engineering CNE'07*, 2007, pp. 130-133.

[53] P. H. Schiller, "The ON and OFF channels of the visual system.," *Trends in neurosciences,* vol. 15, pp. 86-92, 1992.

[54] E. J. Tehovnik and W. M. Slocum, "Microstimulation of macaque V1 disrupts target selection: effects of stimulation polarity," *Exp Brain Res,* vol. 148, pp. 233-237, Jan 2003.

[55] D. H. Hubel and T. N. Wiesel, "Receptive fields and functional architecture of monkey striate cortex," *J Physiol,* vol. 195, pp. 215-243, Mar 1968.

[56] E. J. Tehovnik and W. M. Slocum, "Phosphene induction by microstimulation of macaque V1," *Brain Res Rev,* vol. 53, pp. 337-343, Feb 2007.

[57] E. J. Tehovnik, W. M. Slocum, C. E. Carvey, and P. H. Schiller, "Phosphene induction and the generation of saccadic eye movements by striate cortex," *J Neurophysiol,* vol. 93, pp. 1-19, Jan 2005.

[58] T. Smith and J. Guild, "The CIE colorimetric standards and their use," *Transactions of the optical society,* vol. 33, pp. 73-134, 1931.

[59] E. J. Tehovnik, W. M. Slocum, S. M. Smirnakis, and A. S. Tolias, "Microstimulation of visual cortex to restore vision," *Progress in brain research,* vol. 175, pp. 347-375, 2009.

[60] G. Dagnelie, "Psychophysical evaluation for visual prosthesis," *Annu. Rev. Biomed. Eng.,* vol. 10, pp. 339-368, 2008.

[61] S. C. Chen, G. J. Suaning, J. W. Morley, and N. H. Lovell, "Simulating prosthetic vision: II. Measuring functional capacity," *Vision research,* vol. 49, pp. 2329-2343, 2009.

[62] J. F. Rizzo III and L. N. Ayton, "Psychophysical testing of visual prosthetic devices: a call to establish a multi-national joint task force," *Journal of neural engineering,* vol. 11, 2014.

[63] N. R. Srivastava, P. R. Troyk, and G. Dagnelie, "Detection, eye-hand coordination and virtual mobility performance in simulated vision for a cortical visual prosthesis device," *J Neural Eng,* vol. 6, Jun 2009.

[64] P. H. Schiller and E. J. Tehovnik, "Visual prosthesis," *Perception,* vol. 37, pp. 1529-1559, 2008.

[65] N. Parikh, L. Itti, M. Humayun, and J. Weiland, "Performance of visually guided tasks using simulated prosthetic vision and saliency-based cues," *Journal of neural engineering,* vol. 10, 2013.

[66] G. Dagnelie, P. Keane, V. Narla, L. Yang, J. Weiland, and M. Humayun, "Real and virtual mobility performance in simulated prosthetic vision," *J Neural Eng,* vol. 4, pp. S92-101, Mar 2007.

[67] S. M. Smirnakis, A. A. Brewer, M. C. Schmid, A. S. Tolias, A. Schuz, M. Augath, *et al.*, "Lack of long-term cortical reorganization after macaque retinal lesions," *Nature,* vol. 435, pp. 300-307, May 19 2005.

[68] J. S. Espinosa and M. P. Stryker, "Development and plasticity of the primary visual cortex," *Neuron,* vol. 75, pp. 230-249, Jul 26 2012.

[69] H. A. Baseler, A. Gouws, K. V. Haak, C. Racey, M. D. Crossland, A. Tufail, *et al.*, "Large-scale remapping of visual cortex is absent in adult humans with macular degeneration," *Nature Neuroscience,* vol. 14, pp. 649-655, May 2011.

[70] Y. M. Chino, J. H. Kaas, E. L. Smith, 3rd, A. L. Langston, and H. Cheng, "Rapid reorganization of cortical maps in adult cats following restricted deafferentation in retina," *Vision Res,* vol. 32, pp. 789-796, May 1992.

[71] C. Dariansmith and C. D. Gilbert, "Topographic Reorganization in the Striate Cortex of the Adult Cat and Monkey Is Cortically Mediated," *Journal of Neuroscience,* vol. 15, pp. 1631-1647, Mar 1995.

[72] C. D. Gilbert and T. N. Wiesel, "Receptive field dynamics in adult primary visual cortex," *Nature,* vol. 356, pp. 150-152, Mar 12 1992.

[73] J. H. Kaas, L. A. Krubitzer, Y. M. Chino, A. L. Langston, E. H. Polley, and N. Blair, "Reorganization of retinotopic cortical maps in adult mammals after lesions of the retina," *Science,* vol. 248, pp. 229-231, Apr 13 1990.

[74] J. P. Rauschecker, "Compensatory plasticity and sensory substitution in the cerebral cortex," *Trends Neurosci,* vol. 18, pp. 36-43, Jan 1995.

[75] B. Röder, W. Teder-Salejarvi, A. Sterr, F. Rosler, S. A. Hillyard, and H. J. Neville, "Improved auditory spatial tuning in blind humans," *Nature,* vol. 400, pp. 162-166, Jul 8 1999.

[76] D. Bavelier and H. J. Neville, "Cross-modal plasticity: where and how?," *Nature Rev. Neurosci.,* vol. 3, pp. 443–452, 2002.

[77] A. Amedi, N. Raz, P. Pianka, R. Malach, and E. Zohary, "Early 'visual' cortex activation correlates with superior verbal memory performance in the blind," *Nature Neuroscience,* vol. 6, pp. 758-766, Jul 2003.

[78] H. Burton, A. Z. Snyder, T. E. Conturo, E. Akbudak, J. M. Ollinger, and M. E. Raichle, "Adaptive changes in early and late blind: a fMRI study of Braille reading," *J Neurophysiol,* vol. 87, pp. 589-607, Jan 2002.

[79] E. R. Gizewski, T. Gasser, A. de Greiff, A. Boehm, and M. Forsting, "Cross-modal plasticity for sensory and motor activation patterns in blind subjects," *Neuroimage,* vol. 19, pp. 968-975, Jul 2003.

[80] A. Pascual-Leone and R. Hamilton, "The metamodal organization of the brain," *Prog Brain Res,* vol. 134, pp. 427-445, 2001.

[81] N. Sadato, A. Pascual-Leone, J. Grafman, M. P. Deiber, V. Ibanez, and M. Hallett, "Neural networks for Braille reading by the blind," *Brain,* vol. 121 (Pt 7), pp. 1213-1229, Jul 1998.

[82] N. Sadato, A. Pascual-Leone, J. Grafman, V. Ibanez, M. P. Deiber, G. Dold, *et al.*, "Activation of the primary visual cortex by Braille reading in blind subjects," *Nature,* vol. 380, pp. 526-528, Apr 11 1996.

[83] L. G. Cohen, P. Celnik, A. Pascual-Leone, B. Corwell, L. Falz, J. Dambrosia, *et al.*, "Functional relevance of cross-modal plasticity in blind humans," *Nature,* vol. 389, pp. 180-183, Sep 11 1997.

[84] R. Kupers, M. Pappens, A. M. de Noordhout, J. Schoenen, M. Ptito, and A. Fumal, "rTMS of the occipital cortex abolishes Braille reading and repetition priming in blind subjects," *Neurology,* vol. 68, pp. 691-693, 2007.

[85] L. G. Cohen, R. A. Weeks, N. Sadato, P. Celnik, K. Ishii, and M. Hallett, "Period of susceptibility for cross-modal plasticity in the blind," *Annals of neurology,* vol. 45, pp. 451-460, 1999.

[86] R. Hamilton, J. P. Keenan, M. Catala, and A. Pascual-Leone, "Alexia for Braille following bilateral occipital stroke in an early blind woman," *Neuroreport,* vol. 11, pp. 237-240, Feb 7 2000.

[87] R. Weeks, B. Horwitz, A. Aziz-Sultan, B. Tian, C. M. Wessinger, L. G. Cohen, *et al.*, "A positron emission tomographic study of auditory localization in the congenitally blind," *J Neurosci,* vol. 20, pp. 2664-2672, Apr 1 2000.

[88] B. Röder, O. Stock, S. Bien, H. Neville, and F. Rosler, "Speech processing activates visual cortex in congenitally blind humans," *Eur J Neurosci,* vol. 16, pp. 930-936, Sep 2002.

[89] A. Pascual-Leone, A. Amedi, F. Fregni, and L. B. Merabet, "The plastic human brain cortex," *Annu Rev Neurosci,* vol. 28, pp. 377-401, 2005.

[90] B. D. a. N. H. J, "Cross-modal plasticity: where and how?." *Nature Reviews Neuroscience,* vol. 3, pp. 443-452, 2002.

[91] D. S. Lee, J. S. Lee, S. H. Oh, S. K. Kim, J. W. Kim, J. K. Chung, *et al.*, "Cross-modal plasticity and cochlear implants," *Nature,* vol. 409, pp. 149-150, Jan 11 2001.

[92] E. Fernández, F. Pelayo, S. Romero, M. Bongard, C. Marin, A. Alfaro, *et al.*, "Development of a cortical visual neuroprosthesis for the blind: the relevance of neuroplasticity," *J Neural Eng,* vol. 2, pp. R1-12, Dec 2005.

[93] R. A. Normann, B. Greger, P. House, S. F. Romero, F. Pelayo, and E. Fernandez, "Toward the development of a cortically based visual neuroprosthesis," *J Neural Eng,* vol. 6, Jun 2009.

[94] R. L. Goris, J. A. Movshon, and E. P. Simoncelli, "Partitioning neuronal variability," *Nat Neurosci,* vol. 17, pp. 858-865, Jun 2014.

[95] A. Benucci, A. B. Saleem, and M. Carandini, "Adaptation maintains population homeostasis in primary visual cortex," *Nat Neurosci,* vol. 16, pp. 724-9, Jun 2013.

[96] C. Morillas, S. Romero, A. Martinez, F. Pelayo, L. Reyneri, M. Bongard, *et al.*, "A neuroengineering suite of computational tools for visual prostheses," *Neurocomputing,* vol. 70, pp. 2817-2827, Oct 2007.

[97] F. Rattay, "The basic mechanism for the electrical stimulation of the nervous system," *Neuroscience,* vol. 89, pp. 335-346, 1999.

[98] W. Gobel and F. Helmchen, "In vivo calcium imaging of neural network function," *Physiology,* vol. 22, pp. 358-365, 2007.

[99] M. H. Histed, V. Bonin, and R. C. Reid, "Direct activation of sparse, distributed populations of cortical neurons by electrical microstimulation," *Neuron,* vol. 63, pp. 508-522, 2009.

[100] I. Ferezou, F. Haiss, L. J. Gentet, R. Aronoff, B. Weber, and C. C. Petersen, "Spatiotemporal dynamics of cortical sensorimotor integration in behaving mice," *Neuron,* vol. 56, pp. 907-923, 2007.

[101] E. Seidemann, A. Arieli, A. Grinvald, and H. Slovin, "Dynamics of depolarization and hyperpolarization in the frontal cortex and saccade goal," *Science,* vol. 295, pp. 862-865, 2002.

[102] H. Asanuma, A. Arnold, and P. Zarzecki, "Further study on the excitation of pyramidal tract cells by intracortical microstimulation," *Experimental Brain Research,* vol. 26, pp. 443-461, 1976.

[103] S. Stoney, W. Thompson, and H. Asanuma, "Excitation of pyramidal tract cells by intracortical microstimulation: effective extent of stimulating current," *Journal of neurophysiology,* vol. 31, pp. 659-669, 1968.

[104] Y. Shinoda, A. Arnold, and H. Asanuma, "Spinal branching of corticospinal axons in the cat," *Experimental brain research,* vol. 26, pp. 215-234, 1976.

[105] T. Akaike, V. Fanardjian, M. Ito, M. Kumada, and H. Nakajima, "Electrophysiological analysis of the vestibulospinal reflex pathway of rabbit. I. Classification of tract cells," *Experimental brain research,* vol. 17, pp. 477-496, 1973.

[106] B. Gustafsson and E. B. Jankowska, "Direct and indirect activation of nerve cells by electrical pulses applied extracellularly," *The Journal of Physiology,* vol. 258, pp. 33-61, 1976.

[107] E. Jankowska and W. J. Roberts, "An electrophysiological demonstration of the axonal projections of single spinal interneurones in the cat," *J Physiol,* vol. 222, pp. 597-622, May 1972.

[108] D. Robinson and A. Fuchs, "Eye movements evoked by stimulation of frontal eye fields," *Journal of Neurophysiology,* pp. 637-648, 1969.

[109] J. B. Ranck, "Which elements are excited in electrical stimulation of mammalian central nervous system: a review," *Brain research,* vol. 98, pp. 417-440, 1975.

[110] A. S. Tolias, F. Sultan, M. Augath, A. Oeltermann, E. J. Tehovnik, P. H. Schiller, *et al.*, "Mapping cortical activity elicited with electrical microstimulation using FMRI in the macaque," *Neuron,* vol. 48, pp. 901-911, 2005.

[111] J. H. Maunsell and D. C. van Essen, "Topographic organization of the middle temporal visual area in the macaque monkey: representational biases and the relationship to callosal connections and myeloarchitectonic boundaries," *Journal of Comparative Neurology,* vol. 266, pp. 535-555, 1987.

[112] C. M. Murasugi, C. D. Salzman, and W. T. Newsome, "Microstimulation in visual area MT: effects of varying pulse amplitude and frequency," *Journal of Neuroscience,* vol. 13, pp. 1719-1729, 1993.

[113] N. K. Logothetis, M. Augath, Y. Murayama, A. Rauch, F. Sultan, J. Goense, *et al.*, "The effects of electrical microstimulation on cortical signal propagation," *Nature neuroscience,* vol. 13, pp. 1283-1291, 2010.

[114] M. R. Behrend, A. K. Ahuja, M. S. Humayun, J. D. Weiland, and R. H. Chow, "Selective labeling of retinal ganglion cells with calcium indicators by retrograde loading in vitro," *Journal of neuroscience methods,* vol. 179, pp. 166-172, 2009.

[115] D. K. Freeman, D. K. Eddington, J. F. Rizzo, and S. I. Fried, "Selective activation of neuronal targets with sinusoidal electric stimulation," *Journal of neurophysiology,* vol. 104, pp. 2778-2791, 2010.

[116] S. Butovas and C. Schwarz, "Spatiotemporal effects of microstimulation in rat neocortex: a parametric study using multielectrode recordings," *Journal of neurophysiology,* vol. 90, pp. 3024-3039, 2003.

[117] A. R. Houweling and M. Brecht, "Behavioural report of single neuron stimulation in somatosensory cortex," *Nature,* vol. 451, p. 65, 2008.

[118] D. Huber, L. Petreanu, N. Ghitani, S. Ranade, T. Hromádka, Z. Mainen, *et al.*, "Sparse optical microstimulation in barrel cortex drives learned behaviour in freely moving mice," *Nature,* vol. 450, pp. 61-64, 2007.

[119] S. Joucla and B. Yvert, "Modeling extracellular electrical neural stimulation: from basic understanding to MEA-based applications," *Journal of Physiology-Paris,* vol. 106, pp. 146-158, 2012.

[120] F. Rattay and C. Wenger, "Which elements of the mammalian central nervous system are excited by low current stimulation with microelectrodes?," *Neuroscience,* vol. 170, pp. 399-407, 2010.

[121] H. Meffin, B. Tahayori, E. N. Sergeev, I. M. Mareels, D. B. Grayden, and A. N. Burkitt, "Modelling extracellular electrical stimulation: III. Derivation and interpretation of neural tissue equations," *Journal of neural engineering,* vol. 11, 2014.

[122] C. Overstreet, J. Klein, and S. H. Tillery, "Computational modeling of direct neuronal recruitment during intracortical microstimulation in somatosensory cortex," *Journal of neural engineering,* vol. 10, 2013.

[123] L. Manola, J. Holsheimer, P. Veltink, and J. R. Buitenweg, "Anodal vs cathodal stimulation of motor cortex: a modeling study," *Clinical neurophysiology,* vol. 118, pp. 464-474, 2007.

[124] C. C. McIntyre and W. M. Grill, "Selective microstimulation of central nervous system neurons," *Annals of biomedical engineering,* vol. 28, pp. 219-233, 2000.

[125] Q. Wang, D. C. Millard, H. J. Zheng, and G. B. Stanley, "Voltage-sensitive dye imaging reveals improved topographic activation of cortex in response to manipulation of thalamic microstimulation parameters," *Journal of neural engineering,* vol. 9, 2012.

[126] B. A. Bari, D. R. Ollerenshaw, D. C. Millard, Q. Wang, and G. B. Stanley, "Behavioral and electrophysiological effects of cortical microstimulation parameters," *PloS one,* vol. 8, 2013.

[127] M. Abramian, N. H. Lovell, A. Habib, J. W. Morley, G. J. Suaning, and S. Dokos, "Quasi-monopolar electrical stimulation of the retina: a computational modelling study," *Journal of neural engineering,* vol. 11, 2014.

[128] H. Lorach, G. Goetz, Y. Mandel, X. Lei, T. I. Kamins, K. Mathieson, *et al.*, "Performance of photovoltaic arrays in-vivo and characteristics of prosthetic vision in animals with retinal degeneration," *Vision research,* vol. 111, pp. 142-148, 2015.

[129] K. Mathieson, J. Loudin, G. Goetz, P. Huie, L. Wang, T. I. Kamins, *et al.*, "Photovoltaic retinal prosthesis with high pixel density," *Nature photonics,* vol. 6, pp. 391-397, 2012.

[130] P. B. Matteucci, S. C. Chen, D. Tsai, C. W. Dodds, S. Dokos, J. W. Morley, *et al.*, "Current steering in retinal stimulation via a quasimonopolar stimulation paradigmquasimonopolar retinal stimulation paradigm," *Investigative ophthalmology & visual science,* vol. 54, pp. 4307-4320, 2013.

[131] L. Wang, K. Mathieson, T. I. Kamins, J. D. Loudin, L. Galambos, G. Goetz, *et al.*, "Photovoltaic retinal prosthesis: implant fabrication and performance," *Journal of neural engineering,* vol. 9, 2012.

[132] J. Loudin, D. Simanovskii, K. Vijayraghavan, C. Sramek, A. Butterwick, P. Huie, *et al.*, "Optoelectronic retinal prosthesis: system design and performance," *Journal of neural engineering,* vol. 4, 2007.

[133] L. H. Jepson, P. Hottowy, K. Mathieson, D. E. Gunning, W. Dąbrowski, A. M. Litke, *et al.*, "Spatially patterned electrical stimulation to enhance resolution of retinal prostheses," *Journal of Neuroscience,* vol. 34, pp. 4871-4881, 2014.

[134] C. Sekirnjak, P. Hottowy, A. Sher, W. Dabrowski, A. M. Litke, and E. Chichilnisky, "High-resolution electrical stimulation of primate retina for epiretinal implant design," *Journal of Neuroscience,* vol. 28, pp. 4446-4456, 2008.

[135] M. Sahin and Y. Tie, "Non-rectangular waveforms for neural stimulation with practical electrodes," *Journal of neural engineering,* vol. 4, pp. 227-233, 2007.

[136] N. I. Krouchev, S. M. Danner, A. Vinet, F. Rattay, and M. Sawan, "Energy-optimal electrical-stimulation pulses shaped by the least-action principle," *PloS one,* vol. 9, 2014.

[137] J. M. Rebesco, I. H. Stevenson, K. P. Körding, S. A. Solla, and L. E. Miller, "Rewiring neural interactions by micro-stimulation," *Frontiers in systems neuroscience,* vol. 4, 2010.

[138] W. Song, C. C. Kerr, W. W. Lytton, and J. T. Francis, "Cortical plasticity induced by spike-triggered microstimulation in primate somatosensory cortex," *PloS one,* vol. 8, 2013.

[139] J. D. Weiland, S. T. Walston, and M. S. Humayun, "Electrical stimulation of the retina to produce artificial vision," *Annual review of vision science,* vol. 2, pp. 273-294, 2016.

[140] P. Twyford and S. Fried, "The retinal response to sinusoidal electrical stimulation," *IEEE Transactions on Neural Systems and Rehabilitation Engineering,* vol. 24, pp. 413-423, 2016.

[141] G. A. Orban, "Higher order visual processing in macaque extrastriate cortex," *Physiological reviews,* vol. 88, pp. 59-89, 2008.

[142] M. Mishkin and L. G. Ungerleider, "Contribution of striate inputs to the visuospatial functions of parieto-preoccipital cortex in monkeys," *Behavioural brain research,* vol. 6, pp. 57-77, 1982.

[143] E. T. Carlson, R. J. Rasquinha, K. Zhang, and C. E. Connor, "A sparse object coding scheme in area V4," *Current Biology,* vol. 21, pp. 288-293, 2011.

[144] K. Tsunoda, Y. Yamane, M. Nishizaki, and M. Tanifuji, "Complex objects are represented in macaque inferotemporal cortex by the combination of feature columns," *Nature neuroscience,* vol. 4, p. 832, 2001.

[145] S.-R. Afraz, R. Kiani, and H. Esteky, "Microstimulation of inferotemporal cortex influences face categorization," *Nature,* vol. 442, pp. 692-695, 2006.

[146] T. Yang and J. H. Maunsell, "The effect of perceptual learning on neuronal responses in monkey visual area V4," *Journal of Neuroscience,* vol. 24, pp. 1617-1626, 2004.

[147] C. J. Duffy, "MST neurons respond to optic flow and translational movement," *Journal of neurophysiology,* vol. 80, pp. 1816-1827, 1998.

[148] Y. Gu, G. C. DeAngelis, and D. E. Angelaki, "Causal links between dorsal medial superior temporal area neurons and multisensory heading perception," *Journal of Neuroscience,* vol. 32, pp. 2299-2313, 2012.

[149] P. J. Mineault, F. A. Khawaja, D. A. Butts, and C. C. Pack, "Hierarchical processing of complex motion along the primate dorsal visual pathway," *Proceedings of the National Academy of Sciences,* vol. 109, pp. E972-E980, 2012.

[150] T. Aflalo, S. Kellis, C. Klaes, B. Lee, Y. Shi, K. Pejsa, *et al.*, "Decoding motor imagery from the posterior parietal cortex of a tetraplegic human," *Science,* vol. 348, pp. 906-910, 2015.

[151] M. S. Beauchamp, D. Oswalt, P. Sun, B. L. Foster, J. F. Magnotti, S. Niketeghad, *et al.*, "Dynamic Stimulation of Visual Cortex Produces Form Vision in Sighted and Blind Humans," *Cell,* vol. 181, pp. 774-783. e5, 2020.

[152] A. B. Graf, A. Kohn, M. Jazayeri, and J. A. Movshon, "Decoding the activity of neuronal populations in macaque primary visual cortex," *Nat Neurosci,* vol. 14, pp. 239-45, Feb 2011.

[153] E. M. Meyers, D. J. Freedman, G. Kreiman, E. K. Miller, and T. Poggio, "Dynamic population coding of category information in inferior temporal and prefrontal cortex," *Journal of neurophysiology,* vol. 100, pp. 1407-1419, 2008.

[154] R. Q. Quiroga, L. H. Snyder, A. P. Batista, H. Cui, and R. A. Andersen, "Movement intention is better predicted than attention in the posterior parietal cortex," *Journal of neuroscience,* vol. 26, pp. 3615-3620, 2006.

[155] C. Cortes and V. Vapnik, "Support-vector networks," *Machine learning,* vol. 20, pp. 273-297, 1995.

[156] R. Kohavi, "A study of cross-validation and bootstrap for accuracy estimation and model selection," in *Ijcai*, 1995, pp. 1137-1145.

[157] C.-W. Hsu, C.-C. Chang, and C.-J. Lin, "A practical guide to support vector classification," 2003.

[158] T. Fawcett, "An introduction to ROC analysis," *Pattern recognition letters,* vol. 27, pp. 861-874, 2006.

[159] P. Daniel and D. Whitteridge, "The representation of the visual field on the cerebral cortex in monkeys," *The Journal of physiology,* vol. 159, pp. 203-221, 1961.

[160] R. Gattass, A. Sousa, and C. Gross, "Visuotopic organization and extent of V3 and V4 of the macaque," *Journal of Neuroscience,* vol. 8, pp. 1831-1845, 1988.

[161] M. A. Smith and A. Kohn, "Spatial and temporal scales of neuronal correlation in primary visual cortex," *J Neurosci,* vol. 28, pp. 12591-603, Nov 26 2008.

[162] M. R. Cohen and A. Kohn, "Measuring and interpreting neuronal correlations," *Nat Neurosci,* vol. 14, pp. 811-9, Jul 2011.

[163] E. Zohary, M. N. Shadlen, and W. T. Newsome, "Correlated neuronal discharge rate and its implications for psychophysical performance," *Nature,* vol. 370, p. 140, 1994.

[164] S. C. Chen, G. J. Suaning, J. W. Morley, and N. H. Lovell, "Simulating prosthetic vision: I. Visual models of phosphenes," *Vision research,* vol. 49, pp. 1493-1506, 2009.

[165] R. A. Normann, B. A. Greger, P. House, S. F. Romero, F. Pelayo, and E. Fernandez, "Toward the development of a cortically based visual neuroprosthesis," *Journal of neural engineering,* vol. 6, p. 035001, 2009.

[166] E. Schmidt, M. Bak, F. Hambrecht, C. Kufta, D. O'rourke, and P. Vallabhanath, "Feasibility of a visual prosthesis for the blind based on intracortical micro stimulation of the visual cortex," *Brain,* vol. 119, pp. 507-522, 1996.

[167] M. Bak, J. Girvin, F. Hambrecht, C. Kufta, G. Loeb, and E. Schmidt, "Visual sensations produced by intracortical microstimulation of the human occipital cortex," *Medical and Biological Engineering and Computing,* vol. 28, pp. 257-259, 1990.

[168] K. Torab, T. Davis, D. Warren, P. House, R. Normann, and B. Greger, "Multiple factors may influence the performance of a visual prosthesis based on intracortical microstimulation: nonhuman primate behavioural experimentation," *Journal of neural engineering,* vol. 8, p. 035001, 2011.

[169] P. Troyk, M. Bak, J. Berg, D. Bradley, S. Cogan, R. Erickson, *et al.*, "A model for intracortical visual prosthesis research," *Artificial organs,* vol. 27, pp. 1005-1015, 2003.

[170] D. C. Bradley, P. R. Troyk, J. A. Berg, M. Bak, S. Cogan, R. Erickson, *et al.*, "Visuotopic mapping through a multichannel stimulating implant in primate V1," *Journal of neurophysiology,* vol. 93, pp. 1659-1670, 2005.

[171] T. Davis, R. Parker, P. House, E. Bagley, S. Wendelken, R. Normann, *et al.*, "Spatial and temporal characteristics of V1 microstimulation during chronic implantation of a microelectrode array in a behaving macaque," *Journal of neural engineering,* vol. 9, p. 065003, 2012.

[172] E. J. Tehovnik and W. M. Slocum, "Microstimulation of macaque V1 disrupts target selection: effects of stimulation polarity," *Experimental brain research,* vol. 148, pp. 233-237, 2003.

[173] E. J. Tehovnik, W. M. Slocum, and P. H. Schiller, "Differential effects of laminar stimulation of V1 cortex on target selection by macaque monkeys," *European Journal of Neuroscience,* vol. 16, pp. 751-760, 2002.

[174] W. H. Bosking, P. Sun, M. Ozker, X. Pei, B. L. Foster, M. S. Beauchamp, *et al.*, "Saturation in phosphene size with increasing current levels delivered to human visual cortex," *Journal of Neuroscience,* vol. 37, pp. 7188-7197, 2017.

[175] A. Pouget, P. Dayan, and R. S. Zemel, "Inference and computation with population codes," *Annual Review of Neuroscience,* vol. 26, pp. 381-410, 2003.

[176] M. Jazayeri and J. A. Movshon, "Optimal representation of sensory information by neural populations," *Nature Neuroscience,* vol. 9, pp. 690-696, May 2006.

[177] A. Kohn and M. A. Smith, "Stimulus dependence of neuronal correlation in primary visual cortex of the macaque," *J Neurosci,* vol. 25, pp. 3661-73, Apr 6 2005.

[178] A. Belitski, A. Gretton, C. Magri, Y. Murayama, M. A. Montemurro, N. K. Logothetis, *et al.*, "Low-frequency local field potentials and spikes in primary visual cortex convey independent visual information," *J Neurosci,* vol. 28, pp. 5696-709, May 28 2008.

[179] I. Nauhaus, L. Busse, M. Carandini, and D. L. Ringach, "Stimulus contrast modulates functional connectivity in visual cortex," *Nat Neurosci,* vol. 12, pp. 70-6, Jan 2009.

[180] S. Ray and J. H. R. Maunsell, "Differences in Gamma Frequencies across Visual Cortex Restrict Their Possible Use in Computation," *Neuron,* vol. 67, pp. 885-896, Sep 9 2010.

[181] M. Besserve, S. C. Lowe, N. K. Logothetis, B. Scholkopf, and S. Panzeri, "Shifts of Gamma Phase across Primary Visual Cortical Sites Reflect Dynamic Stimulus-Modulated Information Transfer," *PLoS Biol,* vol. 13, p. e1002257, 2015.

[182] S. Ray and J. H. Maunsell, "Network rhythms influence the relationship between spike-triggered local field potential and functional connectivity," *Journal of Neuroscience,* vol. 31, pp. 12674-12682, 2011.

[183] N. Ramalingam, J. N. McManus, W. Li, and C. D. Gilbert, "Top-down modulation of lateral interactions in visual cortex," *Journal of Neuroscience,* vol. 33, pp. 1773-1789, 2013.

[184] J. M. McFarland, A. G. Bondy, B. G. Cumming, and D. A. Butts, "High-resolution eye tracking using V1 neuron activity," *Nature communications,* vol. 5, p. 4605, 2014.

[185] B. Lima, W. Singer, N. H. Chen, and S. Neuenschwander, "Synchronization Dynamics in Response to Plaid Stimuli in Monkey V1," *Cerebral Cortex,* vol. 20, pp. 1556-1573, Jul 2010.

[186] X. Yue, I. S. Pourladian, R. B. Tootell, and L. G. Ungerleider, "Curvature-processing network in macaque visual cortex," *Proceedings of the National Academy of Sciences,* vol. 111, pp. E3467-E3475, 2014.

[187] A. Pasupathy and C. E. Connor, "Responses to contour features in macaque area V4," *Journal of Neurophysiology,* vol. 82, pp. 2490-2502, 1999.

[188] V. Gilja, C. A. Chestek, I. Diester, J. M. Henderson, K. Deisseroth, and K. V. Shenoy, "Challenges and opportunities for next-generation intracortically based neural prostheses," *IEEE Transactions on Biomedical Engineering,* vol. 58, pp. 1891-1899, 2011.

[189] B. Pesaran, J. S. Pezaris, M. Sahani, P. P. Mitra, and R. A. Andersen, "Temporal structure in neuronal activity during working memory in macaque parietal cortex," *Nature neuroscience,* vol. 5, p. 805, 2002.

[190] H. Scherberger, M. R. Jarvis, and R. A. Andersen, "Cortical local field potential encodes movement intentions in the posterior parietal cortex," *Neuron,* vol. 46, pp. 347-354, 2005.

[191] A. Kandel and G. Buzsáki, "Cellular–synaptic generation of sleep spindles, spike-and-wave discharges, and evoked thalamocortical responses in the neocortex of the rat," *Journal of Neuroscience,* vol. 17, pp. 6783-6797, 1997.

[192] C. E. Schroeder, A. D. Mehta, and S. J. Givre, "A spatiotemporal profile of visual system activation revealed by current source density analysis in the awake macaque," *Cerebral cortex (New York, NY: 1991),* vol. 8, pp. 575-592, 1998.

[193] U. Mitzdorf, "Current source-density method and application in cat cerebral cortex: investigation of evoked potentials and EEG phenomena," *Physiological reviews,* vol. 65, pp. 37-100, 1985.

[194] M. Okun, A. Naim, and I. Lampl, "The subthreshold relation between cortical local field potential and neuronal firing unveiled by intracellular recordings in awake rats," *Journal of neuroscience,* vol. 30, pp. 4440-4448, 2010.

[195] G. Buzsáki, C. A. Anastassiou, and C. Koch, "The origin of extracellular fields and currents—EEG, ECoG, LFP and spikes," *Nature reviews neuroscience,* vol. 13, p. 407, 2012.

[196] S. Katzner, I. Nauhaus, A. Benucci, V. Bonin, D. L. Ringach, and M. Carandini, "Local origin of field potentials in visual cortex," *Neuron,* vol. 61, pp. 35-41, 2009.

[197] D. Xing, C.-I. Yeh, and R. M. Shapley, "Spatial spread of the local field potential and its laminar variation in visual cortex," *Journal of neuroscience,* vol. 29, pp. 11540-11549, 2009.

[198] S. Venkatraman and J. M. Carmena, "Behavioral modulation of stimulus-evoked oscillations in barrel cortex of alert rats," *Frontiers in integrative neuroscience,* vol. 3, p. 10, 2009.

[199] K. J. Otto, P. J. Rousche, and D. R. Kipke, "Cortical microstimulation in auditory cortex of rat elicits best-frequency dependent behaviors," *Journal of neural engineering,* vol. 2, p. 42, 2005.

[200] N. K. Logothetis, M. Augath, Y. Murayama, A. Rauch, F. Sultan, J. Goense, *et al.*, "The effects of electrical microstimulation on cortical signal propagation," *Nature neuroscience,* vol. 13, p. 1283, 2010.

[201] M. B. Voigt, P. A. Yusuf, and A. Kral, "Intracortical microstimulation modulates cortical induced responses," *Journal of Neuroscience,* vol. 38, pp. 7774-7786, 2018.

[202] W. H. Dobelle, "Artificial vision for the blind by connecting a television camera to the visual cortex," *ASAIO journal,* vol. 46, pp. 3-9, 2000.

[203] W. Dobelle and M. Mladejovsky, "Phosphenes produced by electrical stimulation of human occipital cortex, and their application to the development of a prosthesis for the blind," *The Journal of physiology,* vol. 243, pp. 553-576, 1974.

[204] W. H. Dobelle, M. Mladejovsky, and J. Girvin, "Artificial vision for the blind: electrical stimulation of visual cortex offers hope for a functional prosthesis," *Science,* vol. 183, pp. 440-444, 1974.

[205] G. S. Brindley and W. Lewin, "The sensations produced by electrical stimulation of the visual cortex," *The Journal of physiology,* vol. 196, pp. 479-493, 1968.

[206] T. P. Zanos, P. J. Mineault, K. T. Nasiotis, D. Guitton, and C. C. Pack, "A sensorimotor role for traveling waves in primate visual cortex," *Neuron,* vol. 85, pp. 615-627, 2015.

[207] G. M. Ghose and D. Y. Ts' O, "Form processing modules in primate area V4," *Journal of Neurophysiology,* vol. 77, pp. 2191-2196, 1997.

[208] T. P. Zanos, P. J. Mineault, and C. C. Pack, "Removal of spurious correlations between spikes and local field potentials," *Journal of neurophysiology,* vol. 105, pp. 474-486, 2011.

[209] R. Q. Quiroga, Z. Nadasdy, and Y. Ben-Shaul, "Unsupervised spike detection and sorting with wavelets and superparamagnetic clustering," *Neural Computation,* vol. 16, pp. 1661-1687, Aug 2004.

[210] S. Neupane, D. Guitton, and C. C. Pack, "Two distinct types of remapping in primate cortical area V4," *Nature communications,* vol. 7, 2016.

[211] T. Joachims, "Making large-scale SVM learning practical," Technical report, SFB 475: Komplexitätsreduktion in Multivariaten …1998.

[212] V. Vapnik, *The nature of statistical learning theory*: Springer science & business media, 2013.

[213] I. Guyon, J. Weston, S. Barnhill, and V. Vapnik, "Gene selection for cancer classification using support vector machines," *Machine learning,* vol. 46, pp. 389-422, 2002.

[214] D. Arthur and S. Vassilvitskii, "k-means++: The advantages of careful seeding," in *Proceedings of the eighteenth annual ACM-SIAM symposium on Discrete algorithms*, 2007, pp. 1027-1035.

[215] M. A. Smith and M. A. Sommer, "Spatial and temporal scales of neuronal correlation in visual area V4," *Journal of Neuroscience,* vol. 33, pp. 5422-5432, 2013.

[216] M. M. Churchland, M. Y. Byron, J. P. Cunningham, L. P. Sugrue, M. R. Cohen, G. S. Corrado, *et al.*, "Stimulus onset quenches neural variability: a widespread cortical phenomenon," *Nature neuroscience,* vol. 13, p. 369, 2010.

[217] D. A. Gutnisky and V. Dragoi, "Adaptive coding of visual information in neural populations," *Nature,* vol. 452, p. 220, 2008.

[218] G. Purushothaman and D. C. Bradley, "Neural population code for fine perceptual decisions in area MT," *Nature neuroscience,* vol. 8, p. 99, 2005.

[219] T. Hastie, R. Tibshirani, J. Friedman, and J. Franklin, "The elements of statistical learning: data mining, inference and prediction," *The Mathematical Intelligencer,* vol. 27, pp. 83-85, 2005.

[220] R. Biran, D. C. Martin, and P. A. Tresco, "Neuronal cell loss accompanies the brain tissue response to chronically implanted silicon microelectrode arrays," *Experimental neurology,* vol. 195, pp. 115-126, 2005.

[221] D. J. Edell, V. V. Toi, V. M. McNeil, and L. Clark, "Factors influencing the biocompatibility of insertable silicon microshafts in cerebral cortex," *IEEE Transactions on biomedical engineering,* vol. 39, pp. 635-643, 1992.

[222] C. Bjornsson, S. J. Oh, Y. Al-Kofahi, Y. Lim, K. Smith, J. Turner, *et al.*, "Effects of insertion conditions on tissue strain and vascular damage during neuroprosthetic device insertion," *Journal of neural engineering,* vol. 3, p. 196, 2006.

[223] P. A. House, J. D. MacDonald, P. A. Tresco, and R. A. Normann, "Acute microelectrode array implantation into human neocortex: preliminary technique and histological considerations," *Neurosurgical focus,* vol. 20, pp. 1-4, 2006.

[224] S. Brummer, L. Robblee, and F. Hambrecht, "Criteria for selecting electrodes for electrical stimulation: theoretical and practical considerations," *Annals of the New York Academy of Sciences,* vol. 405, pp. 159-171, 1983.

[225] J. R. Bartlett, R. W. Doty sr, B. B. Lee, N. Negrão, and W. H. Overman jr, "Deleterious effects of prolonged electrical excitation of striate cortex in macaques," *Brain, behavior and evolution,* vol. 14, pp. 46-66, 1977.

[226] D. McCreery, W. Agnew, T. Yuen, and L. Bullara, "Comparison of neural damage induced by electrical stimulation with faradaic and capacitor electrodes," *Annals of biomedical engineering,* vol. 16, pp. 463-481, 1988.

[227] D. McCreery, V. Pikov, and P. R. Troyk, "Neuronal loss due to prolonged controlled-current stimulation with chronically implanted microelectrodes in the cat cerebral cortex," *Journal of neural engineering,* vol. 7, p. 036005, 2010.

[228] D. B. McCreery, W. F. Agnew, T. G. Yuen, and L. Bullara, "Charge density and charge per phase as cofactors in neural injury induced by electrical stimulation," *IEEE Transactions on Biomedical Engineering,* vol. 37, pp. 996-1001, 1990.

[229] R. J. Coffey, R. Kalin, and J. M. Olsen, "Magnetic resonance imaging conditionally safe neurostimulation leads: investigation of the maximum safe lead tip temperature," *Neurosurgery,* vol. 74, pp. 215-225, 2013.

[230] Y. Bengio, A. Courville, and P. Vincent, "Representation learning: a review and new perspectives," *IEEE Trans Pattern Anal Mach Intell,* vol. 35, pp. 1798-828, Aug 2013.

[231] Y. LeCun, Y. Bengio, and G. Hinton, "Deep learning," *Nature,* vol. 521, pp. 436-444, 2015.

[232] D. K. Murphey, J. H. Maunsell, M. S. Beauchamp, and D. Yoshor, "Perceiving electrical stimulation of identified human visual areas," *Proc Natl Acad Sci U S A,* vol. 106, pp. 5389-93, Mar 31 2009.

[233] M. S. Beauchamp, W. Bosking, P. Sun, B. Foster, S. Niketeghad, N. Pouratian, *et al.*, "Dynamic Electrical Stimulation of Sites in Visual Cortex Produces Form Vision in Sighted and Blind Humans," *bioRxiv,* p. 462697, 2018.

[234] G. P. Moore, J. P. Segundo, D. H. Perkel, and H. Levitan, "Statistical signs of synaptic interaction in neurons," *Biophysical journal,* vol. 10, pp. 876-900, 1970.

[235] W. W. Lytton and T. J. Sejnowski, "Simulations of cortical pyramidal neurons synchronized by inhibitory interneurons," *Journal of Neurophysiology,* vol. 66, pp. 1059-1079, 1991.

[236] A. Arieli, A. Sterkin, A. Grinvald, and A. Aertsen, "Dynamics of ongoing activity: explanation of the large variability in evoked cortical responses," *Science,* vol. 273, pp. 1868-1871, 1996.

[237] M. Tsodyks, T. Kenet, A. Grinvald, and A. Arieli, "Linking spontaneous activity of single cortical neurons and the underlying functional architecture," *Science,* vol. 286, pp. 1943-1946, 1999.

[238] J. Fiser, C. Chiu, and M. Weliky, "Small modulation of ongoing cortical dynamics by sensory input during natural vision," *Nature,* vol. 431, p. 573, 2004.

[239] B. B. Averbeck, P. E. Latham, and A. Pouget, "Neural correlations, population coding and computation," *Nat Rev Neurosci,* vol. 7, pp. 358-66, May 2006.

[240] B. B. Averbeck and D. Lee, "Effects of noise correlations on information encoding and decoding," *Journal of neurophysiology,* vol. 95, pp. 3633-3644, 2006.

[241] B. N. Bushnell, P. J. Harding, Y. Kosai, and A. Pasupathy, "Partial occlusion modulates contour-based shape encoding in primate area V4," *Journal of Neuroscience,* vol. 31, pp. 4012-4024, 2011.

APPENDIX A SUPPLEMENTARY MATERIAL FOR CHAPTER 4

In this section we have presented supplementary material for chapter 4 which includes further analysis results.

Results of Fixation on Upper Middle Dot

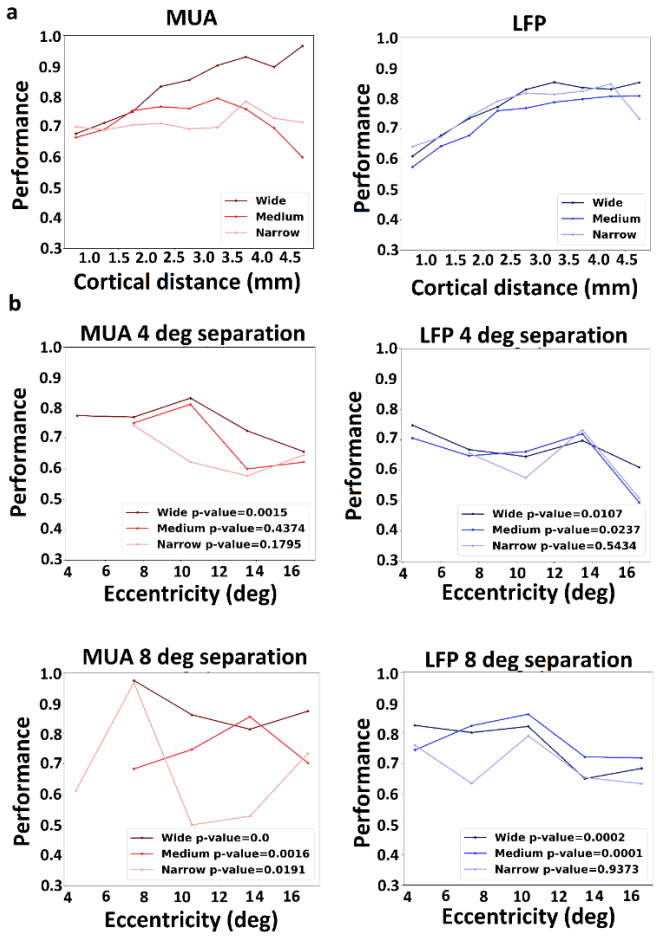

Figure A.1 V4 ensemble response allows spatial discrimination. Darker colors correspond to the wider response windows. The linear SVM was used for classification of the response data. The performances are validation scores of 5-fold cross validation measured as the area under the ROC curve. (a) Discrimination performance versus cortical distance (in mm) for MUA in red (left) and LFP in blue (right) based on responses defined on wide, medium, and narrow windows (darker to lighter). The cortical distance values are divided into 0.5 mm bins and the discrimination performances of pairs with cortical distances within each bin were averaged. (b) Discrimination

performances of pairs with 4° and 8° separation distances as a function of pairs' eccentricity (in deg) for MUA (left) and LFP (right) for responses defined over wide, medium, and narrow windows. Significance (p-values) of correlation between performance and eccentricity for each response window is presented in the plot. Eccentricity values are divided into 3° bins and the discrimination performances of pairs with eccentricity within each bin were averaged.

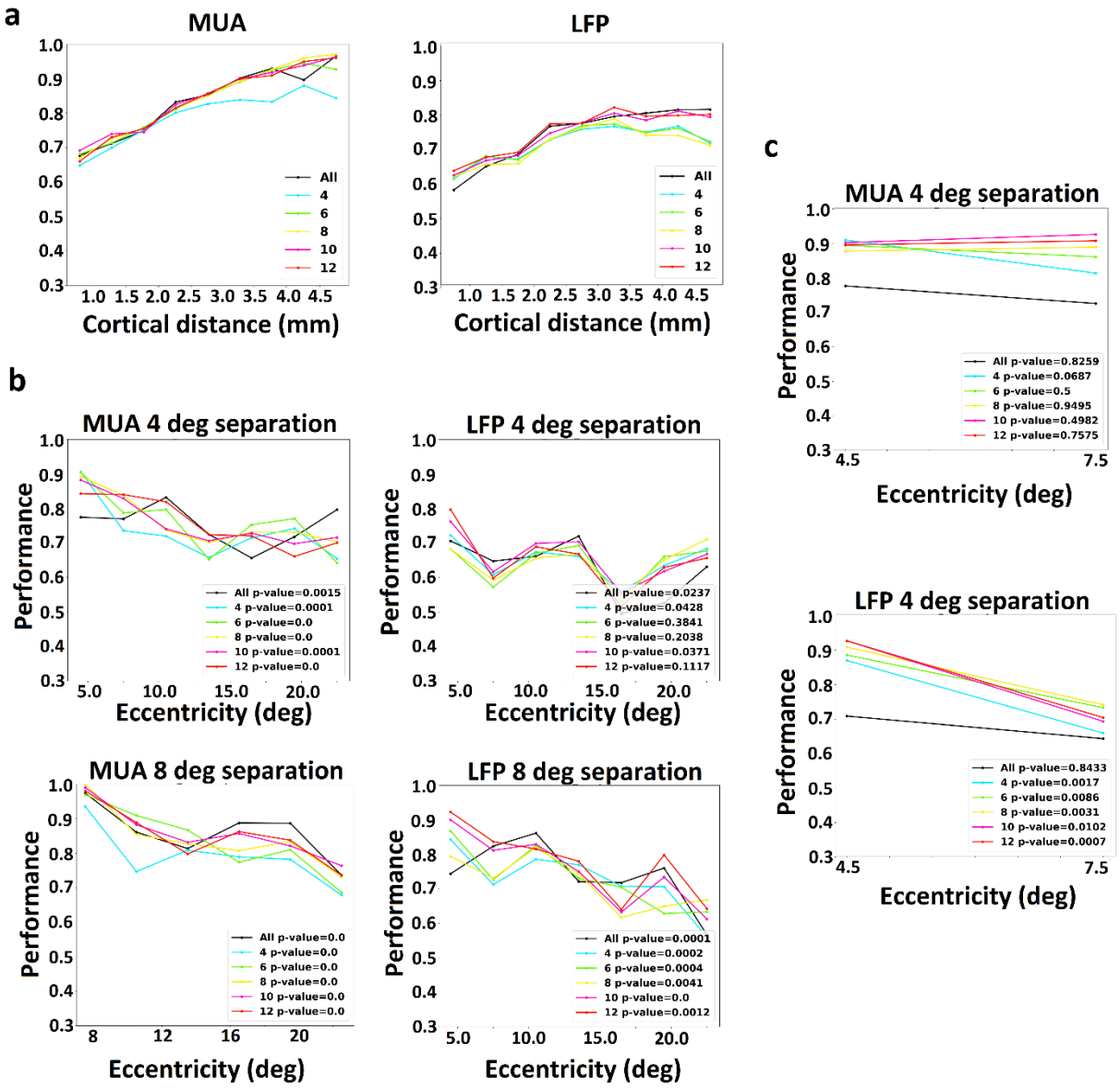

Figure A.2 Results of discrimination analysis with the best (most important) 4 (blue), 6 (green), 8 (yellow), 10 (purple), and 12 (red) electrodes. Discrimination performance using all the

electrodes is shown in black. (a) Discrimination performance versus cortical distance (in millimeters) for MUA (left) and LFP (right) with different sets of the best electrodes. The cortical distance values are divided into 0.5 mm bins and the discrimination performances of pairs with cortical distances within each bin were averaged. (b) Discrimination of probes with 4° (top) and 8° (bottom) separation versus the mean eccentricity of the pairs in visual degrees using the same sets of the best electrodes as (a). MUA results are presented on the left and LFP on the right. Pearson correlation significance (p-values) are presented on each plot associated to the results obtained with each electrode set. Eccentricity values are divided into 3° bins and the discrimination performances of pairs with eccentricity within each bin were averaged. (c) Selecting the best electrodes using importance values obtained by averaging over discriminations with 4° probe separation and <8° pairs eccentricity. The electrodes were sorted by these new importance values. As only the closer eccentricities were important, the plots are illustrated for smaller range of eccentricities.

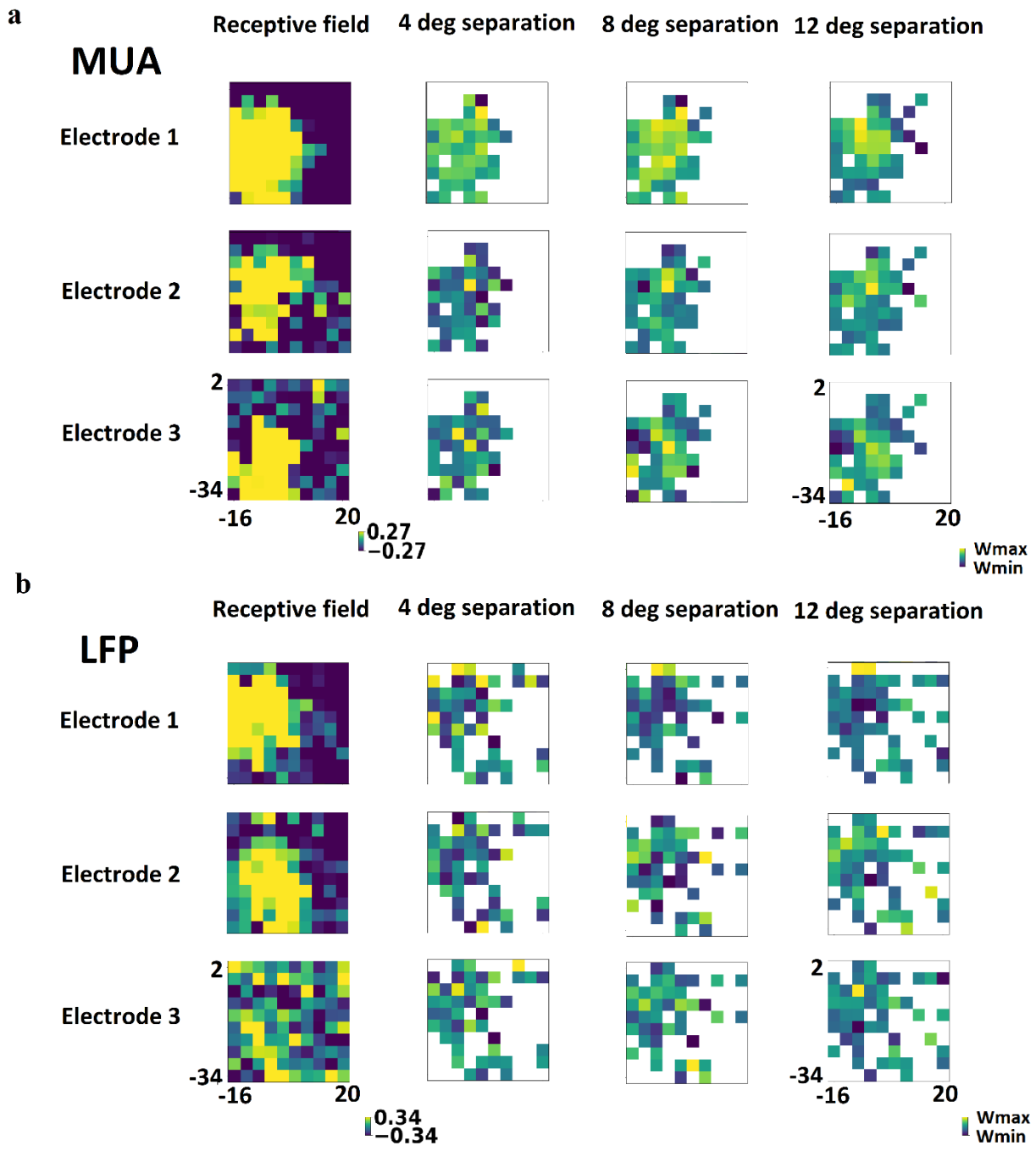

Figure A.3 The coding strategy of individual sites for position discrimination of small and large separations. The degree of color lightness indicates polarity of values; lighter colors show more positive and darker blue colors show more negative values. Spatial receptive field profile is shown for each electrode on the left. The spatial distribution of the weights assigned to each site for discrimination of a probe from the other ones with a fixed distance. This value is calculated for each probe and is presented at its location on the grid. The change in the coding strategy can

be observed from 4° to 12° separation in the visual field (left to right). The values of the discrimination weights are visualized over the ranges between their maximum and minimum to capture the weight variations specific to each separation distance. (a) MUA results: The range of response values for the receptive fields are set to -0.27 to 0.27. The best three electrodes for MUA are selected for this analysis. (b) LFP results. The range of response values for the receptive fields are set to -0.34 to 0.34. The best three electrodes for LFP are selected for this analysis. As the LFP respond by negative peaks, the darker colors are the representative of targets in the weight distribution.

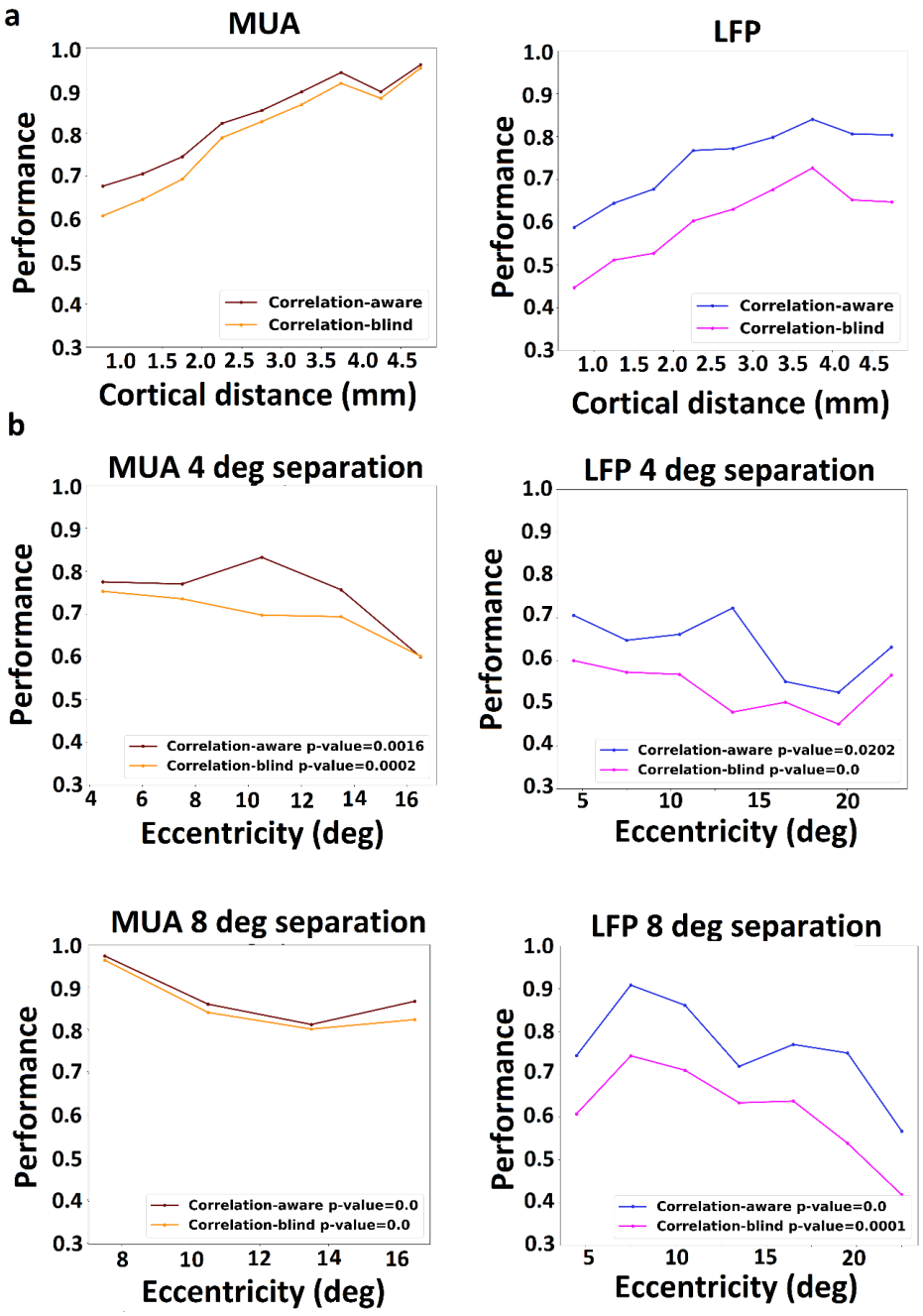

Figure A.4 Effect of noise correlations on spatial discrimination. Dark red and orange colors represent correlation-aware and correlation-blind performances of MUA respectively, while blue and purple colors are representative of the same measures in the LFP. The correlation-blind performances are the cross-validation scores when SVM is trained on the shuffled data but validated on the unshuffled data. (a) Discrimination performance versus cortical distance for correlation-blind versus correlation-aware responses. (left) MUA (right) LFP. The cortical

distance values are divided into 0.5 mm bins and the discrimination performances of pairs with cortical distances within each bin were averaged. (b) Discrimination performance as a function of eccentricity for 4° (top) and 8° (bottom) separations comparing correlation-blind and correlation-aware response data (left) MUA (right) LFP. Pearson correlation p-values are shown on each plot indicating the significance of the relationship. Eccentricity values are divided into 3° bins and the discrimination performances of pairs with eccentricity within each bin were averaged.

Results Using Another Session

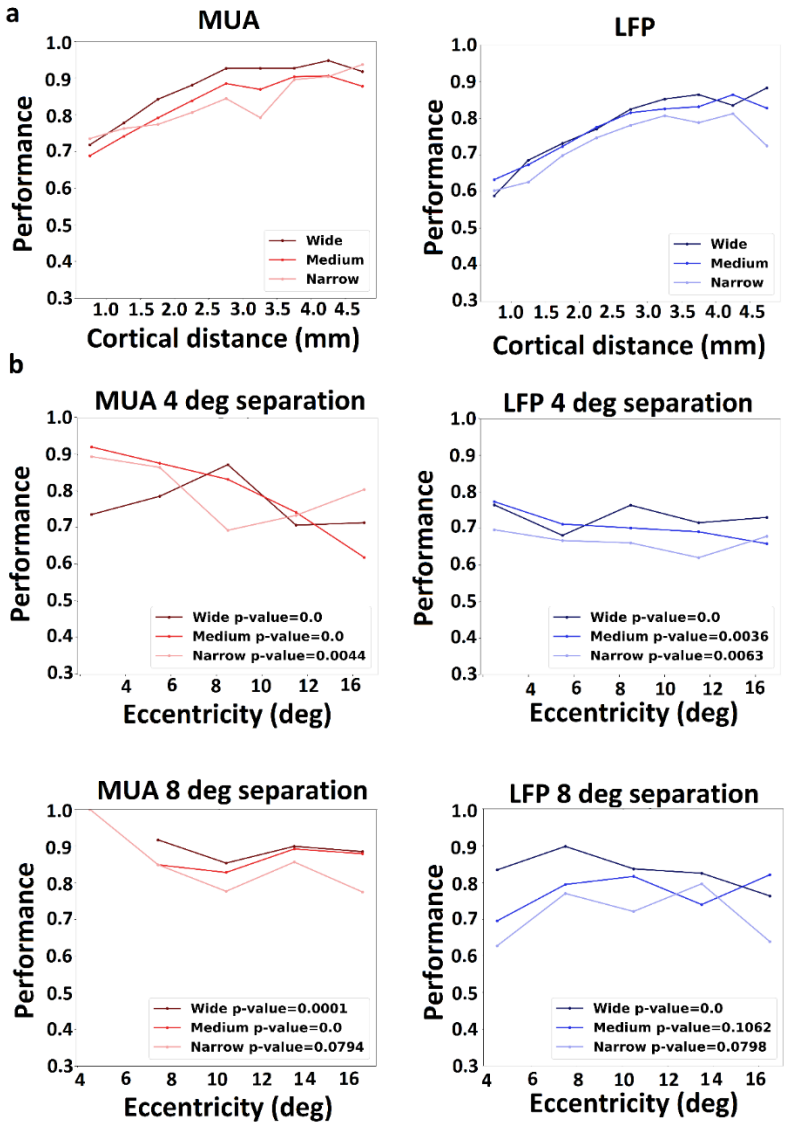

Figure A.5 V4 ensemble response allows spatial discrimination. Darker colors correspond to the wider response windows. The linear SVM was used for classification of the response data. The performances are validation scores of 5-fold cross validation measured as the area under the ROC curve. (a) Discrimination performance versus cortical distance (in mm) for MUA in red (left) and LFP in blue (right) based on responses defined on wide, medium, and narrow windows (darker to lighter). The cortical distance values are divided into 0.5 mm bins and the discrimination performances of pairs with cortical distances within each bin were averaged. (b) Discrimination performances of pairs with 4° and 8° separation distances as a function of pairs' eccentricity (in deg) for MUA (left) and LFP (right) for responses defined over wide, medium, and narrow

windows. Significance (p-values) of correlation between performance and eccentricity for each response window is presented in the plot. Eccentricity values are divided into 3° bins and the discrimination performances of pairs with eccentricity within each bin were averaged.

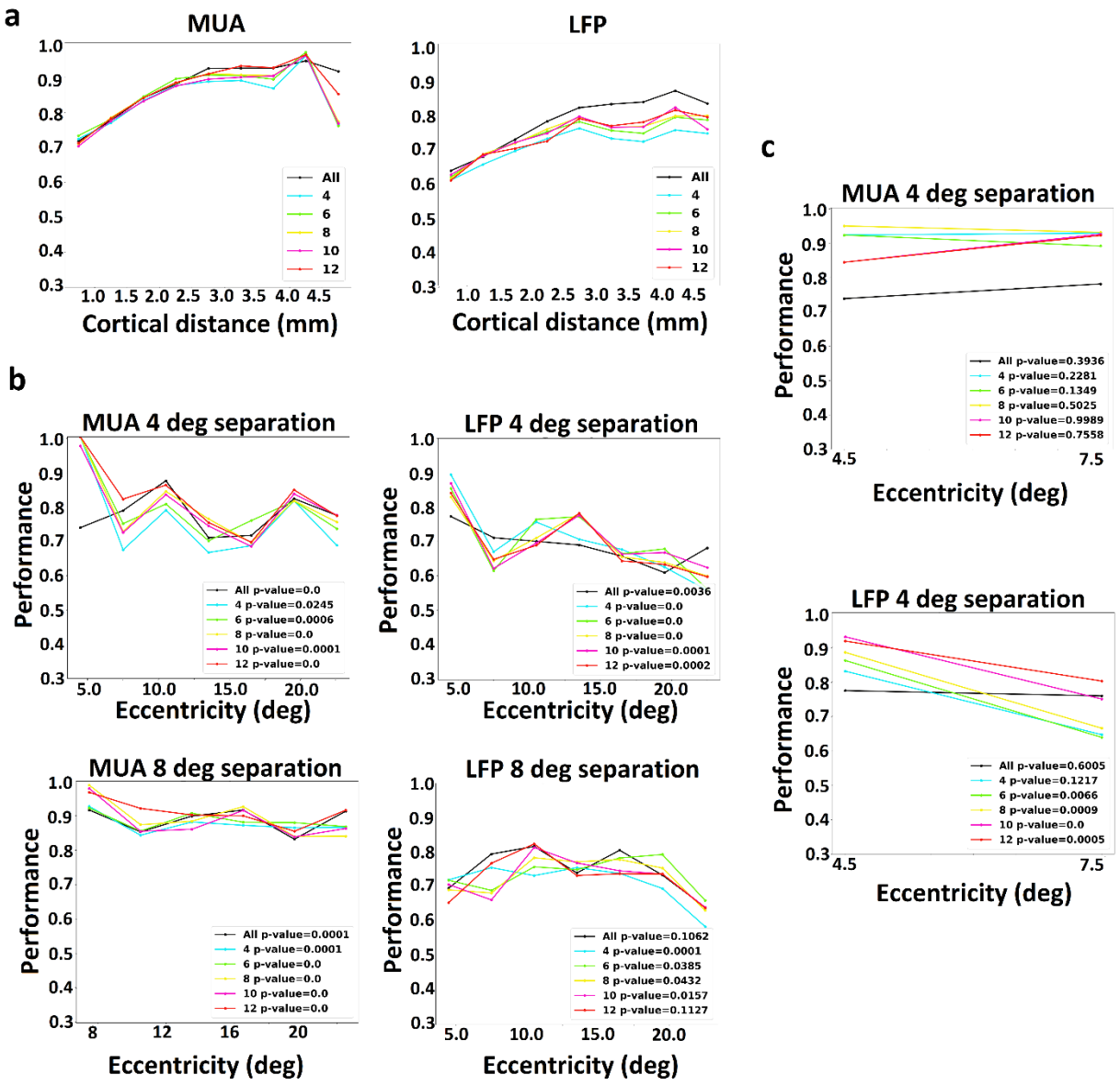

Figure A.6 Results of discrimination analysis with the best (most important) 4 (blue), 6 (green), 8 (yellow), 10 (purple), and 12 (red) electrodes. Discrimination performance using all the electrodes is shown in black. (a) Discrimination performance versus cortical distance (in

millimeters) for MUA (left) and LFP (right) with different sets of the best electrodes. The cortical distance values are divided into 0.5 mm bins and the discrimination performances of pairs with cortical distances within each bin were averaged. (b) Discrimination of probes with 4° (top) and 8° (bottom) separation versus the mean eccentricity of the pairs in visual degrees using the same sets of the best electrodes as (a). MUA results are presented on the left and LFP on the right. Pearson correlation significance (p-values) are presented on each plot associated to the results obtained with each electrode set. Eccentricity values are divided into 3° bins and the discrimination performances of pairs with eccentricity within each bin were averaged. (c) Selecting the best electrodes using importance values obtained by averaging over discriminations with 4° probe separation and <8° pairs eccentricity. The electrodes were sorted by these new importance values. As only the closer eccentricities were important, the plots are illustrated for smaller range of eccentricities.

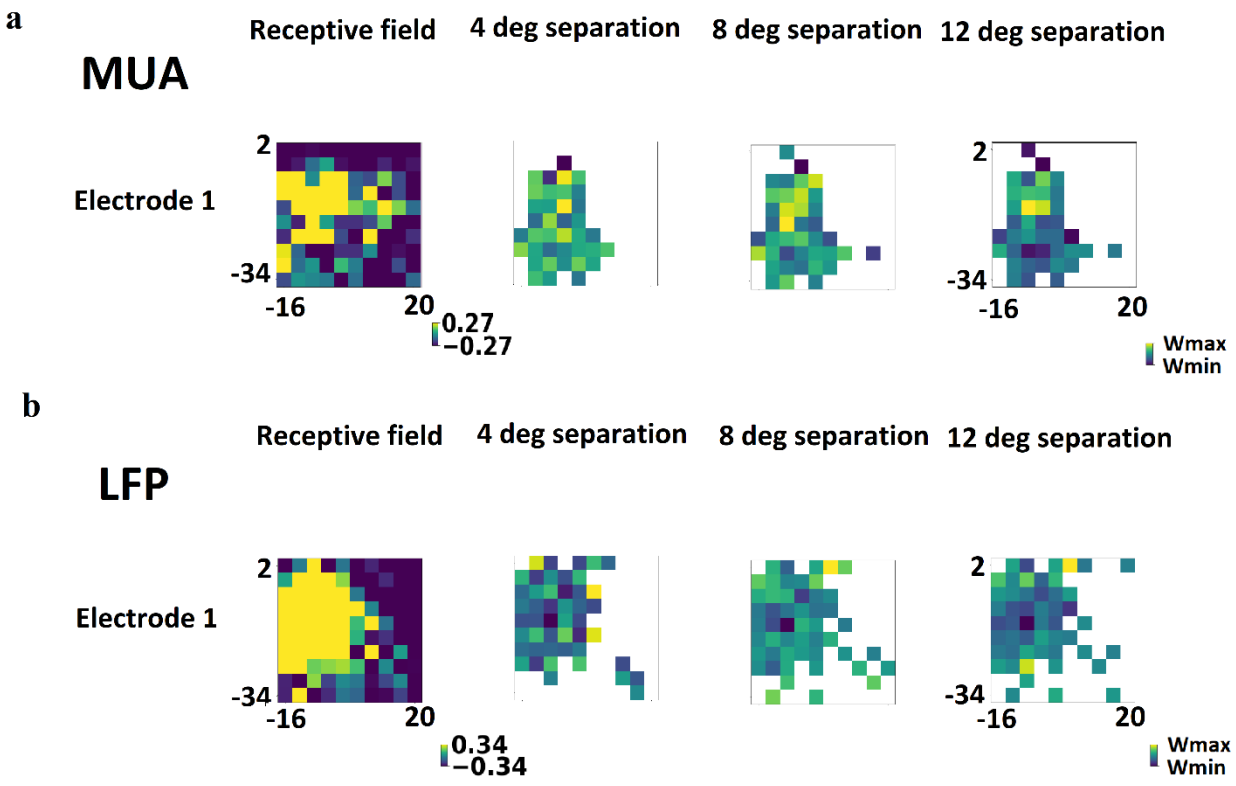

Figure A.7 The coding strategy of individual sites for position discrimination of small and large separations. The degree of color lightness indicates polarity of values; lighter colors show more positive and darker blue colors show more negative values. Spatial receptive field profile is shown for each electrode on the left. The spatial distribution of the weights assigned to each site for discrimination of a probe from the other ones with a fixed distance. This value is calculated for each probe and is presented at its location on the grid. The change in the coding strategy can be observed from 4° to 12° separation in the visual field (left to right). The values of the discrimination weights are visualized over the ranges between their maximum and minimum to capture the weight variations specific to each separation distance. (a) MUA results: The range of response values for the receptive fields are set to -0.27 to 0.27. A good electrode for MUA is selected for this analysis. (b) LFP results. The range of response values for the receptive fields are set to -0.34 to 0.34. A good electrode for LFP is selected for this analysis. As the LFP respond by negative peaks, the darker colors are the representative of targets in the weight distribution.

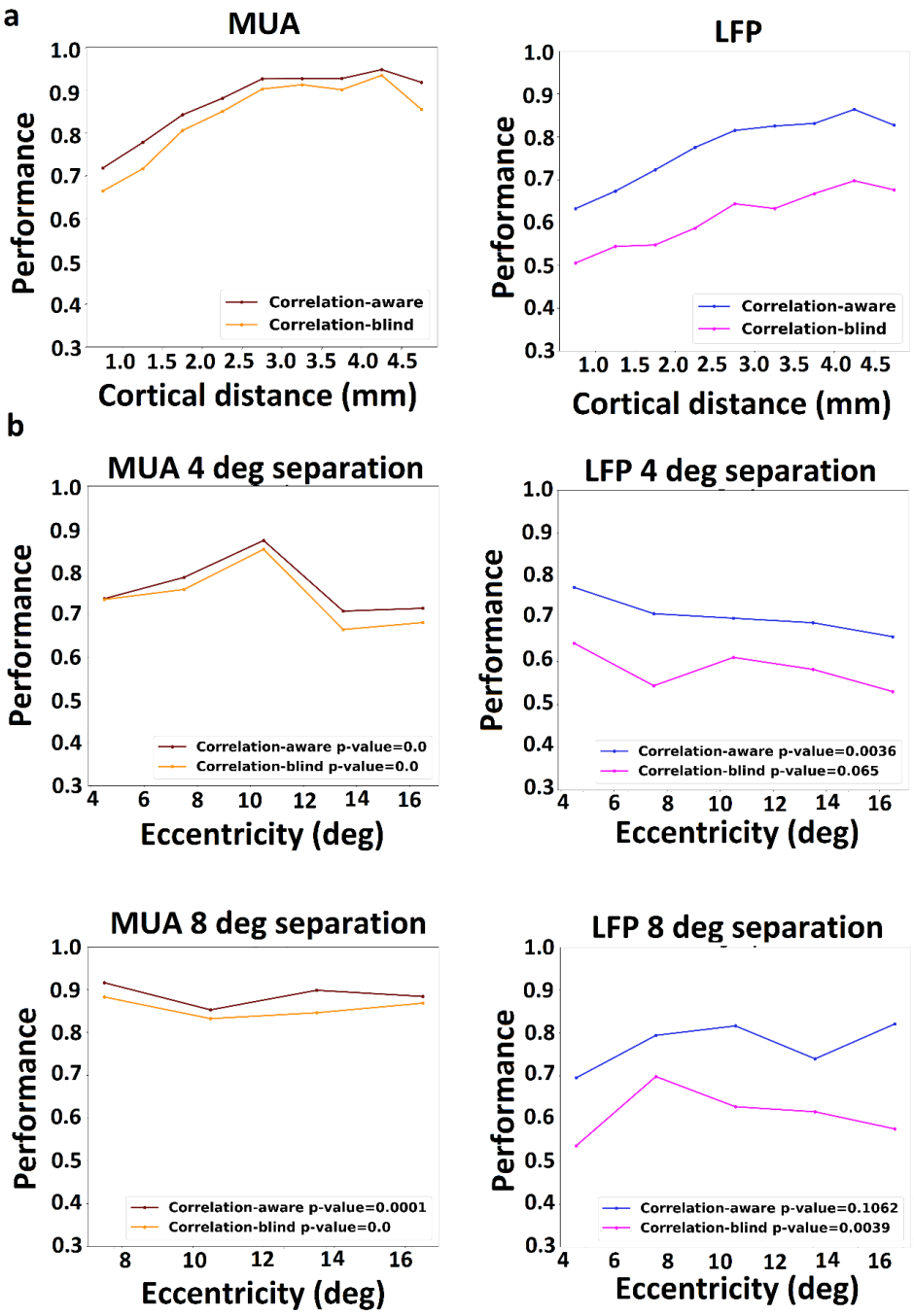

Figure A.8 Effect of noise correlations on spatial discrimination. Dark red and orange colors represent correlation-aware and correlation-blind performances of MUA respectively, while blue and purple colors are representative of the same measures in the LFP. The correlation-blind performances are the cross-validation scores when SVM is trained on the shuffled data but validated on the unshuffled data. (a) Discrimination performance versus cortical distance for correlation-blind versus correlation-aware responses. (left) MUA (right) LFP. The cortical

distance values are divided into 0.5 mm bins and the discrimination performances of pairs with cortical distances within each bin were averaged. (b) Discrimination performance as a function of eccentricity for 4° (top) and 8° (bottom) separations comparing correlation-blind and correlation-aware response data (left) MUA (right) LFP. Pearson correlation p-values are shown on each plot indicating the significance of the relationship. Eccentricity values are divided into 3° bins and the discrimination performances of pairs with eccentricity within each bin were averaged.

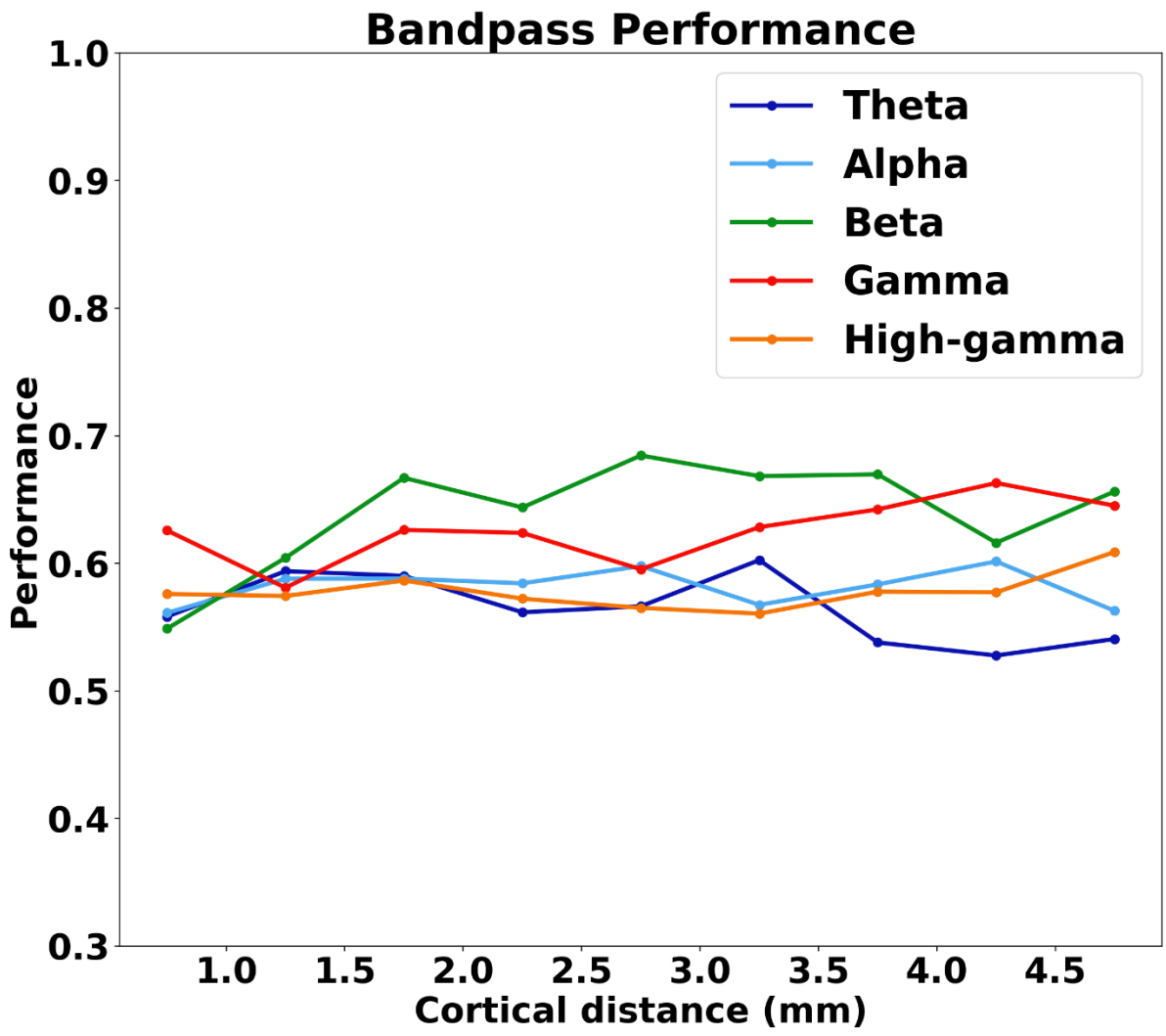

Figure A.9 Discrimination performance of band passed LFPs. Responses for each band passed signal were calculated using the medium window. The band passed LFP performance versus cortical distance for theta (4-8 Hz), alpha (8-12 Hz), beta (12-30 Hz), gamma (30-50 Hz), and high gamma (50-80 Hz) frequency bands. The cortical distance values are divided into 0.5 mm

bins and the discrimination performances of pairs with cortical distances within each bin were averaged.

Results Using Another Monkey

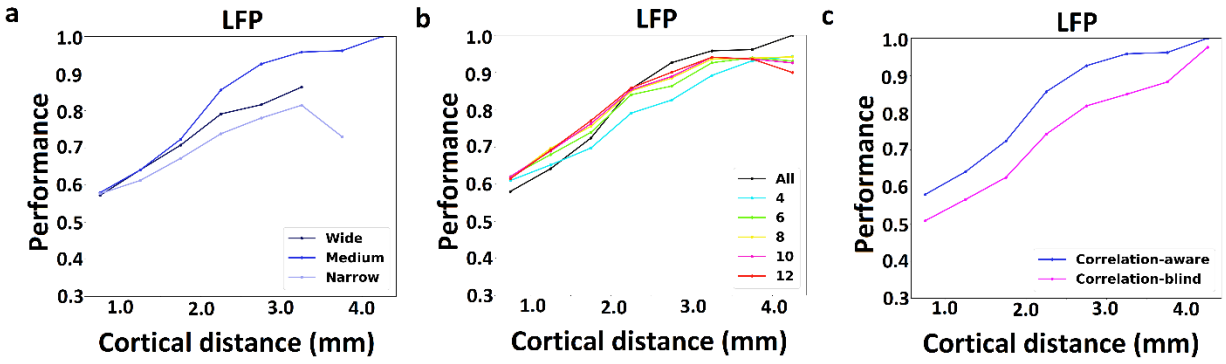

Figure A.10 Discrimination performance versus cortical distance (in mm) for LFP responses in V4. The cortical distance values are divided into 0.5 mm bins and the discrimination performances of pairs with cortical distances within each bin were averaged. (a) Comparing the results obtained using wide, medium, and narrow windows. Darker blue corresponds to the wider response window. The linear SVM was used for classification of the response data. The performances are validation scores of 5-fold cross validation measured as the area under the ROC curve. (b) Spatial discrimination with the best 4, 6, 8, 10, and 12 electrodes in blue, green, yellow, purple, and red colors respectively. Discrimination with all the electrodes is shown in black. (c) Effect of noise correlations on spatial discrimination. Blue and purple colors represent correlation-aware and correlation-blind performances respectively. The correlation-blind performances are the cross-validation scores when SVM is trained on the shuffled data but validated on the unshuffled data.

Comparing the Results Before and After Correction for the Eye Movement

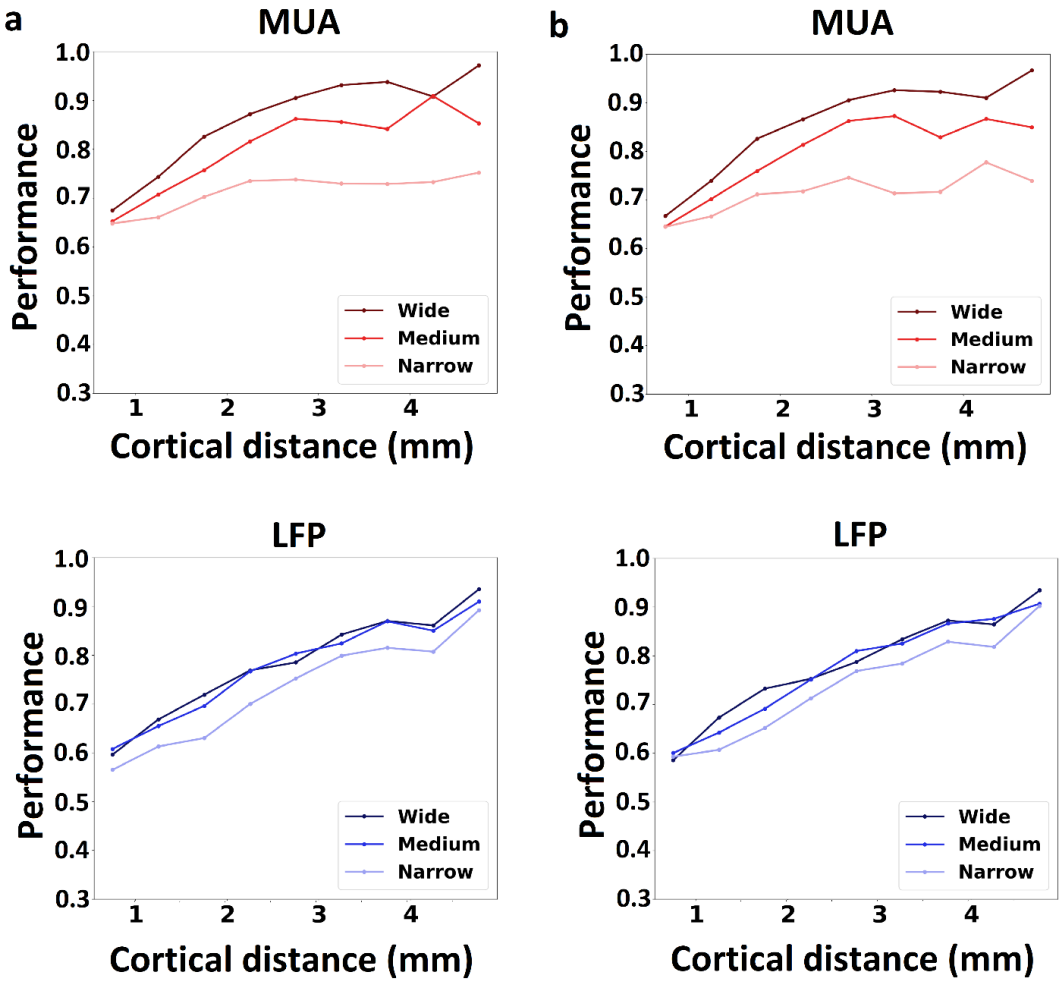

Figure A.11 Comparing the spatial discrimination before and after correction for the eye dispersion. Darker colors correspond to the wider response windows. The linear SVM was used for classification of the response data. The performances are validation scores of 5-fold cross validation measured as the area under the ROC curve. Discrimination performance versus cortical distance (in mm) for MUA in red (top) and LFP in blue (bottom). The cortical distance values are divided into 0.5 mm bins and the discrimination performances of pairs with cortical distances within each bin were averaged. (a) before correction for the eye dispersion (b) after correction for the eye dispersion.

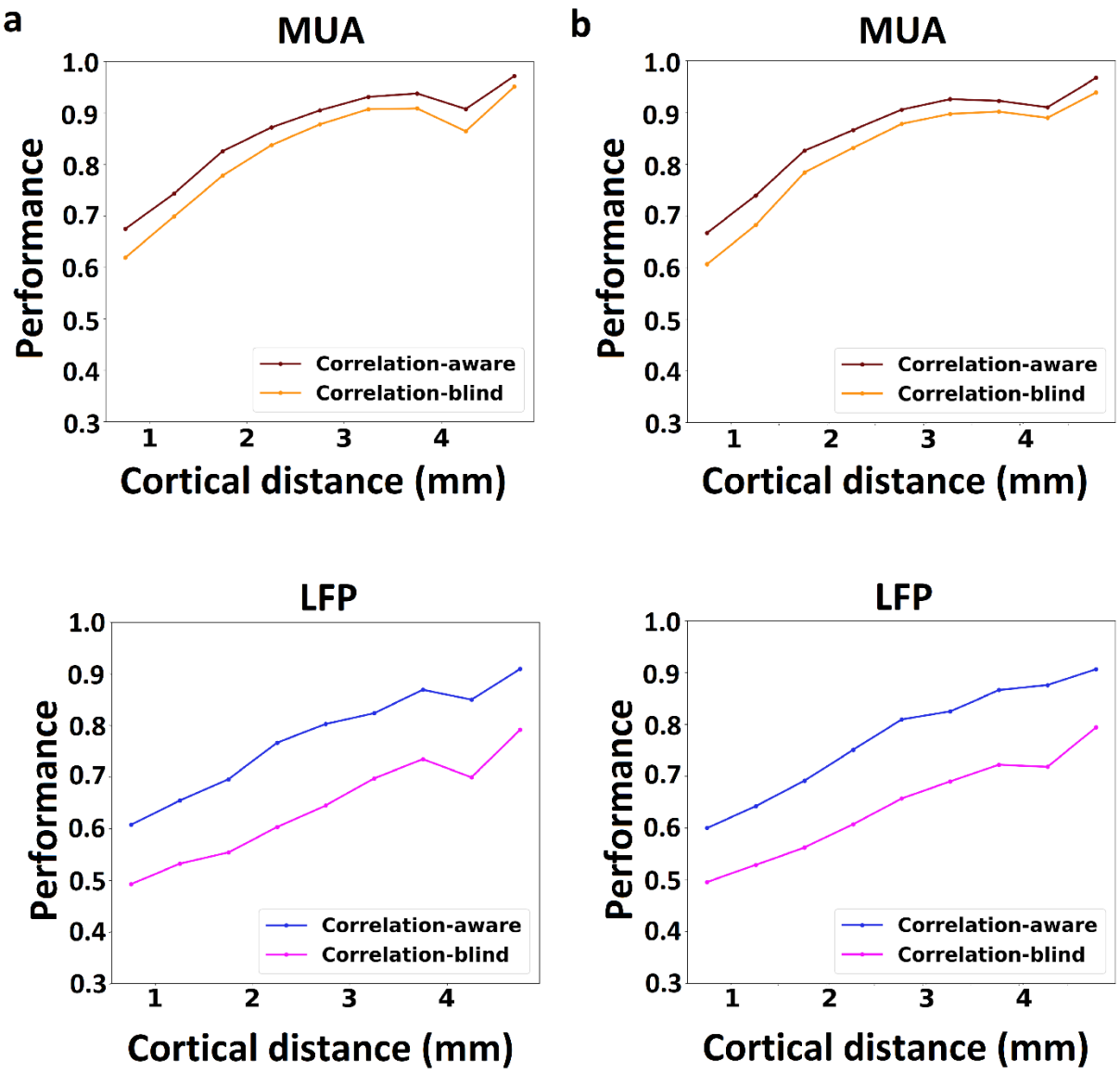

Figure A.12 Comparing the effect of noise correlation on spatial discrimination before and after correction for the eye dispersion. Dark red and orange colors represent correlation-aware and correlation-blind performances of MUA respectively, while blue and purple colors are representative of the same measures in the LFP. The correlation-blind performances are the cross-validation scores when SVM is trained on the shuffled data but validated on the unshuffled data. Discrimination performance versus cortical distance for correlation-blind versus correlation-aware responses. (top) MUA (bottom) LFP. The cortical distance values are divided into 0.5 mm bins and the discrimination performances of pairs with cortical distances within each bin were averaged. (a) before correction for the eye dispersion (b) after correction for the eye dispersion.

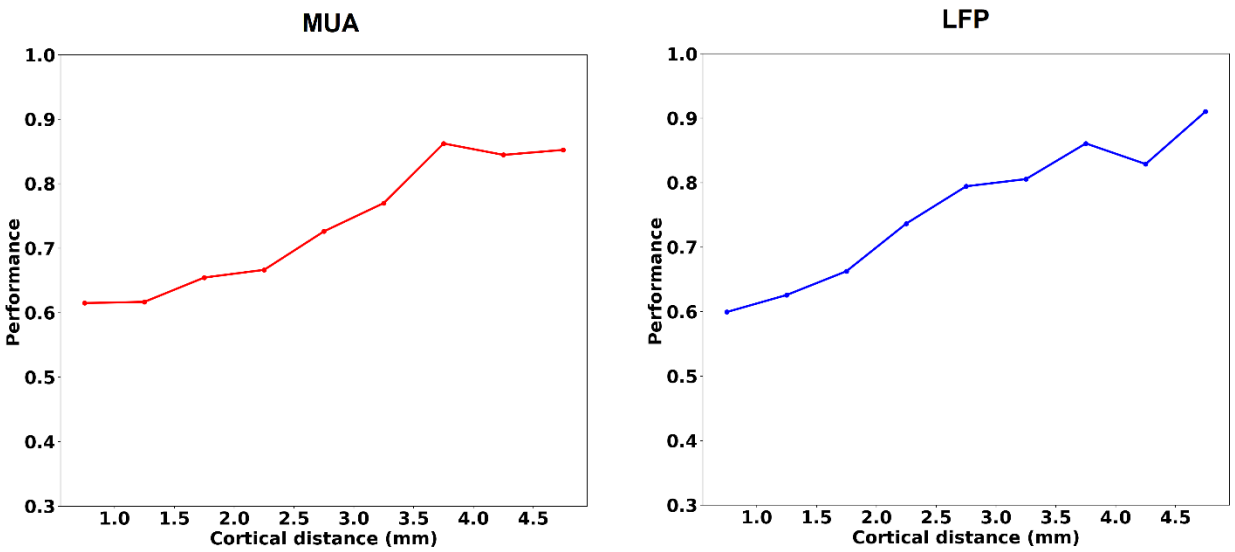

Figure A.13. Spatial discrimination performance versus cortical distance using all the electrodes except the best 12 electrodes (i.e. 84 electrodes): red color for MUA and blue for LFPs. These curves show that the electrodes contain redundant and highly correlated information.

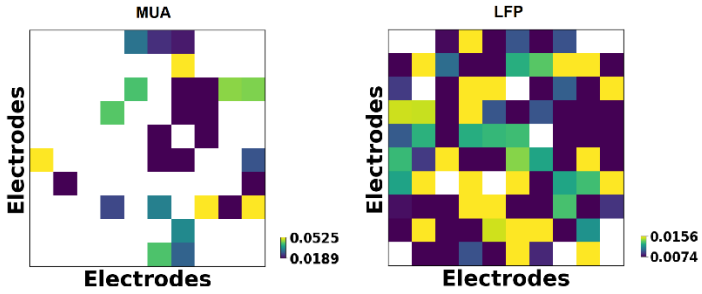

Figure A.14. Distribution of importance values on the electrode array. Yellower electrodes are the most important ones.